OXFORD Regenerative Biomaterials

Regenerative Biomaterials, 2023, **10**, rbac094
https://doi.org/10.1093/rb/rbac094
Advance Access Publication Date: 24 November 2022
Review

Functional engineering strategies of 3D printed implants for hard tissue replacement

Cen Chen[1], Bo Huang[1], Yi Liu[2], Fan Liu[2] and In-Seop Lee[1,3]*

[1]College of Life Sciences and Medicine, Zhejiang Sci-Tech University, Hangzhou 310018, PR China
[2]Department of Orthodontics, School of Stomatology, China Medical University, Shenyang 110002, PR China
[3]Institute of Human Materials, Suwon 16514, Republic of Korea

*Correspondence address. E-mail: inseop@yonsei.ac.kr

Abstract

Three-dimensional printing technology with the rapid development of printing materials are widely recognized as a promising way to fabricate bioartificial bone tissues. In consideration of the disadvantages of bone substitutes, including poor mechanical properties, lack of vascularization and insufficient osteointegration, functional modification strategies can provide multiple functions and desired characteristics of printing materials, enhance their physicochemical and biological properties in bone tissue engineering. Thus, this review focuses on the advances of functional engineering strategies for 3D printed biomaterials in hard tissue replacement. It is structured as introducing 3D printing technologies, properties of printing materials (metals, ceramics and polymers) and typical functional engineering strategies utilized in the application of bone, cartilage and joint regeneration.

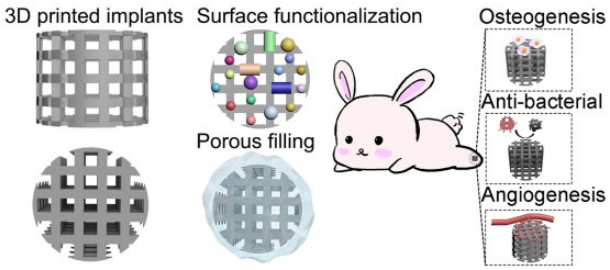

Keywords: hard tissue replacement; bone regeneration; 3D printing; additive manufacturing; functional engineering

Introduction

Bone acts as the supportive framework, protecting vital organ and maintaining multiple functions of human body. The bone disorders, referring to the structural and/or functional abnormities of bones, seriously affect patients' physical function and mental health. Indeed, the ageing population and unhealthy life styles result in an increasing occurrence of bone defect, including fracture, osteoporosis, osteoarthritis, congenital deformity, traumatic injury and oncologic resection [1]. As a result, bone is the second most frequently transplanted tissue worldwide, with over two million maxillofacial surgeries and 2.2 million orthopedic surgeries in China every year.

The development of bone defect treatment starts from bone biology. Structurally, bone is composed of the dense and solid cortical bone, which presents highly peripheral supporting structure, and cancellous bone providing honeycomb-like network with lamellar trabecula inside [2]. The main compositions of bone are inorganic minerals, extracellular matrix (ECM) and various growth factors (GFs). Partial nanostructured ECM produced by osteoblasts provides favorable platform for cell adhesion, proliferation and differentiation. Mineralized portion of ECM undergoes the deposition of calcium-phosphates in the form of hydroxyapatite (HA) interacting with type I collagen and other non-collagenous proteins [3, 4]. Bone homeostasis depends on the dynamic metabolism of bone resorption and formation. Normally, the physiological bone remodeling ensures small bone deformities to be cured through host tissue self-regeneration. However, critical-size bone deformities need bone transplantation through surgical operation. Ideally, non-immunogenic autograft is the best choice based on bone biology mentioned above. Whereas, it requires a second operation for tissue harvest, and the limit sources become the main obstacle for large-sized defects. Although allograft is an alternative choice, immunological rejection and infection need to be carefully handled. Therefore, the development of artificial bone substitutes is essential for bone tissue engineering. Bone tissue engineering includes the utilization of biomimetic scaffolds, inducible cells and growth factors. Among them, porous scaffolds that mimic the ECM component and structure, provide mechanical supporting and biological environment for cell attachment, thereby forming new bone in defect area [5–7].

Three-dimension printing (3DP), also named as additive manufacturing (AM), was first used for fabricating models and prototypes in 1980s [8]. Compared with traditional manufacturing methods that proceed by removal of material to obtain the 3D object, AM is unique in their layer-by-layer adding and bonding material fashions to form solid 3D objects, enabling manufacturing

Received: June 03, 2022. **Revised:** October 20, 2022. **Accepted:** October 27, 2022

processes that automatically produce complex structures directly from computer-aided design (CAD) models with high resolution and sophistication. These technologies are based on a layered manufacturing paradigm that builds solid objects by incremental material deposition and fusion of cross-sectional layers. By breaking down complex 3D shapes into simple 2D layers, the assembling of complex structures can be dramatically simplified under the instruction of CAD models [9–11].

In the last decades, the rapid development of AM technology has been widely recognized as a promising way to fabricate bioartificial bone tissues. Importantly, ideal bone scaffolds require various properties, including biocompatibility, mechanical integrity, bioprintability and osteoconductivity, which are mainly determined by the physical and/or chemical properties of printing materials [12]. Metals, ceramics and polymers are widely used as printing materials in bone tissue engineering [13–16]. After scaffolds implantation, the interaction of materials and surrounding tissues could directly attract cell adhesion and modulate cell behaviors including adhesion, proliferation, differentiation and apoptosis, thereby affecting biocompatibility and osteogenesis of bone scaffolds [17]. Apart from the decoration of bioactive interface above, biomimetic strategies to incorporating functional materials inspired by the chemical compositions and structures of biomolecules or their specific functionalities into implants during 3D printing process provide multi-functions and desired characteristics which can be applied in bone tissue engineering under various conditions. 3D printing scaffolds with functionalized characteristics could not only present the capacity of modulating the interaction of cells/biomolecules with scaffolds, but also obtain an optimized functionality to promote the physicochemical and biological performance of scaffolds in bone tissue engineering [18, 19].

This review covers 3D printing technologies, printed materials and functional engineering strategies for hard tissue substitutes. In detail, we provide a comprehensive overview of widely used 3D printing technologies for hard tissue regeneration. The properties of printed materials (metals, ceramics and polymers) for hard tissue implants are outlined. Additionally, typical functional engineering strategies of printed materials in bone, cartilage and joint applications are highlighted.

3D printing technologies for hard tissue replacement

American Society for Testing and Materials (ASTM) has defined AM as 'a process of joining materials to make objects from 3D model data, usually layer upon layer, as opposed to subtractive manufacturing methodologies' [20]. Two main groups are divided for 3D printing in medical application: cell-free printing technologies and cell-laden bioprinting technologies [21, 22]. Obviously, the requirements of printing materials are different: metals, ceramics and some synthetic polymers that possess non-toxic and high stability are mostly used for cell-free printing technologies. Otherwise, cell-laden bioprinting technologies refer to living cells and materials are simultaneously printed, which had certain restrictions of printing temperatures and pressures, physical and/or chemical properties of printing materials (also known as 'bioinks'), and cell sources [23]. According to its work principle, AM technologies are divided into powder-based systems, inkjet-based systems, materials extrusion and vat photopolymerization, whose applications are widely including metals, polymers, and ceramics (Fig. 1 and Table 1) [12, 21, 22, 24–42].

AM technologies

Powder-based AM

Powder-based AM technologies utilize thermal energy to selectively fuse regions of a powder bed with metallic and/or ceramic powders, which are divided into powder-bed based printing system and direct energy deposition (DED) system [38, 43].

Powder-bed-based printing system

The representative powder-bed fusion printing system includes selective laser sintering (SLS), selective laser melting (SLM) and electron beam melting (EBM) systems [39]. In SLS or SLM systems, powder particles with mean sizes ranging between 20 and 60 μm are placed on build platform as starting materials. Based on the presetting procedure in computer, a high-power laser as energy source scans the surface in a specific 2D pattern to sinter or melt of the powder particles [44]. After the first layer is created, the fabrication piston is lowered and a fresh layer of powder material is recoated across the top surface by a roller in powder delivery system. The resolution and surface roughness of fabricated objects by SLS are determined by particle size of utilized powders where larger particles generally cause lower spatial resolution and higher surface roughness [45]. One of the disadvantages of SLS is incomplete melting of the powder particles, leading to the porosity between the original particles, which affect density of fabricated objects. The amount of free volume is dependent on particle size distribution, printed materials and printing parameters [46, 47]. Therefore, subsequent post sintering or heating treatment is required to improve properties of fabricated object. While, on the other hand, SLS-fabricated objects are light and porous, that can be advantageous in some specific applications, for example, scaffolds require large surface areas for cell growth in tissue engineering [48, 49]. In SLM system, the material powders are not sintered but completely melted directly at processing point by laser source. Thus, SLM-fabricated parts present an improved surface quality, density and superior mechanical strength by higher laser density [50, 51]. The whole process is performed in an inert gas (i.e. argon or nitrogen) filled chamber, which minimizes the risk of oxygen and hydrogen.

EBM technology applies electron beam energy (>100 kW/cm^2) to melt the metal powder and fabricate metallic object that can have a complex structure. The printing process undergo in a vacuum chamber, preventing the inclusion of oxygen into the system [52]. The beam controlled by electromagnetic lenses initiate heating the powder layer with a higher scan speed, followed by completely melting the powder layer based on the geometry defined by the computer design until the desired object completion. The most common metallic materials for EBM printing include titanium (Ti) alloys (Ti–6Al–4V, Ti–Al–Nb and $\alpha+\beta$ alloys), cobalt–chrome alloys (Co–Cr–Mo, Co–Ni–Cr and Co–Cr–W–Ni), stainless steel (316L) [53, 54]. Fousová *et al.* [55] focused on a comparison of SLM and EBM in terms of the mechanical properties of Ti6Al4V alloy. The internal defects of SLM resulted from insufficient melting, while spherical pores in EBM resulted from gas entrapment. More importantly, due to a higher surface roughness and more harmful defects distributed across the Ti-based samples, fatigue strength reached 115 ± 13 MPa for EBM when compared with 220 ± 24 MPa for SLM, indicating SLM seems to be a better choice for the fabrication of porous structures.

DED system

DED is a 3D printing process that employs focused thermal energy (i.e. laser or electron beam) to produce fully dense and

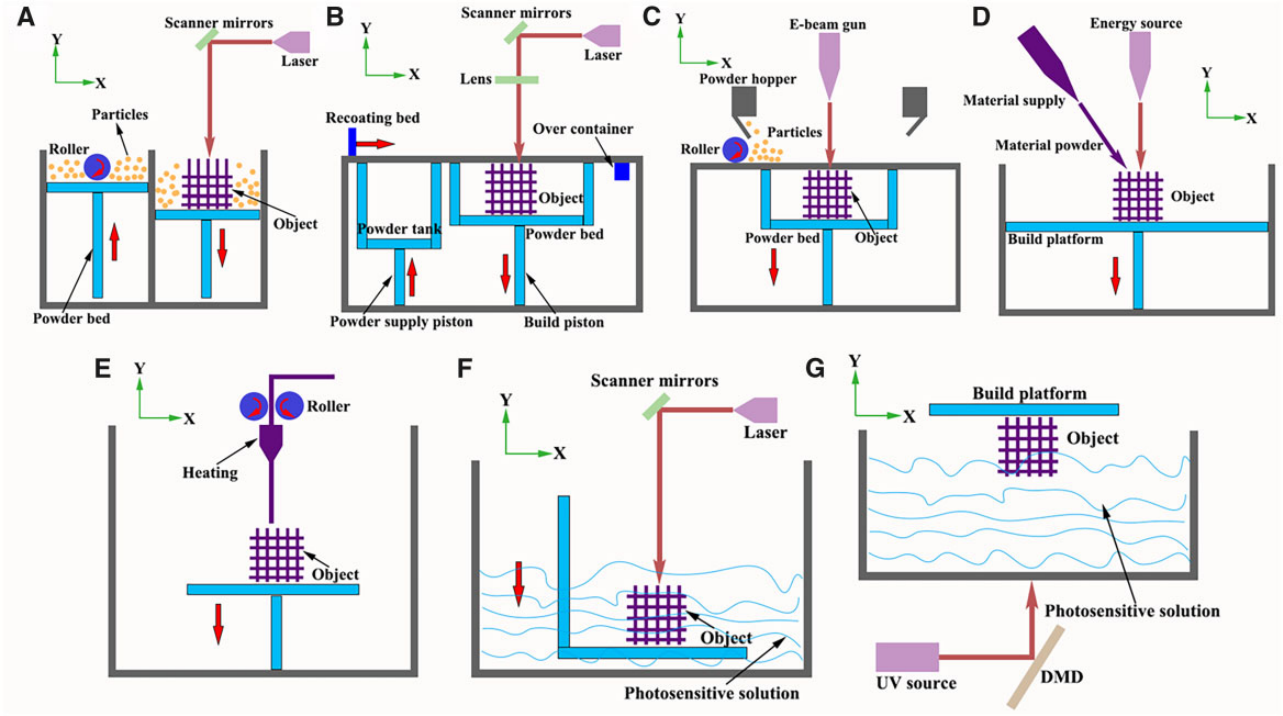

Figure 1. Schematic illustration of commonly used 3D printing technologies [12, 21, 32, 33, 37–39] (**A**: SLS; **B**: SLM; **C**: EBM; **D**: DED; **E**: FDM; **F**: SLA; **G**: DLP).

functional metal implant by depositing fused metal powders. Metals in wire form are melted to form an object in a vacuum chamber. The electron beam melts up the metallic wire and thereby creates a melt pool in which more wire is fed into. A computer guides the movement on a non-stationary build platform so that a material layer is applied to those areas where the desired object needs to be built up, and the process is repeated until the whole object is built up layer by layer [56]. One major advantage of DED is the rapid manufacturing and large building capacity, when compared with powder-bed fusion. Another advantage is that the process of using metallic components with electron beams produces a high vacuum environment, which is a contamination-free work zone, without the need of additional inert gasses that are often used with laser-based processes [57]. DED allows a wide range of different metal materials including Ti, tantalum, stainless steel, aluminum alloys, nickel-based alloys and Ti aluminides. However, the shortcoming is that the accuracy of fabricated object by DED is inferior to other printing technologies. The excess materials on surface structure of fabricated object need to be removed and precisely refined through post printing process [58–60].

Inkjet-based AM

Inkjet-based printing systems refer to the AM process which liquid drops of fabricated materials are selectively deposited in a layer-by-layer manner.

Binder jetting, one of typical types of inkjet-based printing system, is composed of binder solution reservoir, powder reservoir and a build platform. During printing process, powders are firstly sprayed to form one powder layer, followed by jetting binder solution that acts as 'glue' to bond the powder particles together. Once the first layer is formed, the same procedure repeats in a layer-by-layer pattern until the desired object is completed. Compared with other printing technologies, binder jetting is compatible with virtually any powder material. Another advantage of binder jetting is that printing process occurs at room temperature and atmospheric pressure. By avoiding the use of expensive sealed chambers for vacuum, the build volume of binder jetting machines (up to $2200 \times 1200 \times 600$ mm) is among the largest compared with all other AM technologies while still maintaining the high resolution [25]. However, in consideration of the object stability, post-processing steps (curing and densification) are required to enhance mechanical properties.

In addition to non-biological materials for binder jetting, liquid droplets incorporated of biocompatible polymers and encapsulated cells (also known as 'bioinks') can be printed simultaneously by thermal or piezoelectric printing nozzle [37]. In thermal bioprinters, the increasing pressure resulting from the heating force of bioink droplets to eject on built platform. However, the sizes of liquid droplets are heterogeneous, easily clogging the nozzle [61]. The heating temperature can reach at the maximum of 300°C. Nevertheless, it lasts for very short of time for ejecting process, only resulting in a slight increase of system temperature (4–10°C) [62]. Thus, encapsulated cells can still retain high viabilities. In piezoelectric bioprinters, bioink droplets are generated by piezoelectric actuators, which remain uniform size and shape of liquid droplets.

Materials extrusion AM

In extrusion-based AM, materials are extruded through one or multiple print heads by pneumatic pressure or mechanical force. In printing process, a continuous force allows materials to be extruded as a continuous line of 'printing ink', rather than liquid droplets, through one or multiple micro nozzles.

Fused deposition modeling (FDM), also named as thermoplastic extrusion (one of extrusion-based AM), is the layered deposition of molten thermoplastic materials via a heated nozzle. The filament or pellet forms of thermoplastics are heated into

Table 1. Overview the 3D printing technologies

	Technology	Power source	Printing materials	Print speed	Particle size		Layer thickness		Ref.
Cell-free	DED	Laser/electron beam	Metal	Fast	25–75 μm		250 μm		[40, 41]
	SLS	Laser beam	Metal/ceramic/ polymers	Slow	50–150 μm		20–100 μm		[42]
	SLM		Metal		20–60 μm				[24, 36, 39]
	EBM	Electron beam	Metal	Fast	45–105 μm		50 μm		[39]
	Binder jetting	Thermal source	Metal	Medium (6–14 mm/s)	Submicron–150 μm		15–300 μm		[25]
	FDM	Thermal	Thermoplastics; polymer-metal composites	Slow (200 μm–10 mm/s)	–		100–200 μm		[26, 35]
					Viscosity	**Cell viability**	**Resolution**	**Cell density**	
Cell-free/cell-laden	SLA	UV	photopolymers	Fast	None	>90%	60–150 μm	$<10^8$ cells/ml	[22, 27]
	DLP	UV/visible light	photopolymers	Fast than SLA		Higher than SLA	25–50 μm		[28–31, 34]
Cell-laden	Inkjet bioprinting	Thermal/ piezoelectric	Thermoplastics	Fast (1–10^4 droplets/s)	Low (3.5–12 mPa/s)	>85%	75 μm	$<10^6$ cells/ml	[9, 28]
	Extrusion bioprinting	Pneumatic/pressure	Natural/synthetic polymers	Slow (10–700 mm/s)	High (30–6 × 10^7 mPa/s)	80–90%	200–1000 μm	$>10^8$ cells/ml	[21]

semi-liquid states and extruded onto platform. Most synthetic polymers, including polyurethane (PU), poly-caprolactone (PCL) and poly-lactic acid (PLA) are ideal printing materials for FDM in medical application, which can be used for customized patient-specific medical devices. The obvious advantage of FDM is quickly building construct with geometric accuracy and excellent mechanical properties. Meanwhile, bioactive substances including growth factors, antibiotics, drugs, can be incorporated into thermoplastic polymers to enhance the biological properties of fabricated objects, whereas the use of FDM is limited for living cell printing directly under the high temperature of melting [63].

Unlike FDM, extrusion bioprinting do not involve any heating process, indicating polymeric hydrogels with living cells and other bioactive substances can be extruded through nozzles by pneumatic pressure or physical force in a controllable manner. The solidification of polymeric hydrogels is achieved by physico-chemical crosslinking (i.e. sol–gel transformation, polymerization and enzymatic reaction). However, the viscosities of printing hydrogels are crucial for cell viabilities. Generally, higher viscous bioinks extruded from nozzles results in higher shear-stress, which is detrimental to cell viabilities. Additionally, the printing resolution is limited, with the range between 200 and 1000 μm, compared with other technologies [64].

Vat photopolymerization

Vat photopolymerization is an AM process in which liquid photopolymer in a vat is selectively cured by light-activated polymerization. Stereolithography (SLA) and digital light processing (DLP) are two main lithography-based 3D bioprinting technologies.

Basis of SLA is a basin filled with liquid photopolymer, which can solidify after a certain exposure time. In printing process, liquid material is exposed by using light beam to form first layer of fabricated object on the platform. After the platform goes down by the height of one layer, the first layer is covered with photopolymer in the basin and repeated the same procedure until the desired object completion [9]. DLP follows the similar working principle as SLA. However, the light source cures the photopolymer as first layer by a digital micromirror device, which is composed of approximately 1 million micromirrors, rather than linear light beam in SLA [30, 32]. As a result, an entire layer can be cured at a time, indicating DLP exhibits a faster printing speed than SLA. Moreover, visible light can be adopted in DLP system as light source, which supports long-term cell viabilities [65]. Both SLA and DLP are safe for cell incorporation since they avoid high printing temperature and shear stress.

Functional engineering strategies of metallic materials for hard tissue repairment

Compared with other materials, metallic materials are mostly used for hard tissue regeneration, especially for orthopedic and dental application. The requirements of implantable metallic materials include corrosion resistance, proper mechanical strength (specific strength, endurance strength and impact toughness) and high biocompatibility [66–69]. Another important issue for metallic implants is stress shielding, which could increase the risk of bone resorption and fracture [70].

Printable metallic materials

Cobalt–chromium alloys

Cobalt–chromium (Co–Cr) alloys have been used for medical implants since the 1930s [71]. The chromium forms a protective Cr_2O_3 film when exposed to the physiological environment, presenting excellent corrosion resistant and wear resistance [72, 73]. The face-centered cubic crystal structure of Co is the predominant metal element (>60%) in Co–alloys, which is believed to be associated to high yield strength, high work-hardening rates, limited fatigue damage under cyclic stresses [74]. Cr is the primary alloying element which increases strength due to carbide formation. Co–Cr alloys are often used in permanent load-bearing implants in the orthopedic and dental fields [54, 75]. For example, Co–Cr alloys are often used for removable partial denture (RPD) frameworks [76]. Compared with conventional casting or milling methods, higher mechanical strength of dental Co–Cr alloys were achieved by using SLM technology [77]. Murr *et al.* [54] fabricated open-cellular structures of Co–29Cr–6Mo for femoral application by using EBM technology, and achieved proper Young's modulus that matched the stiffness of knee.

Titanium

Pure Ti (CP–Ti) and its alloys (Ti6Al4V) have been introduced in biomedical implants since the 1970s. They exhibit excellent physical properties as bone scaffolds, especially in load-bearing sites of bone defects, which are the most widely used materials for hard tissue replacement (Fig. 2) [78–80]. To be specific, CP–Ti is a relatively weak α-type alloy that cannot be strengthened by heat treatment, while Ti6Al4V is an (α + β)-type alloy whose mechanical strength can be increased up to 50% by heat treatment without significantly affecting its Young's modulus. In particular, Young's modulus of CP–Ti and Ti6Al4V is 103–107 and 114–120 GPa, which is significantly higher than that of bone tissue (7–25 GPa), easily causing stress shielding [81]. In detail, 3D printed Ti-based scaffolds could effectively avoid stress shielding, control mechanical properties to targeted implantation area and favor bone ingrowth, which widely used for hip or knee replacements, spine fusion cages, and craniofacial reconstructions [82]. While bulk Ti-based implants mostly used as dental implants with a survival rate of around 95% according to 10-year clinical observations [83–85]. The major complication is peri-implantitis, which can cause bone loss around the implant, eventually resulting in implant failure [86]. Various surface engineering strategies have been made to optimize implants' bioactivity by increasing their surface roughness and performing physicochemical modification.

Tantalum

Tantalum (Ta) has been used in orthopedic surgery since the 1940s. Ta holds anti-corrosion properties *in vivo* by forming an inert oxide coating surface, which prevents electrochemical reactions and other reactions caused by metallic ions. Similar to Ti, Ta has been used as bone-substitute materials for total joint prosthesis, osteonecrosis of femoral head and dental implants [87]. However, extremely high melting temperature of Ta (3017°C), along with its high affinity towards oxygen, makes it difficult to process Ta structures via conventional processing methods [58]. Thus, SLM and EBM are commonly applied for the fabrication of Ta implants [88, 89]. Luo *et al.* [90] identified that porous tantalum scaffolds with pore size of 400–600 μm and porosity of 75% showed better performance of bone ingrowth and integration. Furthermore, some researchers verified 3D printed Ta scaffolds are superior to Ti scaffolds in resistance to compression and deformation [88, 91]. Tang *et al.* [91] achieved satisfied outcomes in 27 clinical applications (hip, fibula and femur) of EBM-fabricated Ta bone implants since 2016, indicating the potential application as bone-substitute materials (Fig. 3) [92].

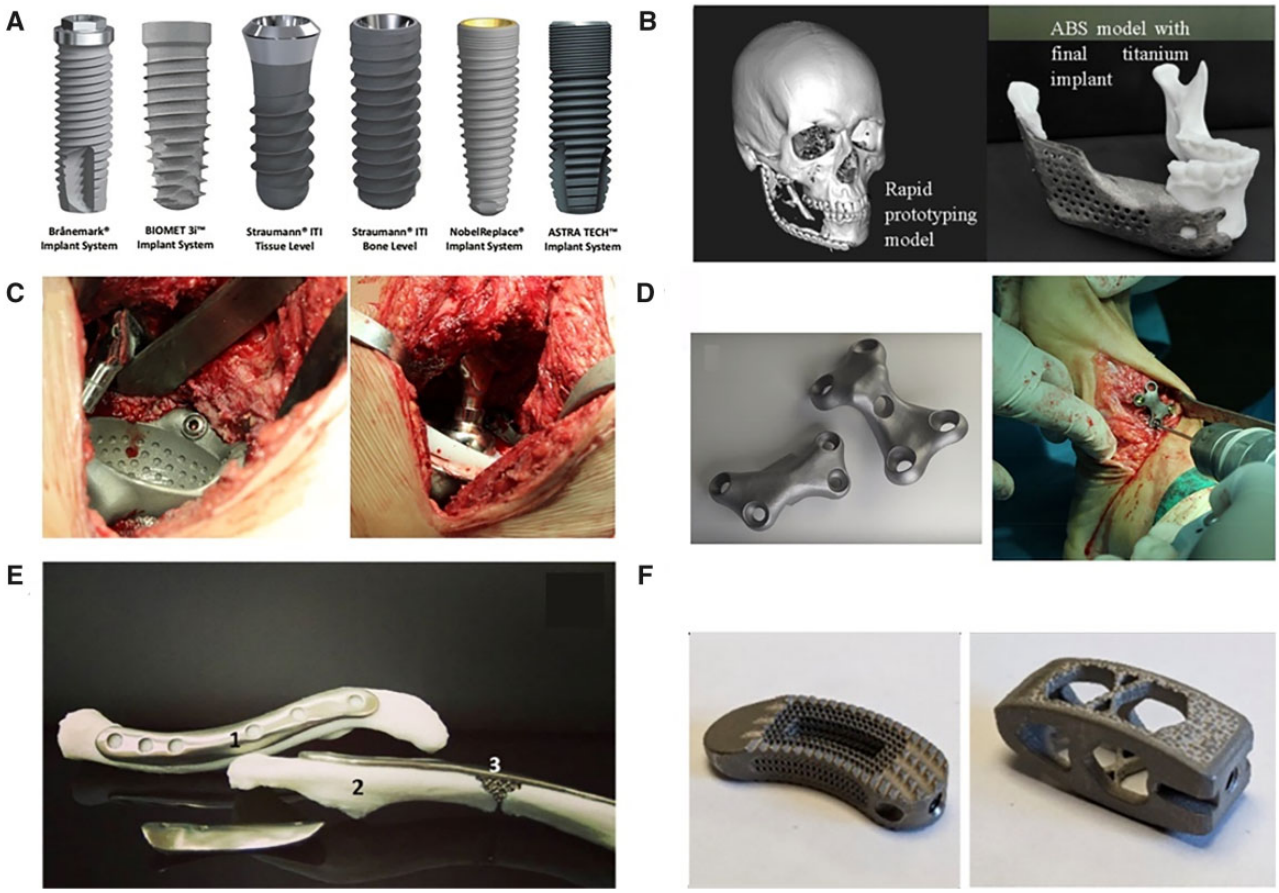

Figure 2. The clinical application of Ti-based implants [78–80]. (**A**: Commercially available dental implants. Reproduced with permission from Ref. [80] Copyright 2020 Japanese Society for Dental Materials and Devices. **B**: The anatomic design of the mandibular implant with a lattice structure. **C**: Hip replacement of Ti6Al4V implant using EBM technology; **D**: patient-specific Ti6Al4V implants in foot osteotomy; **E**: 3D printed Ti implant with lattice structured insert by TechMed Technion for clavicular reconstruction. Reproduced with permission from Ref. [78] Copyright 2018 Springer Nature. **F**: Activated Ti interbody cages. Reproduced with permission from Ref. [79] Copyright 2021 Springer Nature.).

More importantly, Ta is also used as coating material on account of good corrosion resistance. Several researches illustrated Ta provided high wettability and surface energy at bone-to-implant interface, facilitating favorable microenvironment for cell adhesion [92–95]. Wang *et al.* [96] provided a novel understanding on the molecular mechanism underlying the excellent biological performance of Ta coating of Ti implant under diabetic condition. Ta coating could promote the proliferation and osteogenic differentiation of osteoblast by suppressing ROS-mediated p38 pathway *in vitro*, and induced more new bones, enhancing osteointegration at bone-to-implant interfaces under diabetic sheep models.

Magnesium

Magnesium (Mg) is commonly known as a degradable metal for orthopedic use [97]. Therefore, the long-term side-effects of Mg implants could be minimized or avoided, and the released Mg ions may facilitate bone regeneration [98]. Another advantage is that Mg presents more comparable modulus to bone, which reduces the detrimental effects of stress shielding [99]. Somehow, it is difficult to fabricate Mg parts through 3D printing due to its highly reactive activity. The surface energy of raw Mg powders or wires increase and present a higher risk of reacting with atmospheric oxygen to enable combustion. An inert atmosphere is required to prevent exposure to oxygen. Selective laser melting, directed energy deposition and binder jetting are commonly used for the fabrication of Mg-based implants [100, 101]. Ideal Mg-based orthopedic fixators including plate, screw, pin, scaffold and ring, have strong initial mechanical strength to support the fractured bone in the early healing stages, and their proper degradation behavior match the healing process of the fractured bone [102–105].

Similar to Ti, Mg-based implants are demonstrated as clinical success especially for orthopedic bone screws. MgYReZr alloy screws (MAGNEZIX®) have been approved for clinical use since 2013 and extended to over 50 countries [106]. In 2015, Korea Food and Drug Administration has approved another MgCaZn screws for clinical use, in consideration of the complete healing performance of distal radius fracture after six months post-fixation [99, 107]. In China, pure Mg screws (purity: 99.99%) are widely used to repair head and neck factures with a lower rate of complication [108, 109].

Functional engineering strategies of metallic materials

Metallic implants are most commonly used for load-bearing implant applications. The modification strategies of metallic materials including suitable physicochemical properties (i.e. fatigue and wear resistance, modulus and density) and biological properties (i.e. biocompatibility, osteoconductivity and osteoinductivity), providing functionalized bone-to-implant interfaces, which achieve long-term stabilities [110–112]. In this section,

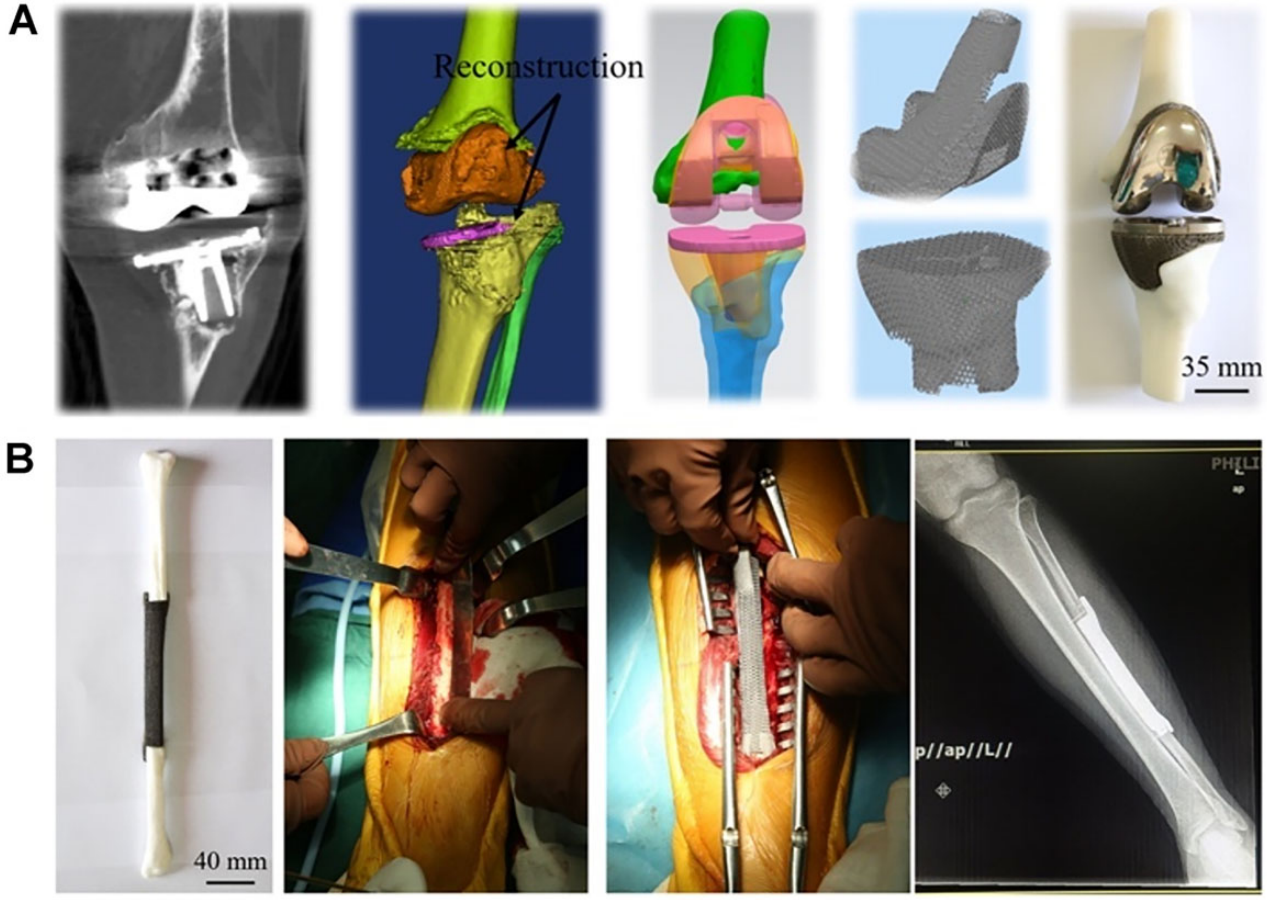

Figure 3. The clinical application for tantalum implants [92]. (**A**: EBM-fabricated ta lattice implants for hip reconstruction; **B**: EBM-fabricated ta fibula lattice implants.) reproduced with permission from Ref. [92] Copyright 2020 Spring Nature.

modification strategies of metallic-based implants based on post-printing treatment, physicochemical modification and surface coating are outlined (Table 2) [95, 96, 113–120].

Post-printing treatment

Three-dimensional printed metallic implants exhibited different microstructures with improved physical properties when compared with those fabricated by traditional casting or milling methods. However, during printing process of EBM or SLM, the recurrent melting and cooling of metal powders easily result in poor surface finish, high porosity and the formation of residual stress, which affects stability or accuracy of desired objects [121, 122]. Apart from pre-heating feedstock powder and substrate before printing for reducing the residual stress, the post-treatments after printing are necessary to improve physical properties (especially for fatigue performance) of metallic implants [123]. Post sintering or heating treatment for optimizing microstructure is required to improve properties of fabricated object. Mierzejewska *et al.* [38] demonstrated the strength and Young's modulus of Ti6Al4V alloy fabricated by direct metal laser sintering (DMLS) before heat treatment was higher, when compared with cast and forged samples. Importantly, a decrease in hardness of DMLS samples were observed after heat treatment, indicating the significant change of microstructures. Another research by Jaber *et al.* [124] proved that the tensile strength/ductility of the Ti6Al4V alloy produced by SLM was determined by the post-heat treatment. The best mechanical properties were obtained by heat treatment at 850°C followed by cooling in the furnace, which increased ductility from 8% to 13%. The improvements in the mechanical properties after post heat-treatment are mainly due to the elimination of thermal stresses and the changes of microstructures [111, 125].

Physical and chemical modification

Apart from heat treatment that has been proved to especially improve mechanical properties, physical and/or chemical modification could provide macro/micro/nano-scale surface roughness that enhancing both physicochemical and biological properties of metallic implants [126].

In terms of 3D solid Ti implants (i.e. dental implants, screws and nails), mechanical modification has been used to improve surface roughness, hardness, wear resistance, corrosion resistance and wettability. Peening including shot peening, ultrasonic impact peening and laser shock peening have been widely perceived as simple and effective post-processing methods to eliminate residual stresses in the lateral direction, effectively increasing the fatigue strength of 3D printed objects [127]. Surface mechanical attrition treatment (SMAT) is one of effective methods that obtain a nanostructured layer in the treated surface of metals, which could significantly improve the friction and wear resistance of metallic materials (Fig. 4A) [122, 128, 129]. The basic principle of SMAT is the modification on surface layer of a bulk metallic materials, such as Fe, stainless steel, Ti, Co–Cr and Mg, though repeatedly impacted by multidirectional flying balls (diameter: 1–10 mm) [128, 130]. Several studies have confirmed

Table 2. Representative examples of modification strategies on metallic implants

Substrate	Coating method	Loading material	Effects	Ref.
Ti–6Al–4V disc	Alkali-treatment; Dopamine grafting	Gentamicin (GS)/agarose	The released GS from composite hydrogel layer were able to efficiently inhibit bacterial activity.	[113]
Ti disc	Biomimetic deposition	CS		[114]
Ti mesh	Anodization	Sr/CaPs	Sr-droped CaPs/Ti mesh exhibited the higher gene expressions related to osteogenesis, and resulted in new bone formation *in vivo*.	[115]
Ti disc	Microarc oxidization	antimiR138/CS/HA	Ti with functionalized layer enhanced the osteogenesis of MSCs *in vitro*, and promoted osteointegration in rat model *in vivo*	[119]
Ti disc	Biomimetic deposition	Pac-525/PLGA microspheres/HLA	Pac@PLGA/HA coated Ti exhibited a strong cytotoxicity to both Gram-negative bacteria and Gram-positive bacteria	[118]
Ti disc	Electrophoretic deposition	Double layers: Sr/HLA; Vancomycin/CS/Gel	The drug released was more sufficient, providing a more significant anti-bacterial activity for a drug concentration of 2.74 μg.	[120]
Ti scaffold	Biomimetic deposition	BMP-loaded silica/CS	BMP-loaded silica/chitosan scaffolds exhibited the highest e bone regeneration fraction (36%) at 4 weeks	[116]
Ta scaffold	Electrostatic self-assembly	DOX/HEMA-MMA-MAA	The release of DOX from the functionalized Ta implants was up to 1 month, and inhibited the proliferation of chondrosarcoma cells	[117]
Ti–6Al–4V disc	Vacuum plasma spraying	Porous Ta	Porous Ta coating s promoted BMSCs adhesion, proliferation, osteogenesis *in vitro*, and promoted osseointegration, leading more bone formation *in vivo*	[95]
Ti scaffolds	Chemical vapor deposition	Porous Ta	Porous Ta coating promoted osteointegration by suppressing the ROS-mediated p38 pathway under diabetic condition.	[96]

CS, chitosan; HLA, hyaluronic acid; DOX, doxorubicin; HEMA-MMA-MAA, hydroxylethyl methacrylate-methyl methacrylate-methylacrylic acid; BMSCs, bone mesenchymal stem cells.

SMAT-treated metals promoted the focal adhesion, proliferation and differentiation of MSCs [129, 131, 132].

Grit-blasting or sand-blasting/acid-etching (SLA) are commonly used physical modification methods for Ti-based materials (Fig. 4B). The macroroughness fabricated by grit-blasting is interspersed with irregularly shaped micropores while acid treatment is a simple method to provide micro/nano-structure of Ti implant [133]. Meanwhile, the acid-treated surface is usually followed by other modification strategies, including hydrothermal treatment [134]. Usually, strong acid solutions, such as HNO_3/HF mixture or HCl/H_2SO_4 mixture are used to remove the oxide layer and some underlying material, as well as the contaminants on the surface of Ti implants, resulting in homogenous irregularities and increasing functional surface area and roughness [135]. TiZr alloy implants with the SLActive® surface provided a long-term safe and reliable alternative to dental implants (Ti, Grade IV) [136]. The increased wettability with a micro-rough surface treated by SLA and plasma treatment could reduce M1 macrophages recruitment that were responsible for chronic inflammation, and result in the high expression level of anti-inflammatory activated macrophages (M2), which synergistically yield a microenvironment suitable to reduce healing time and enhance osseointegration [137]. In summary, compared with smooth surface, micro-topographies (surface area roughness of 1–2 μm) by SLA have been proved as an improvement in osseointegration, accelerating cell processes and shortening healing time. More importantly, metallic implants are commonly modified by sand-blasting and acid-etching to reach at commercial level before clinical use.

Physical vapor deposition (PVD) and ion implantation are another two prevalent methods to improve the properties of anti-corrosion and fatigue resistance, which are expected to significantly enhance the long-term safety of Ti implants [138–140].

Besides, the activation of 3D solid metallic implants can be achieved by multiple chemical technologies including anodic oxidation, alkaline heated-treatment, plasma oxidation, which can alter the surface topography of metallic implants and benefit bone healing [141, 142]. Alkaline heated-treatment can obtain unique surface topography and provide Ti–OH sites of Ti implants, facilitating protein adsorption and reducing bacterial adhesion [143].

The increasing hydrophilicity of Ti implants, especially dental implants, can shorten the healing period by enhancing the early osteointegration while inhibiting hydrophobic bacterial adhesion [144, 145]. Usually, the implants have to be hydroxylated, rinsed under nitrogen protection, and stored in an isotonic saline solution until their use. Plasma oxidation can also be used to increase the wettability of the Ti surface [146]. Moreover, the hydrophilic surface by chemical modification has a favorable affinity to proteins and is capable to maintain the proper conformation and function of the absorbed proteins, and subsequentially encourage cell adhering onto the implant, as well as promote osteoblast differentiation [147, 148].

Micro-arc oxidation (MAO), also named as plasma electrolytic oxidation, generates a homogeneous oxide layer in the plasma state that is fabricated by applying an extremely high voltage in a suitable electrolyte (Fig. 4G) [149]. It is a well-developed method which could not only provide micro/submicron-roughness

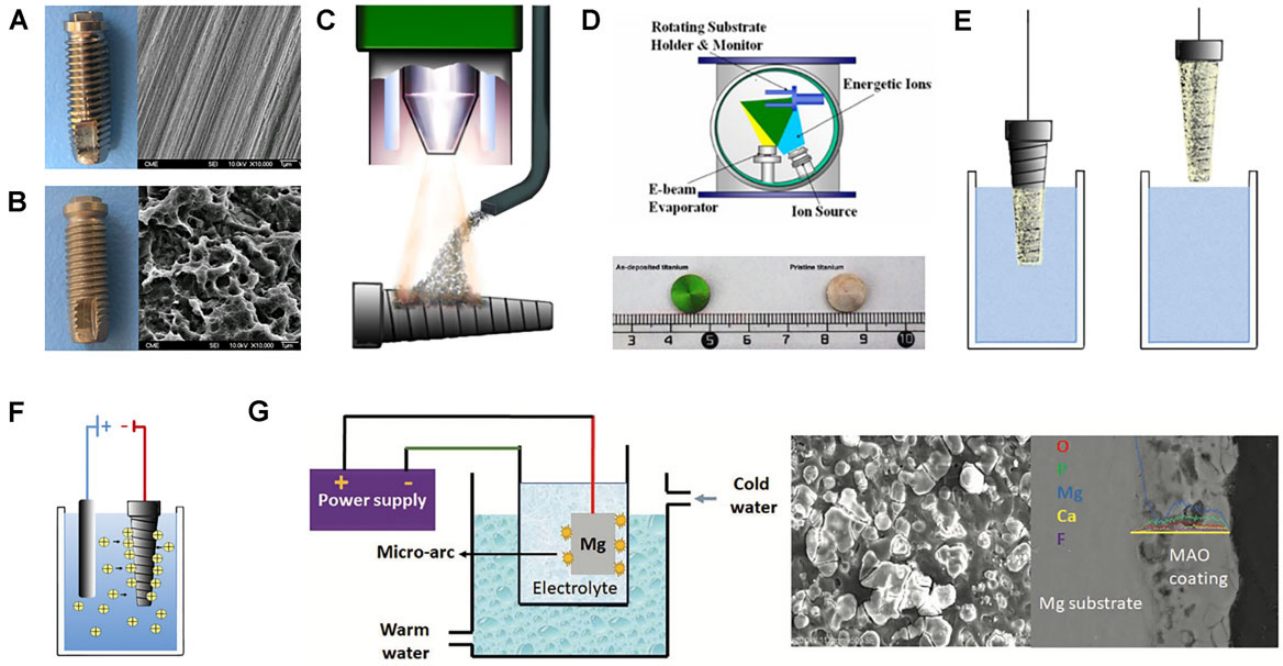

Figure 4. Representative examples of surface modification strategies [107, 153]. (**A**: Machined surface of Ti implant. **B**: Sand-blasted and then acid-etched implant. **C**: Plasma-spraying, to form an oxide film on the Ti surface and allows ceramic coating formation. **D**: IBAD, able to prepare bio-coatings with considerably higher adhesion strength. **E**: Dipping, sol–gel and biomimetic coating, known as simple operation and cost-effective methods. **F**: EPD, utilizing two electrodes to induce the migration of particles in solution towards the surface to be coated. Reproduced with permission from Ref. [107] Copyright 2020 John Wiley and Son. **G**: MAO treatment of Mg-based metals to form a CaPs coating. Reproduced with permission from Ref. [153] Copyright 2017 American Chemical Society).

(1–20 μm) to maximize the interlocking between mineralized bone and implant surface, but also produce a porous and firmly adhesive coating on Ti surface [110, 150]. After MAO has been performed, hydrothermal treatments are usually conducted to improve its apatite-inducing ability [151]. In addition, various kinds of bioactive elements, such as Ca, P, Si and Ag, can be incorporated into fabricated layer formed by MAO to enhance the biological performance both in *vitro* and in *vivo*.

Surface coating

Various surface modification methods for solid metallic implants we mentioned above could provide bioactive sites on the surface that facilitate other substances to be incorporated, as well as provide multiple functions (i.e. anti-corrosion, osteogenesis, anti-bacteria and anti-inflammatory) [152, 153].

Calcium-based coating

In term of surface coating for metal-based implants, inorganic components, including Ca, Si, Ag or Mg, which are involved in bone metabolism and can favor bone homeostasis and augment mineralization and angiogenesis [154]. Among them, calcium-based depositions, which often refer to calcium phosphates (CaPs), are main modification strategy to form strong fixation at the bone-to-implant interface. Numerous researches have demonstrated HA layer coated on Ti implants could significantly promote osteogenic differentiation of MSCs, and induce new bone formation for bone repair *in vivo* [155, 156]. Chen *et al.* [157] gave a statement that HA coating could improve the postoperative mean Harris hip score, reduce the incidence of thigh pain and the incidence of femoral osteolysis in hip arthroplasty. More clinical studies coating demonstrated dental implants with HA coating exhibited high survival rate (97–98%) in more than 5-year follow-up studies [158, 159]. Moreover, due to the porous structures of mineral layer, bioactive molecules/antibiotics/drugs could be incorporated into CaPs layers to achieve both enhanced osteoinductivity and antibacterial effect. However, surface modification technologies are quite different between solid metal implants and porous metal scaffolds as we mention above. Therefore, we take Ti-based solid/porous implants as example, several representative Ca-based coating methods will be introduced in this section (Table 3) [160–172].

In term of solid Ti implants, CaPs deposition can be achieved by biomimetic precipitation, electrochemical deposition, MAO, plasma spray, sol–gel and hydrothermal deposition.

The plasma spraying deposition on metallic surface is one of physical modification methods for HA or calcium silicate coating (Fig. 4C). The molten particles are sprayed on the surface of metallic substrates at high temperature to augment their wear and corrosion resistance and bioactivity [173, 174].

Ion-beam assisted deposition (IBAD) is a vacuum deposition process based on the combination of ion-beam bombardment and PVD (Fig. 4D) [175, 176]. IBAD has the ability to prepare bio-coatings with considerably higher adhesion strength as compared with traditional coating methods. The high adhesion strength is the result of interaction between the substrate and coating atoms, assisted by ion bombardment [169, 176].

Solution-deposited biomimetic coating refers to mineral layer is nucleated and grown on the Ti substrate in solution containing Ca^{2+} (Fig. 4E). Usually, Ti substrates are firstly alkali-treated to provide Ti–O sites and immersed into Dulbecco's phosphate-buffered saline solution under physiological conditions [177]. Biomimetic coating is a cost-effective and environment-friendly method with simple operation. Another advantage of this method is the ability to incorporate bioactive molecules that can be co-precipitated with the inorganic components [164, 172, 177, 178].

Table 3. Overview of bioceramic coating methods

Methods	Description	Parameter	Thickness	Advantage	Limitation	Ref.
Electrochemical deposition (ED)	Charged particles in a dispersion are migrated under electrical field towards the substrate electrode	Solution: NaH_2PO_3 (6 mM)/Ca $(NO_3)_2$ (10 mM) Electric current density: 20 mA/cm^2 Temperature: 30–90°C (20 min)	50–500 μm	Simple operation; cost-effective; high deposition rate	Low adhesion strength cracking of the coating	[160, 161, 165]
Plasma spray	Molten HA particles are sprayed on the surface of metal substrate at high temperature	Plasma gas/argon gas: 50 l/min; electric current: 600 A	<20 μm	Highly crystallized HA with fine microstructure	Low adhesion strength; uncontrollable surface morphology	[160, 166]
Ion-beam assisted deposition (IBAD)	Vacuum deposition process based on ion-beam bombardment and PVD	Chamber pressure: 3×10^{-4} Pa Voltage of electron beam evaporator: 8.5 kV; electric current: 0.1 A	500 nm	Strong adhesion strength Thin coating	Expensive device	[167–169]
Acid/alkali-heat treatment+ Biomimetic deposition	Acids help to clean the surface of metals, followed by alkali-heat treatment to provide Ti–OH sites	$HCl:H_2SO_4:H_2O$ = 1:1:2 (30 min); 1 M NaOH (140°C, 6 h) Deposition: DPBS solution with 100 mg/l $CaCl_2$ (24 h)	<30 μm	Simple operation; cost-effective; incorporation of biologically active molecules	Low adhesion strength; long time of coating process (few days)	[164, 170]
Micro-arc oxidation (MAO)	Electrochemical surface treatment technique for generating oxide coatings on metals	Electrolyte: 0.2 M $C_4H_6CaO_4$/0.04 M $C_3H_7Na_2O_6P{\cdot}5H_2O$ Eclectic current: 0.3 A Pulsation frequency: 800 Hz; Oxidation time: 5 min	200 μm	Homogenous oxide film layer	Microcracks	[18, 171]
Sol–gel coating	Produce almost any single- or multi-component oxide layer on metals	Preparation of HA sol: Ca/P precursors; Dip coating/spin coating	<1 μm	Low coating temperature; cost-effective; thin coating	Low wear-resistance; difficulty of porosity control	[162]
Pulsed laser deposition (PLD)	The high-power laser provides the energy source to melt, vaporize and deposit thin films	Chamber pressure: 10^{-4}–10^{-1} Torr; Laser wavelength: 248 nm Pulsation frequency: 10 Hz	0.05–5 μm	Low deposition temperature Highly crystalline HA	Texturing step before coating; splashing nanoparticles on the film	[163, 172]

In summary, more clinical studies demonstrated dental implants with HA coating exhibited high survival rate (97–98%) in more than 5-year follow-up studies [158, 159]. Although various surface modification methods have been introduced above, only a limited number of solid implant modification technologies have been applied for clinical trials and further commercialization, while the vast majority of coatings are still in the preclinical phase.

Unlike the solid implants, porous metallic implants (i.e. cages and scaffolds) preferred a distance osteogenesis pattern which bone grows from the periphery towards the inner scaffold [179]. Thus, the remodeling of in-growth bone needs a challenging modification strategy of internal surface. However, Common-used methods for CaPs coating including plasma spraying, IBAD deposition and electrospray deposition are not appliable for porous Ti implants, while biomimetic coating is also difficult to form uniform HA layer within internal surface of porous scaffolds. Xiu *et al.* [180] fabricated micro/nano-scale TiO_2 coatings containing CaPs on both inner surface (4.4 μm) and outer surface (4.8 μm) of 3D printed micro-porous scaffolds, which exhibited a high efficiency in the enhancement of osteointegration of porous TiAl64 via optimizing the patterns of bone in-growth and bone/implant interlocking (Fig. 5A). Li *et al.* [181] improved biomimetic coating of HA on porous Ti6Al4V scaffolds by the introduction of polydopamine films formed by self-polymerization. The uniform HA coating on entire pore structure enhanced proliferation and osteogenic differentiation of MC3T3-E1 cells *in vitro* and improved osteointegration after implantation *in vivo* (Fig. 5B).

Apart from common-used CaPs coating, calcium carbonates ($CaCO_3$) could be fabricated at the hydrogel–Ti interfaces by carbon oxide (CO_2) diffusion [182]. The fabricated $CaCO_3$ mineral layer grew inside hydrogels and wrapped up their polymer networks to provide a strong bonding between hydrogel and Ti substrate. Inspired by *in situ* mineralization method above, our group developed novel modification strategy for porous implants [183]. In detail, UV-responsive methacrylic anhydride chitosan (CSMA) was filled into 3D printed porous Ti implant, followed by the introduction of $CaCl_2$ and *in situ* mineralization by CO_2 diffusion within hydrogel, which could release Ca^{2+} continuously, resulting in promoted proliferation and osteogenesis of MSCs *in vitro* (Fig. 5C).

Polymeric coating

Polymeric coating layer which present highly versatile and flexible structures is another promising strategy for metallic functional modification to improve cell bioactivities [184].

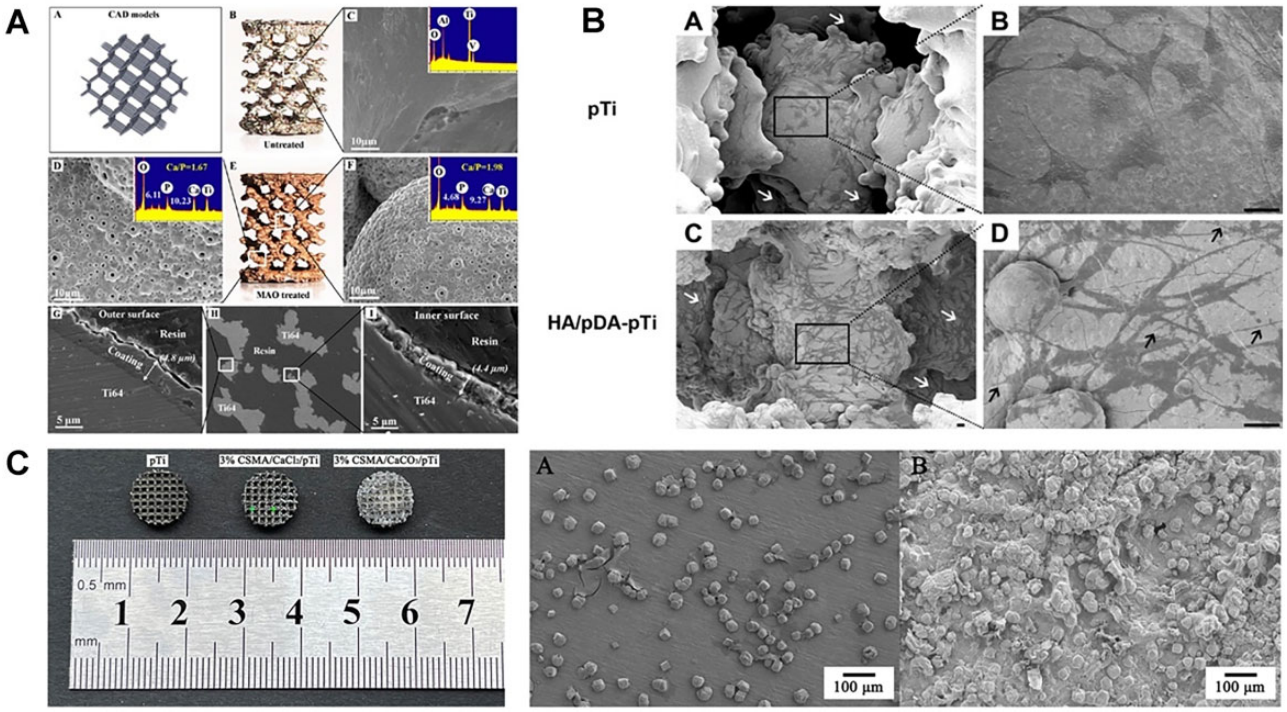

Figure 5. Ca-based coating for the 3D printed porous Ti-based implants (especially for internal surface) [180, 181, 183]. (**A**: the porous Ti6Al4V scaffold after MAO treatment displayed homogeneous layer of microporous titanium oxides coating containing a significant amount of Ca and P. The thickness of coating at the inner and outer surface were 4.4 and 4.8 μm. Reproduced with permission from Ref. [180] Copyright 2016 American Chemical Society. **B**: HA coating was clearly loaded on the inner surfaces of the scaffold with pre-deposited pDA film. Cells were favorably adhered on the inner surfaces (white arrows) with lamellipodia extensions (black arrow) after HA/pDA immobilization. Reproduced with permission from Ref. [181] Copyright 2020 American Chemical Society. **C**: The observation of 3D printed porous titanium filled with mineralized chitosan hydrogel. $CaCO_3$ mineral layer grew inside hydrogels and wrapped up their polymer networks to provide a strong bonding between hydrogel and porous Ti scaffold.)

Common-used fabrication methods (i.e. electrophoretic deposition (EPD), layer-by-layer deposition and electrospinning) and several representative examples are introduced in this section.

Biocompatible natural polymeric coatings are mainly inspired by the inherent structure of human bone to mimic the ECM, which significantly promote biological performance of metallic implants [118, 120]. Chitosan (CS), Alginate (Alg) and collagen type I (Col I) are widely used as modification materials for metallic implants due to their favorable biocompatibility, biodegradability and antibacterial properties. Compared with CaPs coating, the main effort for natural polymeric coatings is to easily load osteogenic particles or drugs along with nanoparticles (i.e. CaPs, silver, graphene oxide or zinc oxide) within orthopedic implants, which improve the bioactivity and cell attachment ability (Fig. 6) [185].

EPD is an effective method for the deposition of charged materials (i.e. chitosan) on the surface of metals. EPD is achieved by the movement of charged particles in a liquid dispersion towards the working electrode. After the deposition, a heat treatment step is normally needed to further densify the deposit and to eliminate the porosity, which could improve the mechanical properties of polymeric-based coating. The surface interactions and EPD parameters (i.e. applied voltage, deposition time and distance between electrodes) play a vital role in the coating efficiency. The cationic nature and high charge density of chitosan (CS) make it ideal for use in EPD. More importantly, CS coatings containing other polymers, nanoparticles and/or antibiotic drugs synergistically impart multifunctionality to the implant surface. Qi *et al.* [186] demonstrated gelatin nanospheres with dexamethasone (DEX) were distributed homogeneously onto chitosan-coated Ti substrate by using EPD technology, which could inhibit inflammation and stimulate osteogenesis with the help of favorable DEX release profile.

Layer-by-layer deposition (LBL) is another promising method for polymeric coating on solid substrate. The basic principle of LBL is to form integrated polyelectrolyte films (PEM) by the alteration of polymeric materials with charged sites or functional groups on their surface. The stability of the coating is determined by the static-attractive force, the strength of hydrogen bonds and covalent bonding [187]. The multilayer films could control loading and release profiles of bioactive molecules, including growth factors, drugs and DNA/RNA molecules [188–190]. Wu *et al.* [119] prepared PEMs by LBL approach with a chitosan-miRNA (CS/antimiR-138) complex and sodium hyaluronate (SH) on microarc-oxidized (MAO) Ti surfaces. The sustained release of CS/antimiR-138 from PEM-functionalized microporous Ti implant could enhance osteogenesis of MSCs *in vitro* and promoted osteointegration in rat model *in vivo*. Chitosan-decorated BSA nanoparticles (CBSA-Ns) and oxide sodium alginate (OSA) were coated on Ti scaffolds by electrostatic interaction. The synergistic effect of the hierarchical structure of assembled films and immobilized BMP2 on the scaffold improved osteogenesis of BMSCs, as well as exhibiting good antibacterial activity when incorporating vancomycin on OSA films [191]. Besides, silver nanoparticles-loaded CS-heparin PEMs were constructed on alkali-heat treated Ti substrates via LbL self-assembly technology, which promoted osteointegration and reduced microbial infection [192].

The physicochemical and biological properties of synthetic polymeric coatings can be tailored by the constituent monomers or polymers. Multiple types of synthetic polymeric coatings including poly(D,L-lactic-co-glycolic acid) (PLGA), PCL, polyvinyl

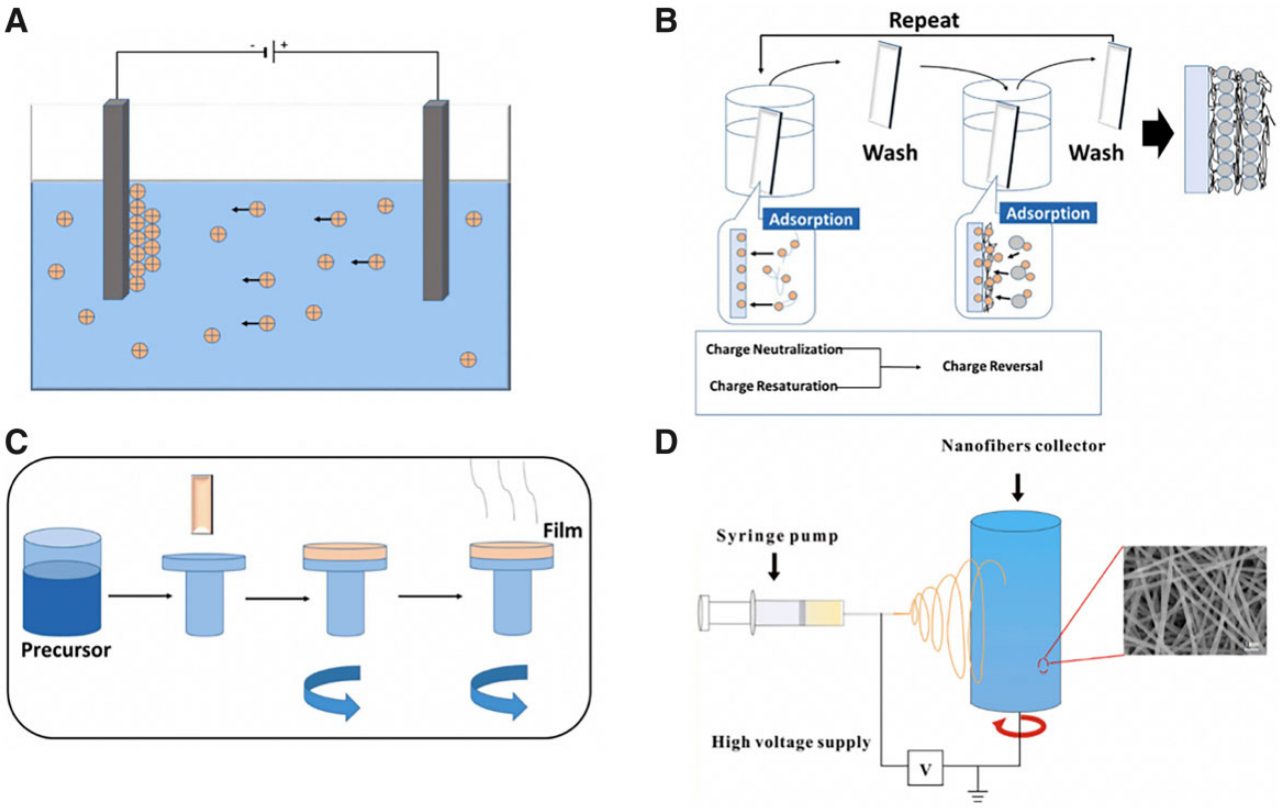

Figure 6. Polymeric coating strategies on metallic implants [185]. (**A**: EPD; B: layer-by-layer assembly; **C**: spinning coating; **D**: electrospinning) reproduced with permission from Ref. [185] Copyright 2021 Elsevier).

alcohol (PVA) and polyethylene glycol (PEG) are frequently used as coatings for metallic implants.

Electrospinning is a promising processing technique that utilizes electrical forces to produce ultrafine polymeric fibers using polymer solutions, which can form polymeric layers (especially synthetic polymers) on solid Ti implants (Fig. 6D). Coaxial doxycycline (Doxy)-doped PCL/PVA nano-fibers were directly deposited on the Ti implant surface by using electrospinning. Doxy-doped nano-fibers coating effectively inhibited bacterial infection and enhanced osseointegration in an infected (*Staphylococcus aureus*) tibia implantation rat model [193]. Biodegradable PLGA coatings with vancomycin through electrospinning method were deposited on the surface of Ti, which exhibited a synergetic effect of antibacteria and osteogenesis *in vitro* and *in vivo* [194]. Lee *et al.* [195] utilized PCL as a polymer coating to improve the initial corrosion resistance of biodegradable Mg. In detail, PEO was performed to increase adhesion between the polymer and the 3D printed Mg. The improved corrosion resistance of the PCL coating resulted in the release of a lower level of magnesium ions than that in the PEO group, which can lead to r more bone formation. Stable PCL nano-fibrous layer on AZ31 magnesium alloy could also be fabricated by using electrospinning which utilizes electrical forces to produce ultrafine polymeric fibers using polymer solutions [196]. The presence of coating can be used to tailor the degradation, as well as improving cell viability, adhesion and proliferation.

Functional engineering strategies of ceramic materials for hard tissue repairment

Ceramics, especially bioceramics, are attracted increasing attention for the application of bone regeneration due to their inherent biocompatibility and bioactivity [197–199]. Traditionally, porous ceramic scaffolds are fabricated by technologies such as freezing casting, gas forming, salt leaching and phase separation [200–203]. The development of ceramic-based printing technology overcomes the limitation of conventional methods, which mostly lack of the precise control of pore structures (i.e. pore size, porosity, inner pore connectivity) [204]. At present, the most commonly used printing technologies for ceramic includes SL, SLS, materials extrusion and BJ. As the main component and self-standing material, the printed bioceramic construct usually needs a sintering process for post-treatment to improve mechanical strength, which brings obvious difficulties to incorporate heat-liable drugs or growth factors in the printing process [205]. Due to the high-performance requirements for printing materials, only a few bioceramics are suitable for 3D printing in bone tissue engineering. Thus, representative bioceramics for 3D printing and their modification strategies as well as applications for hard tissue regeneration will be introduced in this section.

Printable ceramic materials

Calcium phosphates

HA is one of most widely used bioceramics in bone tissue engineering, which is main inorganic component of human natural bone, leading to the affinity for the adhesion and proliferation of osteocytes [206, 207]. More importantly, HA can stimulate endogenous expression of osteogenic growth factors of BMSCs via multiple signal pathways [208–210]. However, the poor mechanical properties (high brittleness/low strength) and slow degradation rate of HA are main challenges in clinical translation for bone substitutes, especially for load-bearing applications [204]. Apart from HA, tricalcium phosphate (TCP) ($Ca_3(PO_4)_2$) is another

well-studied 3D printed bioceramic, with α-phase and β-phase. β-TCP has the crystal structure of a rhombohedral space group, exhibiting more stable structure and higher biodegradation rate than those of α-TCP [211, 212]. Compared with HA, β-TCP has a faster degradation rate and higher solubility. It is proved that the release of Ca^{2+} from β-TCP particles could significantly promoting osteogenesis of BMSCs *in vitro* as well as enhancing new bone formation *in vivo* [213]. Although β-TCP exhibits better bending strength and fracture toughness than HA, it is hardly used alone for load-bearing implants [213]. To solve above problems, biphasic calcium phosphate (BCP), composing HA and β-TCP in a specific ratio, is developed. To optimize the proportion, BCP scaffolds with different ratios of HA and β-TCP were prepared by ZPrinter® 250 printer, the results demonstrated BCP composed of 40 wt% HA and 60 wt% exhibited favorable osteogenic differentiation of BMSCs [214]. Besides, Liu *et al.* [215] utilized DLP technology to fabricate BCP (HA:β-TCP = 4:6) scaffolds with macro-pore sizes and confirmed scaffolds with 800 mm pore size are superior for initial bone formation and maturation in a rabbit calvarial defect. Craniofacial defect, especially for intracranial hemorrhage or infarction, need precisely repair and reconstruction, otherwise, secondary infection or inappropriate substitute implantation could result abnormal swell ratio of brain tissue, which is threaten to life. Compared with Ti mesh and PEEK, bioceramic had a similar chemical composition natural bone. In clinic, 3D customized α-TCP implants were used for bone replacement in frontal-orbital region of human skull [216].

Calcium silicate (Ca–Si/CSi)

$CaSiO_3$ (Ca–Si/CSi) is a kind of promising materials with superior sealing ability and bioactivity in bone tissue engineering [217]. It is proved that Ca–Si cement can form a HA layer on the surface of scaffolds after immersion in simulated body fluid (SBF), which are benefit for enhancing bonding between scaffold and the surrounding bone tissue [218]. Moreover, the release of Si^{2+} could up-regulate the expression level of collagen type I (CoI I), fibronectin (FN) and osteocalcin (OCN) of multiple stem cells via MAPK/ERK and MAPK/p38 signaling pathway [219]. However, the high dissolution rate of Ca–Si ceramics easily results in a high pH value, probably affects cell activities. To solve this problem, the addition of magnesium ion (Mg^{2+}) is found to control the degradation rate of Ca–Si cements and improve bone regeneration [220, 221]. Another important modification strategy of Ca–Si biocaremics is bifunctional Ca–Si scaffolds with photothermal functionalization for bone tumor therapy, which will be introduced in next section.

Bioactive glass (BG)

BGs represent a subgroup of ceramic materials, such as silicate bioactive (45S5 Bioglass®), borate bioactive glass and phosphate bioactive glass. We take 45S5 Bioglass® as an example, which is well studied for biomedical applications [222, 223]. Similar to Ca–Si ceramics, 45S5 glass are able to form a carbonate-substituted HA on glass surface in contact with surrounding body fluids, which is benefit for adsorption of growth factors and recruitment of osteoprogenitor cells [224]. As implantation particles or granules, 45S5 glass could effectively promote bone formation, whereas as porous scaffolds, several limitations need to be addressed [225, 226]. Firstly, crystallization of bioglass occurs close to glass transition (Tg) and impedes sintering by preventing viscous flow. Consequently, bioglass scaffolds are at least partially crystalline and often has poor mechanical properties. Another limitation is the slow degradation rate of bioglass, which cannot match the periods of bone formation [227]. BG granules also can be used as additive materials for large-scale reconstruction. Aitasalo *et al.* [228] designed patient-specific composite implant using resin matrix materials as supporting framework, which was filled with a bioactive glass. No infection or loosen of the implant was found in a 4-year follow-up, indicating the safety and osteoconductivity of bioactive glass reinforced scaffold.

Compared with conventional BG, the development of mesoporous bioglass (MBG) is attracted more attention due to the well-order mesoporous structure. The high specific surface area and large pore volume of MBG is favorable for an enhanced bone-forming ability [229, 230]. Zhang *et al.* [231] fabricated strontium-containing MBG scaffolds with controlled architecture and enhanced mechanical strength. Additionally, calcium sulfate hydrate (CSH)/MBG scaffolds were successfully fabricated using an extrusion-based printer, which had a regular and uniform macroporous structure and high porosity. CSH/MBG scaffolds could promote the adhesion, proliferation, ALP activity and osteogenesis-related gene expression of BMSCs, as well as exhibiting favorable new bone formation in calvarial defects [232].

Functional engineering strategies of ceramic-based implants

Currently, most bioceramic materials have achieved clinical translation in the form of micro/nano particles, cements and scaffolds [204]. In term of identical bioceramic material, 3D design of a bioceramic implants offer anchoring sites to cell extensions, induce cell adhesion and further facilitate cell network formation and tissue ingrowth [233–235]. Thus, the modifications of 3D printed bioceramic scaffolds provide multiple functions, which can synergistically improve the effect of bone regeneration.

Structural modification

The geometrical features of porous scaffolds, including surface curvature, pore shape, pore size and porosity have great impacts on mechanical and biological performances [236–238]. Intrinsically, pore structures are highly related to mechanical behavior under variable loading conditions. Although 3D printing technologies can control identical pore size and porosity of bioceramic implants, the structural design and optimization of 3D printed ceramic scaffold is primary to solve the long-term existing issue of insufficient bone formation in the inner part of large-size scaffolds [239, 240]. Porous ceramic scaffolds are often designed with a hierarchical structure in consist of the macro-/micro- and nanostructures that facilitate bone tissue ingrowth. Generally, porous microstructures like regular strut-based structures arranged at a particular angle and pattern are used for implant and scaffold design [241]. Some specific design of structures for bioceramic implants are much more beneficial for bone regeneration.

Pore shape and orientation are fundamental factors relating to mechanical properties of porous implants [240, 241]. Honeycomb-pore CSi–BG scaffolds exhibited markedly higher compressive strength (~88 MPa) than the scaffolds with other pore shapes (rectangular, parallelogram and Archimedean chord) [242]. The high strength of honeycomb pore structure was mainly attributed to its anisotropic structure and double strut wall architecture, which was widely presented in the biological systems, and had been reported to be responsible for the stability of their macroscopic architectures. Another research demonstrated that hexagonal shapes of HA scaffolds exhibited the highest compressive strength at any given porosity due to increasing contact area

between printed layers, thereby resulting in a highly anisotropic architecture (Fig. 7A) [243].

In addition to mechanical properties, surface area of pore structure has an influence on cell behaviors. Bose *et al.* [244] explored topographical features with different surface area of 3D printed TCP cylindrical scaffolds, which preferably simulated personalized bone implants that could match patient's defect site-specificity to aid bone healing (Fig. 7B). Wu *et al.* [245] prepared hollow-struts-packed (HSP) bioceramic scaffolds with designed macropores and multi-oriented hollow channels via a modified coaxial 3D printing strategy. Due to the larger surface area and higher porosity of bioceramic scaffolds with unique hollow-struts structures, such bone scaffolds significantly possessed a faster degradation rate, promoting the new bone formation in the center area (Fig. 7C).

Furthermore, inspired by the hierarchical structure and functions of bone, the haversian bone-mimicking bioceramics-based multicellular delivery system was designed and fabricated by DLP technology. Haversian canals could disperse the compressive and the flexural stress, which prevented the exceedingly early failure due to the local fracture (Fig. 7D). Also, the unique structure of haversian canals facilitated nutrition delivery, provided proper microenvironment to promote the osteogenic and angiogenic differentiation of cells, as well as enhanced both new bone and blood vessels formation *in vivo* [246].

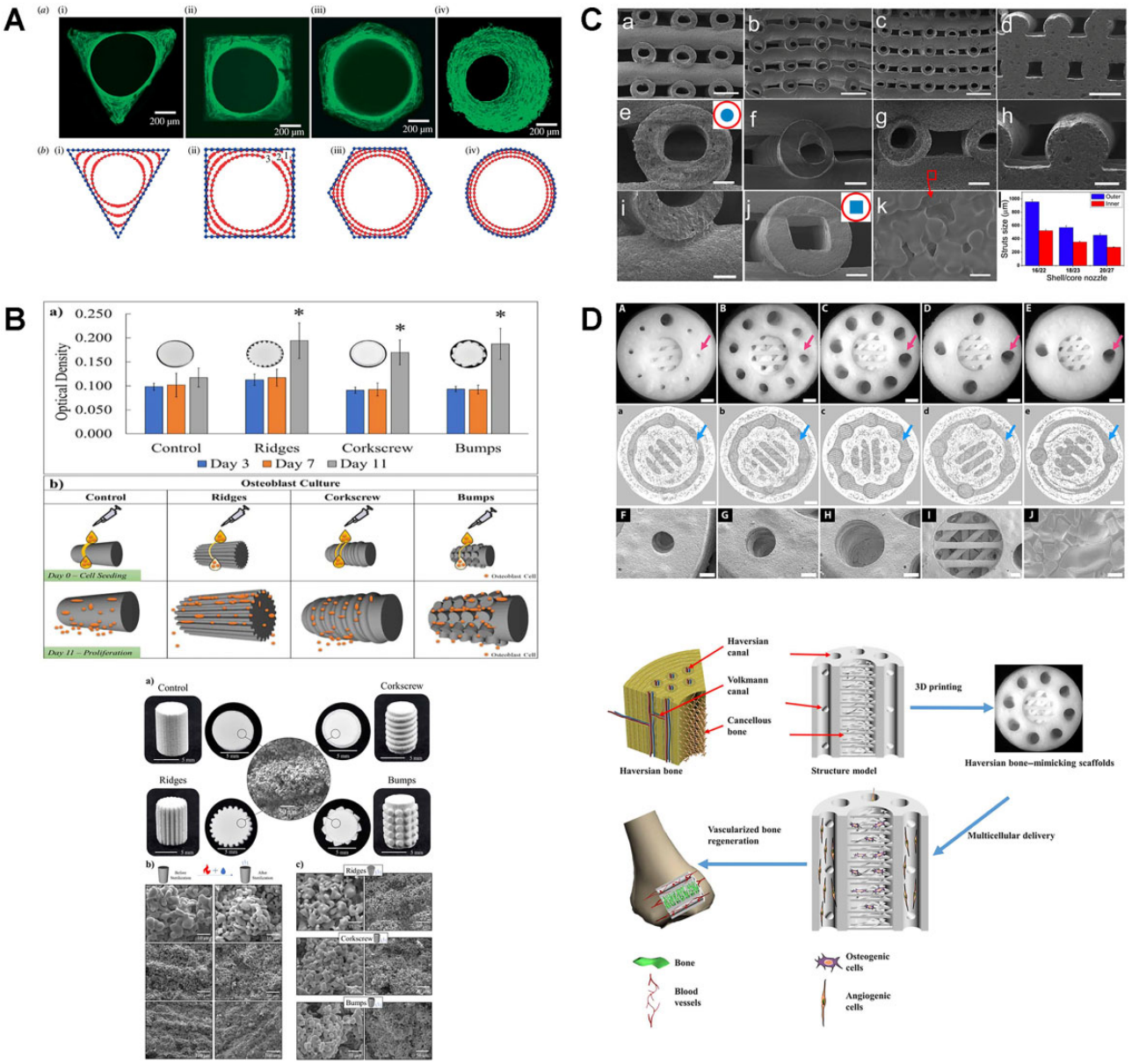

Figure 7. Representative examples of structural modification of bioceramics implants [243–246]. (**A**: Hydroxyapatite channels with controlled cross-sections of different geometries (triangular, square, hexagonal and circular) reproduced with permission from Ref. [243] Copyright 2008 the Royal Society. **B**: Surface topography modification via 3D printing can increase surface area to support enhanced biological response without compromising mechanical properties. Reproduced with permission from Ref. [244] Copyright 2021 Elsevier. **C**: Hollow-struts-packed (HSP) bioceramic scaffolds with designed macropores and multioriented hollow channels via a modified coaxial 3D printing strategy. Reproduced with permission from Ref. [245] Copyright 2015 American Chemical Society. **D**: A haversian bone-mimicking scaffold prepared via DLP printing reproduced with permission from Ref. [246] Copyright 2020 American Association for the advancement of science.)

External surface functionalization

In consideration of the drawbacks of bioceramic scaffolds, external surface functionalization refers to coating of bioactive layers (i.e. protein, polymers and drugs) onto 3D-printed bioceramic structure. Physical (dipping) and/or chemical immobilization (covalent deposition) are common-used methods for external surface functionalization. Physical immobilization is the simplest way to impregnate target protein onto the surface of bioceramics via weak non-covalent interactions, including electrostatic, van der Waals, hydrogen bonding and/or hydrophobic interactions. While, chemical modification is based on altering the surface energy, charge and/or functional groups [247].

Hydrothermal treatment, usually regraded as a post-printing process, is a promising modification method to form needle-shaped crystal nucleation which has a great influence on the morphological and physicochemical features of 3D-printed CaPs scaffolds [248]. Raymond *et al.* [249] reported that α-TCP scaffolds by direct ink writing presented more crystallization nanostructures, and had a major impact on permeability and protein adsorption capacity after hydrothermal processes when compared with biomimetic treatment.

Polymerization of dopamine contains a large number of bioactive groups including catechol moieties, –OH and $–NH_2$, which can bind strongly to different types of materials [250]. Compared with the numerous previous investigations on pore structures of implants, Wu *et al.* [251] fabricated the nanolayers by the self-polymerization of dopamine and apatite mineralization on the strut surface of 3D printed bioceramic scaffolds by simply dropping as-prepared bioceramic scaffolds into dopamine-SBF solution for 4 days. The nanostructure of mineralized polydopamine film on 3D printed scaffolds improved osteogenesis and angiogenesis. Besides, as another biocompatible agent with high photothermal conversion efficiency.

Apart from the intrinsic osteogenic properties, bioceramics, with appropriate functionalization, are excellent candidates to promote bone and tissue regeneration along with bone cancer therapy [252, 253]. From the promises of photothermal therapy (PTT) for localized treatment of bone tumors, Yang *et al.* [254] designed a black phosphorus-reinforced BG scaffolds for the efficient localized treatment of osteosarcoma and enhanced bone formation. The significantly decreased viability of Saos-2 cells and tumor ablation effect in osteosarcoma mice model after near-infrared (NIR) irradiation, strongly demonstrated photothermal-therapeutic effects of BP-BG scaffold. More importantly, BP–BG scaffold are also favorable for biomineralization *in situ*, facilitating osteogenesis both *in vitro* and *in vivo*.

Similarly, carbon nanomaterials are recommended for their photothermal performance in bone tumor therapy [255]. Owing to the unique structure and special properties, graphene oxide (GO) processes favorable thermal conductivity and enhanced osteoinductivity [256]. Ma *et al.* [257] fabricated GO-modified β-TCP composite scaffolds combining a high photothermal effect for tumor therapy and significantly enhanced bone-forming ability by 3D printing and surface-modification strategies. Furthermore, magnetic nanoparticles (Fe_3O_4)-loaded GO nanolayer was prepared for the modification of 3D printed β-TCP scaffolds. The magneto-thermal property of composite scaffolds could effectively kill bone tumor cells in an alternating magnetic field, and significantly promote osteogenesis by the synergistic effect of GO and the released Fe ions.

Ion substitution

Differ from external surface functionalization, ion substitution usually occurs in the preparation of ceramic-based solution, and simultaneously printed as composite construct, which ensures the homogeneous distribution and well protection from degradation of bioceramic materials [225, 231, 258–260].

Ca^{2+} in HA structure can be substituted by other cations, meanwhile substitution of PO_4^{3-} in the HA structure with anionic compounds has also been achieved [252]. Various researches reported that the metal ion-doped HAs stimulated osteoblast proliferation and differentiation [261]. Thus, the addition of trace elements including, molybdenum (Mo), strontium (Sr), manganese (Mn) and magnesium (Mg) into bioceramics during printing process is another important modification strategy to improve the physicochemical and biological properties of composite scaffolds [225, 259, 262, 263]. Although many literatures have reported the successful examples of ions-dropped ceramic scaffolds, conventional methods were mostly applied for these fabrications. Herein, some representative researches related to 3D printed bioceramic scaffolds with trace elements incorporation are listed as Table 4 [231, 259, 262, 264–271]. Apart from the inherent characteristics of biocreamics, additional effect including anti-bacteria, anti-tumor and anti-oxidation are achieved by some specific element nanoparticles. For example, Zhang *et al.* [270] prepared Ag modified β-TCP scaffolds through a combination of a 3D-printing method and a layer-by-layer coating technique, which could effectively kill bacteria, and had positive effects on osteogenesis by promoting the expression of an osteoblast-related gene in BMSCs. The dual effect of anti-tumor and enhanced osteogenesis can be achieved by trace elements-dropped (Cu, Fe, Mn, Co) bioactive glass-ceramic (BGC) scaffolds via 3D printing technology [271]. Under NIR irradiation, the anti-tumor investigation *in vivo* and *in vitro* found all trace elements could effectively kill tumor cells (Cu > Fe > Mn > Co), which were related to the increasing temperature and laser power density. All element-dropped BGC scaffolds could not only stimulate osteogenic differentiation of BMSCs, but also facilitate biomineralization. Among them, 3D printed Fe/BGC and Mn/BGC have great potential as bifunctional scaffolds for photothermal tumor therapy and bone regeneration. However, only a limited number of preclinical researches were performed validate the risks and benefits of 3D printed functionalized bioceramics scaffold with photothermal properties for cancer therapy. It is worth noting that the long-term and wide-spread clinical performances of photothermal bioceramics in cancer therapy need to be comprehensively investigated.

Functional engineering strategies of polymeric materials for hard tissue repairment

Polymers are large molecule materials made up of many smaller and identical repeating units joined together by covalent bonds [21]. Generally, 3D printed polymers can be classified into two major groups according to their original sources. The first group is natural polymers, such as gelatin, alginate, collagen, agarose, chitosan, fibrin and hyaluronic acid (HLA). The other group includes synthetic polymers, such as PEG, PU, pluronic acid and poly(lactide-co-glycolide) (PLGA). A distinction between the natural and synthetic polymers is that natural polymeric chains are full of bioactive groups, while synthetic polymeric networks are repeatable inert units (monomers) [21]. Theoretically, any

Table 4. Representative examples of ion substituted bioceramics in bone tissue engineering

Ceramic-based materials	Ion elements	Post-treatment	Effect	Printing parameters	Ref.
BG	Mo	1350°C, 3 h	BG scaffolds with Mo incorporation enhanced the mechanical strength, and stimulated bioactivities of BMSCs. The release of MoO_4^{2-} could promote chondrogenesis by activating HIF-α pathways and restrained catabolic responses by regulating TIMP3, MMP13 and ADAMTS5	Pressure: 1.5–3.0 bar Printing speed: 5 mm/s	[264]
β-TCP	Ag	1100°C, 3 h	Ag@GO nano composite-modified scaffolds were not only effective in killing bacteria, but also had positive effects on osteogenesis by promoting the expression of an osteoblast-related gene in BMSCs.	Pressure: 3 MPa Nozzle diameter: 0.52 mm Step distance: 1.11 mm	[270]
BG	Cu	1300°C, 3 h	Cu^{2+} facilitated the proliferation and maturation of chondrocytes through activating HIF pathway, and further promoting the anti-inflammatory M2 phenotype and elevating the secretion of anti-inflammatory cytokines in macrophages to reduce the damage of cartilage tissue.	Pressure: 3–6 bar Printing speed: 6 mm/s Nozzle diameter: 0.22 mm	[265]
β-TCP	Mg/Si	1250°C, 2 h	Significantly higher bone and blood vessel formation were observed for the TCP scaffolds with Mg and Si in rat distal femoral defect model.	Not report	[266]
β-TCP	Fe/Si	1250°C, 2 h	The presence of Fe and Si improved mechanical strength of β-TCP scaffolds after sintering, as well as exhibiting an enhanced early-stage osteoconduction and neovascularization *in vivo*.	pure β-TCP layers: 35 μm Doped β-TCP layers: 35 μm	[267]
BG	Cu/Fe/Mn/Co	1300°C, 3 h	Photothermal performance: Cu > Fe > Mn > Co Cu–BG, Fe–BG and Mn–BG scaffolds effectively killed tumor cells *in vitro* and significantly inhibited tumor growth *in vivo*	Not report	[271]
Ca–Si	Sr/Mg	1150°C, 45 min 1150°C, 3 h	Compared with conventional β-TCP scaffold, Sr/Mg/Ca–Si scaffolds had better apatite formation ability and bone induction performance.	Printing speed: 6 mm/s Nozzle diameter: 450 μm Filament spacing: 850 μm	[259]
MBG/AlgMC	Zn	$CaCl_2$ crosslinking, 10 mins	The addition of Zn in BMG/AlgMC ink greatly reduced viscosity.	Nozzle diameter: 410 μm Printing width: 7.75 mm Strand distance: 1.8 mm	[268]
HA/MC	Sr	Glutaraldehyde crosslinking	Sr-HA scaffolds with mineralized collagen improved cell adhesion and proliferation in vitro, and exhibited more bone formation in bone defect.	Pressure: 0.25–0.5 MPa Nozzle diameter: 0.4 mm Filament spacing: 1.1 mm Printing speed: 5–8 mm/s	[262]
MBG	Sr	No	3D printed Sr-MBG scaffolds exhibit good apatite-forming bioactivity and sustained drug delivery properties, facilitating cell proliferation and differentiation	Printing speed: 9–12 mm/s Nozzle diameter: 0.4 mm Pressure: 1.5–3.8 bar	[231]
Ca–Si/PCL	Mg/Sr	No	3D-printed Mg-/Sr-doped Ca–Si-based scaffold stimulated bone regeneration via dual-stimulation of AKT and WNT signaling pathways	Pressure: 200–250 kPa	[269]

AlgMC, alginate-methylcellulose; MC, mineralized collagen.

polymers which have a sol–gel phase transition character can be applied in an extrusion-based bioprinting technology. In fact, very few polymers can be printed in layers at room temperature. Fortunately, polymer chains are more easily be connected to one another physically or chemically, when compared with metals and ceramics. After modification, special physical–chemical characters of polymers in response to various external stimuli, including light, temperature, pH, magnetism and electricity, which enrich the diversity of printing application. Therefore, the modification strategies of representative polymers and their applications for hard tissue replacement are highlighted in this section.

Printable polymeric materials

Alginate

Alginate, an anionic polysaccharide derived from brown algae, have been frequently used as cell-laden 'bioinks' in 3D bioprinting processes, due to its biocompatibility, biodegradable, non-immunogenic and mild gelation characteristics [272]. However, alginate has poor mechanical properties, and uncontrollable degradation in aqueous condition. The free functional moieties, hydroxyl and carboxyl that distribute along the backbone, are benefited for alginate modification [273]. Ooi *et al.* [274] utilized thiol-ene reaction to design a modular alginate-based hydrogel system that extended the biofabrication window of alginate, allowing for printability at a lower concentration (2 wt%) with high cell survivability (>80%) in the creation of stable 3D constructs by extrusion-based bioprinting. Besides, crosslinking is another important part for alginate bioprinting. Prior to crosslinking, alginate solutions behave as non-Newtonian fluids with low viscosities that are unable to acquire a 3D geometrically defined structure. Various divalent cations (i.e. Ca^{2+}, Zn^{2+}, Ba^{2+}) are commonly used as crosslinking agents [275, 276]. Chen *et al.* [277] evaluated the printability, physicochemical properties and osteogenic potential of four common alginate bioinks: alginate-$CaCl_2$, alginate-$CaSO_4$, alginate-gelatin and alginate-nanocellulose for the 3D bioprinting of accurate osteogenic grafts. Effective cell-matrix interactions were only observed in alginate–$CaCl_2$ printed constructs, as well as exhibited significantly enhanced osteogenic differentiation in compared with the other three bioinks.

Gelatin

Gelatin is a partial hydrolyzed protein by breaking the triple helix of collagen into single-strain molecules, and widely applied for 3D printing due to its excellent biocompatibility, high water-adsorbing capacity, rapid biodegradability and non-immunogenicity [278]. Gelatin solution has a unique sol–gel transition at 28°C, which can be tuned and physically cross-linked during bioprinting by heating gelation. However, temperature-induced gelation is typically slow and unstable, which limits its long-term use in tissue engineering [37]. Additionally, the mechanical properties of gelatin need to be improved as bone scaffolds.

Hyaluronic acid

HLA or hyaluronan is a polysaccharide existing in living organisms composed of D-glucuronic acid and N-acetyl-D-glucosamine [279]. Like most of the natural polymers, HLA exhibits excellent biocompatibility and biodegradability, which has played an essential role in cell proliferation, angiogenesis and cell–receptor interactions [280–282]. Whereas, pure or unmodified HLA is seldomly used as printing materials alone [283]. No yield stress and shape fidelity during printing process can be achieved, due to the shear-thinning properties of HLA [283]. Thus, HLA can be employed as the supplemental agent to alter the viscosity of other polymer hydrogels. As an alternative way, HLA is the main component and self-standing material, undergoing single or multiple physical/chemical modification with shear-thinning or post-printing crosslinking for shape retention [284].

Chitosan

Chitosan (CS) is a cationic polysaccharide produced by partial deacetylation of chitin. It has been applied in many biomedical fields, such as bone, skin and cartilage repair, due to its low or non-toxic, antibiotic and biodegradable properties [285]. Furthermore, for drug delivery purpose, bioactive molecules encapsulated CS bioink provides the possibility to print 3D structures to enhance cell responses [286].

Poly(ε-caprolactone)

PCL is one of the non-hazardous polyesters obtained by ring-opening polymerization of ε-caprolactone monomers [287]. PCL exhibits slow degradation, resulting from its less frequent ester bonds per monomer. The melting point of PCL is about 60°C, while glass transition temperature (Tg) is around −60°C [22]. Therefore, it is an ideal structural material for FDM technologies. During the printing processes, PCL molecules maintain crystal states with low or moderate mechanical properties [288]. A major disadvantage of PCL is its intrinsic hydrophobicity and lack of functional groups, resulting in poor cell attachment and proliferation [289]. However, it is an excellent choice as a supporting material, especially for hard tissue replacement.

Polyethylene glycol

PEG is a hydrophilic, biocompatible, non-immunogenic synthetic polyether with a linear and branched structure that has been approved by the FDA as a good candidate for cell encapsulation [290, 291]. PEG hydrogels have been widely applied as fundamental materials for extrusion-based materials [291–293]. For example, a linear PEG with succinimidyl valerate end groups (PEGX) was used to crosslink a variety of polymers including GelMA, fibrinogen, and PEG amine via amino-carboxylic acid coupling. During printing process, extrudable and self-supporting bioink gels from the PEGX method yielded optimal layer-by-layer definition that enabled the ability to print thick, self-supporting constructs. After secondary post-printing crosslinking step, PEGX-gelatin bioink presented stable printed constructs with high cell viabilities [293].

Polyether–ether–ketone

Polyether–ether–ketone (PEEK) is a semi-crystalline synthetic polymer, as well as s a high-performance engineered thermoplastic polymer with potential to use in a variety of metal replacement applications due to its superior mechanical properties [294]. In the last decades, PEEK is considered as an ideal alternative material for Ti, which has been widely served in craniomaxillofacial and spine fusion surgeries [295–298]. Compared with Ti (102–110 GPa), PEEK presents a much lower elastic modulus (3–4 GPa), which is close to human trabecular bone (1 GPa) [299]. The melting temperature and glass transition temperature (Tg) of PEEK are 343 and 143°C, respectively, which indicates thermoplastic PEEK can be printed by SLS and FDM technologies [94].

However, residual stress is accumulated, leading to warping and interlayer delamination during the printing process, which probably effects printing accuracy and mechanical properties [295, 300]. The investigations on mechanical properties of PEEK between 3D printing and conventional approach (injection molding) demonstrated that, FDM-printed PEEK had a wide range of tensile strength and Young's modulus (approximately equaled or slightly exceeded to injection molded PEEK), which were influenced by printing parameters including layer thickness, printing speed, ambient temperature and nozzle temperature [301–303].

PEEK is a typical example for the translation in clinical use (Fig. 8). For example, patients suffering from bone-related tumors are tortured by more than tumor itself, but the tissue defects after tumor resection. Yang *et al.* [304] reported the PEEK replacement in fronto-orbital defects after the resection of fibromatous hyperplasia. The as-fabricated PEEK perfectly matched and easily

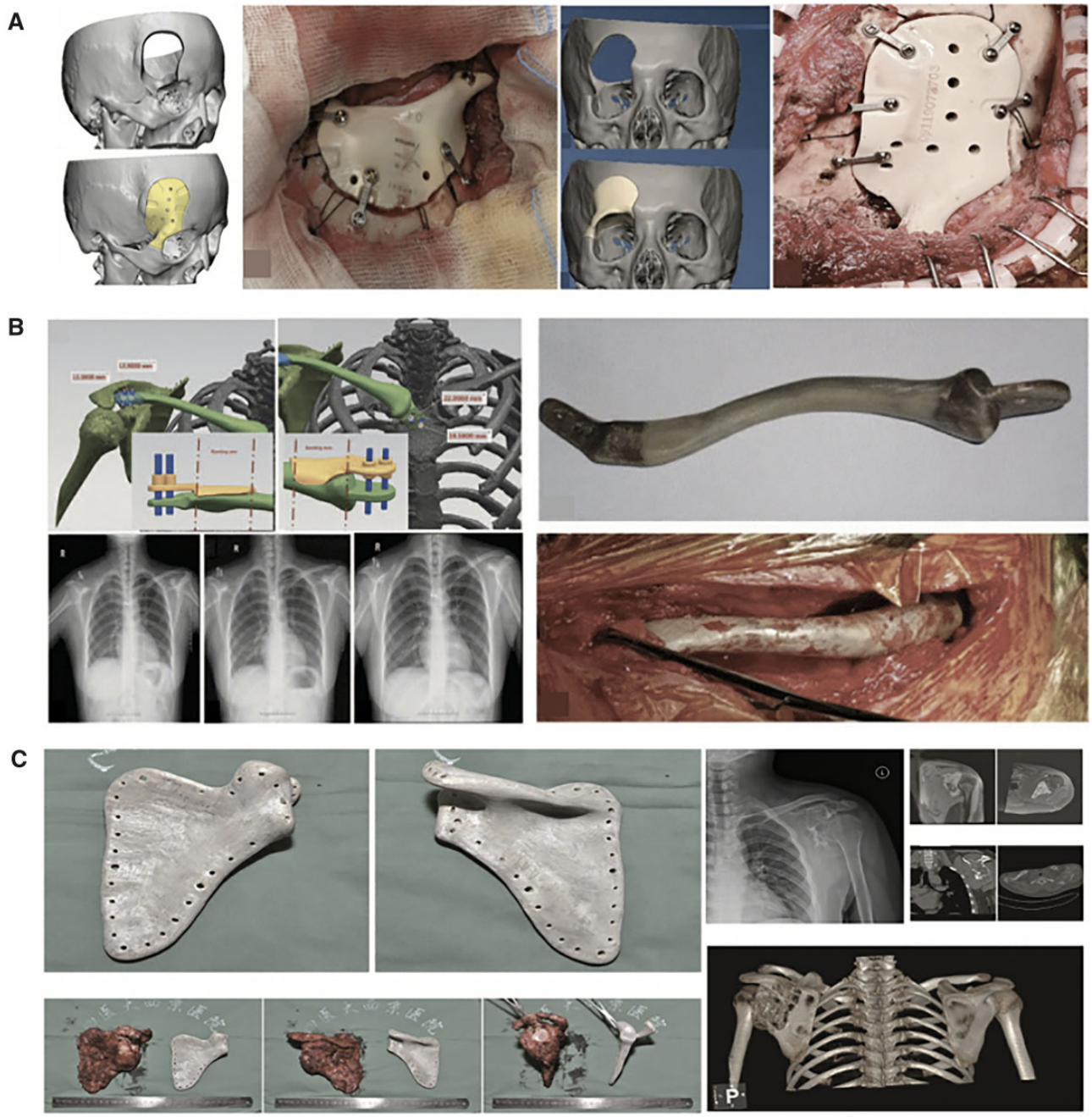

Figure 8. The clinical application for polymeric implants [304–306]. (**A**: 3D printed PEEK for complex craniofacial defect. Reproduced with permission from Ref. [304] Copyright 2021 Wolter's Kluwer Health. Inc. **B**: 3D PEEK implant designed, molded and inserted into defect area in subtotal clavicle reconstruction. Reproduced with permission from Ref. [305] Copyright 2021 Wolter's Kluwer Health. Inc. **C**: PEEK prosthesis for scapular reconstruction. PEEK prosthesis was in normal position from X-ray image after tumor resection. Reproduced with permission from Ref. [306] Copyright 2018 Elsevier.)

embedded into the defect area to achieve individualized reconstruction in one-stage surgery. Another case was reported as reconstruction of complex bone defects in a patient suffering from chronic clavicle osteomyelitis [305]. Three-dimensional-printed PEEK prosthesis was properly fixed into the acromial end and the medullary cavity of the sternal stalk. Satisfactory cosmetic and functional outcomes were achieved after 2-year follow-up. PEEK prosthesis also can be used for the application of large joints replacement in clinic. The X-ray examination after the operation presented a good anatomical position of PEEK prosthesis, allows early functional recovery of the patient [306].

Besides, carbon-fiber-reinforced coating (CFR) is introduced for PEEK modification for clinical use. CF/PEEK is an ideal material for plates and nails due to the flexible fatigue strength and modulus of elasticity, and displayed significantly less artefacts in computed tomography (CT) and magnetic resonance imaging, allowing a precise follow-up radiograph [307]. Laux *et al.* [308] presented clinical cases with application of CF/PEEK implants in orthopedic tumor surgery. However, the failure of CFR–PEEK implants has been reported in clinic, advising the careful use of functionalized PEEK under strict supervision [309, 310].

Functional engineering strategies of polymeric-based implants

Polymers offer greater design flexibility than metals and ceramics [311]. The properties of polymers determine their application for clinical use. In detail, natural polymers are superior to synthetic polymers in terms of biocompatibilities and often employed as cell-laden accommodations [21]. Whereas, most synthetic polymers take advantage at mechanical properties and immunogenic responses that frequently used as supporting structures [22].

Stimulus-responsive polymeric hydrogels

In biomedical applications, there is a great demand for 'smart materials' which are sensitive to external triggers or biological signals for the development of next-generation as precision medicine. Stimulus-responsive hydrogels are defined as the hydrogels with reversible or inversible phase transition *in situ* by light, heat, magnetism and/or force stimulation [312].

Thermo-responsive polymers

Temperature is the most frequently selected stimulus to achieve shape-transformation in bioprinted structures. Most thermo-responsive materials enable reversible deformation, and divided into two groups regarding the critical temperature, the lower critical solution temperature (LCST), and the upper critical solution temperature (UCST) [313]. Polymers are insoluble in water when possessing an UCST and become soluble below UCST [314].

Poly(N-isopropylacrylamide) (PNIPAm) is the most extensively studied thermo-responsive polymer, which is an amphiphilic polymer, possessing both hydrophilic (amide groups) and hydrophobic (isopropyl groups) chains [315]. At a temperature below LCST, PNIPAm molecules in an aqueous environment exhibit a hydrophilic behavior with an extended coil structure. When the temperature increases above the LCST (32°C), hydrophobic groups become more active, resulting in the molecules to transform into a shape resembling a compact globule [316]. Several strategies to introduce PNIPAM within natural or synthetic polymers have been developed. PNIPAm can be conjugated to hyaluronan acid (HLA-PNIPAM) as thermo-responsive HLA hydrogels that present liquid status at room temperature and gel status in the body [317–319]. HLA-PNIPAM hydrogels had great potential to support extrusion of a range of biopolymers which undergo fast gelation, thereby facilitating the printing of cell-ladened cartilage constructs [320].

Photo-responsive polymers

Photo-responsive biomaterials can be activated by light in a relatively wide wavelength range, including NIR, infrared (IR), ultraviolet (UV) regions and visible light [321]. Methacrylation is one of common-used methods to prepare photo-responsive polymers, including gelatin, hyaluronan acid and chitosan. Methacrylate group (MA) including glycidyl methacrylate or methacrylic anhydride can interact with carboxyl, hydroxyl and amine groups of polymers [322].

Gelatin methacryloyl (GelMA), is one typical example of photo-responsive natural polymer for 3D printing, based on a natural gelatin backbone with the introduction of methacrylate groups [323]. Hoch *et al.* [324] developed novel gelatin-based hydrogels by primary amines methacrylation and carboxylic acid moieties acetylation. After crosslinking by photo-initiator (Irgacure 2959), chondrocytes-laden hydrogels were printed by piezoelectric inkjet-based 3D printing. Almost 100% cell viabilities in hydrogels were observed after 6 h incubation. However, GelMA prepolymer solution exhibits a fast sol–gel transition at room temperature, which is a hurdle for its use in stereolithography bioprinting. Kumar *et al.* [31] modified GelMA hydrogels to exhibit slower sol–gel transition at room temperature and faster photopolymerization by optimizing the solvent, the reaction duration and the pH value. They found the modified GelMA exhibited mechanically stable structures with high resolution after DLP printing. Moreover, High cell viability and cell–matrix integration in modified GelMA hydrogels offered the versatility for a wide range of applications in tissue engineering. Although GelMA and Irgacure 2959 form prevalent system of stereolithography-based bioprinting, UV crosslinking limits penetration depth affecting the overall polymerization efficiency for large constructs. Besides, oxygen inhibition during UV irradiation results in insufficient crosslinking, which might directly impact the print fidelity of printed construct [325]. A new sight was developed by Lim *et al.* [326] who utilized visible light and ruthenium (Ru)/sodium persulfate (SPS) as visible-light initiating system to fabricate GelMA-based hydrogel constructs. To be surprised, more than 85% of cell viability was achieved in new visible light system. Meanwhile, printed constructs photopolymerized by new visible light system were completely crosslinking when compared with UV irradiation. It was indicated that optimized visible light system is more suitable for bioprinting of cell-laden constructs with high shape fidelity and cell viability.

Methacrylated HLA (HLAMA) is generated by photochemically crosslinking HLA and methacrylate using UV-light source [327]. The addition of GelMA into HLAMA exhibits tunable physical and biological properties [328]. Such hybrid printing system with two distinct hydrogel inks were developed for cartilage tissue engineering. HLAMA/GelMA provided a suitable environment for chondrogenic cell (ATDC5) encapsulation and proliferation, while cellulose nanocrystals-reinforced HLAMA/GelMA possessed excellent printability and provided adequate structural support to the 3D printed structure. Satisfyingly, the printed construct remained stable during the process of cyclic compression, as well as exhibiting persistently high cell viabilities [329].

Photopolymerization is also the common strategy to improve the strength of CS, allowing photo-responsive CS to retain its shape during the 3D printing process [330]. In term of UV-responsive CSMA, the UV curable chitosan precursor is generally mixed with photo-initiators, and exposed to UV light for crosslinking [331]. Shen *et al.* [32] utilized a LAP (Lithium phenyl-2,4,6-trimethylbenzoylphosphinate) as photo-initiator, which could be exposed to blue light (405 nm) for crosslinking. CSMA with a substitution degree (36%) can be printed into complex 3D hydrogel structures with high-resolution and high-fidelity by DLP technologies. More importantly, when compared with I2959 and UV irradiation, blue light and LAP resulted in less damage to cells.

Surface treatment

Similar to metallic materials, surface topography of polymers, especially synthetic polymeric materials, plays an important role to cell responses after implantation [332]. The fabricated scaffolds could be modified by physicochemical treatments. For example, the printed PCL scaffolds by Bioscaffolder® device were firstly subjected to an oxygen plasma, and grafted by argon 2-aminoethylmethacrylate (AEMA), followed by immobilizing of gelatin and physical adsorbing of FN [333]. The synergistic effect of the scaffold architecture and the biomimetic surface enabled the creation of plotted PCL scaffolds with increasing attachment, proliferation, colonization and differentiation of MC3T3-E1 cells. Park *et al.* [334] modified the surface characteristics of FDM-printed

PCL/HA scaffolds using O_2 plasma and sodium hydroxide. When compared with O_2 plasma treatment, the alkaline treatment was favorable for exposing HA particles embedded in the scaffolds, which promoted cell proliferation and differentiation of hDPSCs. Han *et al.* [335] demonstrated post-treatment of FDM-printed PEEK including polishing and sandblasting could roughen the surface and increase hydrophilicity, facilitating cell adhesion and proliferation. A recent research by Park *et al.* [336] utilized polydopamine coating and HA layer to decorate 3D printed PCL scaffolds for BMP-2 release. The modified PCL/PDA/HA/BMP-2 scaffolds could control BMP-2 release to up to 7 days, promote cell growth, proliferation and osteogenesis *in vitro*. Besides, an injectable thermo-sensitive chitosan hydrogel with BMSCs encapsulation was incorporated into a FDM-printed PCL scaffold. The hybrid construct possessed reinforced compressive strength and favorable micro-environment for cells growth and osteogenesis via sustained release of BMP-2 for more than 1 week [337].

Hybrid composite hydrogels

Synthetic polymers and their composites are of great interest in orthopedic fields due to their mechanical properties that can match bone-related tissues [22]. It is noteworthy that synthetic polymers provided adequate structural support for hard tissue replacement in clinical use, especially in load-bearing sites of bone defects [338]. Thus, the incorporation of natural polymers or bioactive agents into synthetic polymers is a simple and effective way to enhance biological performance of 3D printed scaffolds (Fig. 9) [339]. Some representative examples of modification strategies on polymeric-based hydrogels are list in Table 5 [32, 284, 324, 328, 334, 335, 340–346].

A linear PEG with succinimidyl valerate end groups (PEGX) was used to crosslink a variety of polymers including GelMA, fibrinogen, and PEG amine via amino-carboxylic acid coupling. During printing process, extrudable and self-supporting bioink gels via the PEGX method yield optimal layer-by-layer definition

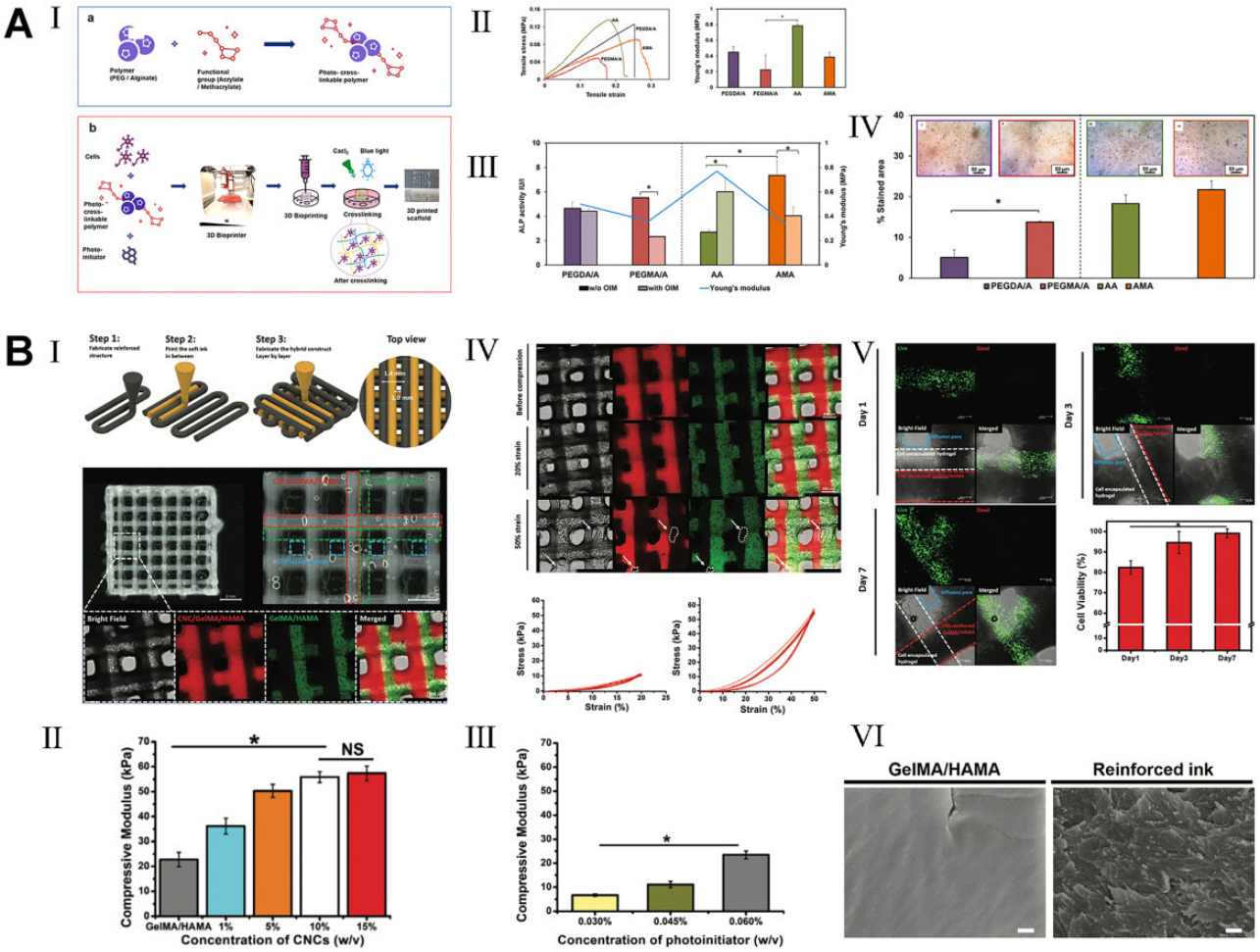

Figure 9. Mechanical reinforcement of composite polymers for 3D printing [329, 339]. (**A**: I. Overall 3D bioprinting process to fabricate functional PEG diacrylate (PEGDA) or PEG dimethacrylate (PEGMA)-Alg acrylate (AA) or alg ormethacrylate (AMA) crosslinked scaffolds. II. Stress-strain curve and young's modulus (MPa) value of different hydrogels indicated the functionalized PEG and alginate gels exhibited high mechanical strength compared with natural materials. III. The ALP activities of functionalized hydrogels demonstrated the favorable osteogenic effects with any additive agents. Reproduced with permission from Ref. [339] Copyright 2021 Elsevier. **B**: I. Illustration of the hybrid printing procedure and the observation of the hybrid printed construct (the hybrid printed constructs were fabricated using the two hydrogel inks: cellulose nanocrystals (CNCs)-reinforced GelMA/HLAMA and GelMA/HLAMA inks, which were defined in the optical microscopic image by red dotted lines and green dotted lines, respectively.) II–III. Compression test for the optimal concentration of GelMA/HLAMA, reinforced hydrogel and photoinitiator. IV. Mechanical results of hybrid printed construct after cyclic compression (structural integrity was retained after 10 cycles of compression with 20% strain. After 10 cycles of compression with 50% strain, the structural defects appeared as marked by the white arrow and dot line). V. Cells remained high viability of 82.4 ± 3.3% at day 1 and reached to 99.1 ± 2.2% at day 7. VI. SEM observation of GelMA/HLAMA ink. Reproduced with permission from Ref. [329] Copyright 2020 John Wiley and Sons.)

Table 5. Representative examples of modification strategies on polymeric-based hydrogels in bone tissue engineering

Printing technologies	Bioinks	Modification strategies	Crosslinking condition	Application	Ref.
Magics EnvisionTEC (extrusion-based)	OA/Gel	Oxidization of alginate	100 mM $CaCl_2$; room temperature	Not mention	[342]
Inkjet printing	Chondrocytes/GMA	Methacrylation and acetylation of gelatin	UV irradiation (Irgacure 2959)	Cartilage	[324]
Extrusion-based	Chondrocytes/GelMA/HA	Methacrylation of gelatin	UV irradiation; 37°C	Cartilage	[343]
Extrusion-based	ADA/Gel	Oxidization of alginate	$BaCl_2$		[344]
Bioscaffolder dispensing system (extrusion-based)	HLAMA	Methacrylation of HA	UV irradiation Irgacure 2959	Bone	[345]
3D FDM printer (piston-based)	Ad-MeHA/CD-MeHA	Adamantane-modified MeHA; cyclodextrin-modified MeHA	UV irradiation (5 min) Irgacure 2959	Not mention	[284]
Beam projector (Stereolithography-based)	Fibroblasts/PEG/GelMA	Methacrylation of gelatin	Visible light eosin Y	Not mention	[346]
DLP	HUVECs/CSMA	Methacrylation of CS	Blue light (405 nm) LAP	Not mention	[32]
FDM	PCL/HA	O_2 plasma and NaOH treatment	–	Bone	[334]
Stereolithography-based	Chondrocytes/GelMA/HLAMA	Methacrylation of Gel and HA	Blue light Ethyl	Cartilage	[328]
Stereolithography-based	MSC/GelMA/PEGDA	Methacrylation of gelatin acrylated PEG	UV irradiation	Cartilage	[341]
FDM	CFR/PEEK	Polish/sandblasting	Post-heat treatment	Bone	[335]
FDM	CHAp/PEEK	Not mention	Not mention	Bone	[340]

OA, oxidized alginate; GMA, methacrylated and acetylated gelatin; HLA, hyaluronic acid; ADA, alginate dialdehyde; AD, adamantane; CD, cyclodextrin; CFR, carbon fiber; CHAp, $Ca_{10}(OH)(PO_4)_3$.

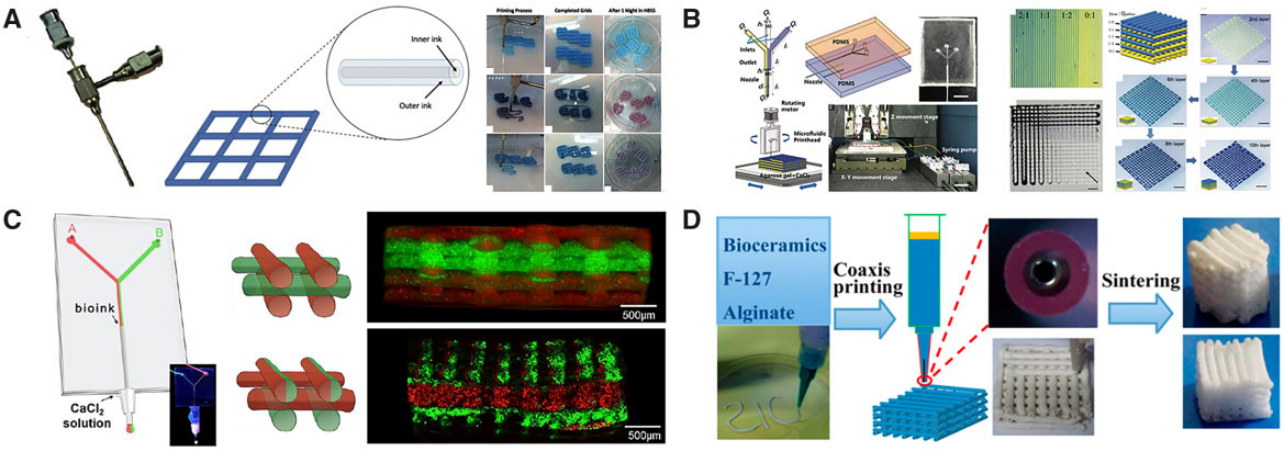

Figure 10. Multi-material bioprinting based on microextrusion technologies with multiple printing-heads [245, 357–359]. (**A**: Coaxial nozzles were design for gird construct with inner/outer layers. Reproduced with permission from Ref. [357] Copyright 2020 Wolters Kluwer. **B**: The design of microfluidic printheads with multiple inlets and an outlet, and the color-coded heterogenous construct. Reproduce with the permission from Ref. [358] Copyright Whioce Publishing. **C**: Microfluidic system ('Y' shaped channel) was used to flow two separate bioinks containing red and green fluorescent beads that through a single extruder. Reproduced with permission from Ref. [359] Copyright 2015 John Wiley and Sons. **D**: Bioceramic powders with F-127 solution and alginate were printed by extrusion printer with coaxial printing nozzle, followed by sintering to achieve mechanically stable construct. Reproduced with permission from Ref. [245] Copyright 2015 American Chemical Society.)

that enabled the ability to print thick, self-supporting constructs. After secondary post-printing crosslinking step, PEGX–gelatin bioink presents stable printed constructs with high cell viabilities [293]. A novel research by Piluso *et al.* [347] reported an engineered RGD modified PEG hydrogel with transient incorporation of low molecular weight gelatin (LMWG) fragments for microcapillary extrusion-based bioprinting system. They demonstrated the incorporation of LMWG fragments enabled the microcapillary-based extrusion of the PEG-based hydrogel with excellent shape fidelity and accuracy. Acrylated PEG (PEGDA) can be synthesized in one step by reacting acryloyl chloride with pendant hydroxyl groups [348]. Zhu *et al.* [341] prepared TGF-β1 encapsulated BSA-PLGA particles via a core-shell electro-spraying technique, and mixed with MSCs, GelMA and PEGDA as bioinks. The printed construct by tabletop stereolithography-based 3D bioprinter could significantly improve printing resolution and compressive modulus with the incorporation of PEGDA. The sustained release of TGF-β1 from composite hydrogel improved chondrogenic differentiation of encapsulated MSCs *in vitro*.

Additionally, homogeneous silicate-coated PEEK through electron beam evaporation could enhance its biological activities by promoting proliferation and osteogenic differentiation of ovariectomized (OVX) BMSCs [349]. Sulfonated PEEK was another modification strategy to enhance antibacterial and osteogenic abilities

both *in vivo* and *in vitro* [350]. To be specific, Gao *et al.* [351] provided a comprehensive understanding on the immune microenvironments in the presence of PEEK with functional layers. Poly(acrylic acid) (PAA) and poly(allylamine hydrochloride) (PAH) films with tunable nanoscale porosity were prepared by self-assembly technology under two pH values. The functional films inhibited the acute inflammatory response of macrophages by down-regulating the expression of integrin and adhesion complexes, and created a favorable microenvironment for osteogenic differentiation of BMSCs, as well as promoted bone formation ability in bone defect models [352–354].

More importantly, hierarchical fabrications of complex construct are recently achieved by multi-material 3D bioprinters, which makes it possible to simultaneously extruding various bioinks with precise printing resolution (Fig. 10). For example, cell-laden natural hydrogels can be printed from one nozzle, and ceramics or synthetic polymers are printed from another nozzle to reinforce the structure stability. Naren *et al.* [360] designed a core-shell structure by a modified bioprinter. Ceramic paste of high viscosity could be extruded from metallic core nozzle, while shell structure consisted of cell-laden alginate hydrogels with low viscosities which were printed through an outer nozzle. After crosslinking by $CaCl_2$, the alginate/bioceramic core/shell-structured 3D scaffold enhanced the mechanical properties and maintained high viability for a long culture period. Additionally, multifunctional 3D bioprinting platform with two kinds of bioprinters were designed to construct hierarchical parts [361]. Cui *et al.* [356] utilized biodegradable polylactide (PLA) fibers and cell-laden GelMA hydrogels through a multifunctional 3D bioprinting platform consisted of a FDM 3D bioprinter and a SLA 3D bioprinter to explore complex vascularized bone constructs.

Challenges and perspectives

As the osteogenesis of 3D printed implants is a primary concern for hard tissue replacement, the implants with multiple functions are one of the most effective strategies to facilitate the osteointegration. In this review, the typical functional engineering strategies based on the properties of printed materials (metals, ceramics and polymers) are highlighted.

In hard tissue engineering, the customized implants by 3D printing technology offers precise control and high accuracy of microarchitecture. Currently, some challenges of 3D printed implants still need to be carefully addressed: (i) accuracy control of 3D printed implants based on natural bone structure; (ii) the mechanical strength of 3D printed implants matching the clinical requirements of implants under various conditions; and (iii) 3D printed implants for repairing large bone defects under various clinical and/or pathological conditions.

Due to the inherent bioinert properties, 3D printed metals mostly need bioactive surface structures after printing, no matter for solid or porous implants. Thus, physical–chemical modification methods are usually applied for the alteration of implant surface, including surface roughness, wettability and hardness. Moreover, biocompatible coating (CaPs and polymeric coating) on metallic implants can provide biomimetic microenvironments for cell responses (i.e. adhesion, proliferation, differentiation) after implantation. Differ from bioinert metals, ceramics themselves present favorable osteogenic capability. The functional engineering strategies of 3D printed ceramics implant mostly focused on the design of biomimetic structure as well as providing multiple functions (i.e. photothermal, osteogenic, antibacterial), synergistically improving the effect of bone regeneration. The properties of polymers depend on the structure of monomers that is smallest repeating unit in the polymer chains and their connections. Thus, polymeric implants are mostly undergoing chemical modification for favorable osteogenesis. Besides, in consideration of different advantages of polymers, the simultaneous or sequential printing of synthetic and natural polymers via multiple bioprinters is a potential method for fabricating multiple-functional implants for hard tissue replacement.

However, multiple functionalized implants still remain some challenges. For example, the efficiency of new bone formation is related to the degree of vascularization, especially for repairing large bone defects. Thus, enhanced angiogenesis is a major concern in cell-laden bioprinting. Antibacterial property is another strategy for researchers to functionalize 3D printed implants. Besides, further development might focus on the drug load/release profile of implants, which are released via an internal or external stimulus in a controllable manner. Although a great number of researches achieved promising results, the fabrication of multiple-functional tissue engineered scaffold is a hindrance, and further clinical translation is still at the primary stage. From general point of view, we expect the next generation of biomaterials with interdisciplinary cooperation and technological innovation will perfectly match bone defects and meet the clinical individualization requirements.

Funding

This work was financially supported partly by the Zhejiang Provincial Natural Science Foundation of China (LY20E010006), and partly by the National Natural Science Foundation of China (51502265 and 81701033).

Conflicts of interest statement. The author(s) declared no potential conflicts of interest with respect to the research, authorship, and/or publication of this article.

References

1. Roseti L, Parisi V, Petretta M, Cavallo C, Desando G, Bartolotti I, Grigolo B. Scaffolds for bone tissue engineering: state of the art and new perspectives. *Mater Sci Eng C Mater Biol Appl* **2017**;78:1246–62.
2. Florencio-Silva R, Sasso GRdS, Sasso-Cerri E, Simões MJ, Cerri PS. Biology of bone tissue: structure, function, and factors that influence bone cells. *Biomed Res Int* **2015**;2015:421746.
3. Feng X, McDonald JM. Disorders of bone remodeling. *Annu Rev Pathol* **2011**;6:121–45.
4. Marie P. Physiology of bone tissue. *Immuno-Anal Biol Spec* **1992**;7:17–24.
5. Turnbull G, Clarke J, Picard F, Riches P, Jia L, Han F, Li B, Shu W. 3D bioactive composite scaffolds for bone tissue engineering. *Bioact Mater* **2018**;3:278–314.
6. Bahraminasab M. Challenges on optimization of 3D-printed bone scaffolds. *Biomed Eng Online* **2020**;19:69.
7. Laird NZ, Acri TM, Chakka JL, Quarterman JC, Malkawi WI, Elangovan S, Salem AK. Applications of nanotechnology in 3D printed tissue engineering scaffolds. *Eur J Pharm Biopharm* **2021**;161:15–28.
8. Nayar S, Bhuminathan S, Bhat WM. Rapid prototyping and stereolithography in dentistry. *J Pharm Bioallied Sci* **2015**;7:S216–9.

9. Liu F, Liu C, Chen Q, Ao Q, Tian X, Fan J, Tong H, Wang X. Progress in organ 3D bioprinting. *Int J Bioprint* **2018**;4. doi: 10.18063/IJB.v4i1.128.
10. Mardis NJ. Emerging technology and applications of 3D printing in the medical field. *Missouri Med* **2018**;115:368–73.
11. Chung JJ, Im H, Kim SH, Park JW, Jung Y. Toward biomimetic scaffolds for tissue engineering: 3D printing techniques in regenerative medicine. *Front Bioeng Biotechnol* **2020**;8:586406.
12. Chen Y, Li W, Zhang C, Wu Z, Liu J. Recent developments of biomaterials for additive manufacturing of bone scaffolds. *Adv Healthcare Mater* **2020**;9:e2000724.
13. Park JY, Park SH, Kim MG, Park S-H, Yoo TH, Kim MS. Biomimetic scaffolds for bone tissue engineering. *Adv Exp Med Biol* **2018**;1064:109–21.
14. Saravanan S, Leena RS, Selvamurugan N. Chitosan based biocomposite scaffolds for bone tissue engineering. *Int J Biol Macromol* **2016**;93:1354–65.
15. Barabaschi GDG, Manoharan V, Li Q, Bertassoni LE. Engineering pre-vascularized scaffolds for bone regeneration. *Adv Exp Med Biol* **2015**;881:79–94.
16. De Witte TM, Fratila-Apachitei LE, Zadpoor AA, Peppas NA. Bone tissue engineering via growth factor delivery: from scaffolds to complex matrices. *Regen Biomater* **2018**;5:197–211.
17. Zhang D, Xu X, Long X, Cheng K, Li J. Advances in biomolecule inspired polymeric material decorated interfaces for biological applications. *Biomater Sci* **2019**;7:3984–99.
18. Liu J, Mohd Rafiq NB, Wong LM, Wang S. Surface treatment and bioinspired coating for 3D-printed implants. *Front Chem* **2021**;9:768007.
19. Yao X, Peng R, Ding J. Cell-material interactions revealed via material techniques of surface patterning. *Adv Mater* **2013**; 25:5257–86.
20. Chhaya MP, Poh PSP, Balmayor ER, van Griensven M, Schantz J-T, Hutmacher DW. Additive manufacturing in biomedical sciences and the need for definitions and norms. *Expert Rev Med Devices* **2015**;12:537–43.
21. Liu F, Chen Q, Liu C, Ao Q, Tian X, Fan J, Tong H, Wang X. Natural polymers for organ 3D bioprinting. *Polymers* **2018**; 10:1278.
22. Liu F, Wang X. Synthetic polymers for organ 3D printing. *Polymers* **2020**;12:1765.
23. Dey M, Ozbolat IT. 3D bioprinting of cells, tissues and organs. *Sci Rep* **2020**;10:14023.
24. Van Hooreweder B, Apers Y, Lietaert K, Kruth JP. Improving the fatigue performance of porous metallic biomaterials produced by selective laser melting. *Acta Biomater* **2017**;47:193–202.
25. Mostafaei A, Elliott AM, Barnes JE, Li F, Tan W, Cramer CL, Nandwana P, Chmielus M. Binder jet 3D printing—process parameters, materials, properties, modeling, and challenges. *Progress Mater Sci* **2021**;119:100707.
26. Walker M, Humphries S. 3D printing: applications in evolution and ecology. *Ecol Evol* **2019**;9:4289–301.
27. Quan H, Zhang T, Xu H, Luo S, Nie J, Zhu X. Photo-curing 3D printing technique and its challenges. *Bioact Mater* **2020**;5: 110–5.
28. Hölzl K, Lin S, Tytgat L, Van Vlierberghe S, Gu L, Ovsianikov A. Bioink properties before, during and after 3D bioprinting. *Biofabrication* **2016**;8:032002.
29. Melchels FPW, Feijen J, Grijpma DW. A review on stereolithography and its applications in biomedical engineering. *Biomaterials* **2010**;31:6121–30.
30. Schmidleithner C, Malferrari S, Palgrave R, Bomze D, Schwentenwein M, Kalaskar DM. Application of high resolution DLP stereolithography for fabrication of tricalcium phosphate scaffolds for bone regeneration. *Biomed Mater* **2019**;14:045018.
31. Kumar H, Sakthivel K, Mohamed MGA, Boras E, Shin SR, Kim K. Designing gelatin methacryloyl (GelMA)-based bioinks for visible light stereolithographic 3D biofabrication. *Macromol Biosci* **2021**;21:2000317.
32. Shen Y, Tang H, Huang X, Hang R, Zhang X, Wang Y, Yao X. DLP printing photocurable chitosan to build bio-constructs for tissue engineering. *Carbohydr Polym* **2020**;235:115970.
33. Daly AC, Freeman FE, Gonzalez-Fernandez T, Critchley SE, Nulty J, Kelly DJ. 3D bioprinting for cartilage and osteochondral tissue engineering. *Adv Healthcare Mater* **2017**;6:1700298.
34. Kumar H, Sakthivel K, Mohamed MGA, Boras E, Shin SR, Kim K. Designing gelatin methacryloyl (GelMA)-based bioinks for visible light stereolithographic 3D biofabrication. *Macromol Biosci* **2021**;21:e2000317.
35. Sa M-W, Nguyen B-NB, Moriarty RA, Kamalitdinov T, Fisher JP, Kim JY. Fabrication and evaluation of 3D printed BCP scaffolds reinforced with ZrO(2) for bone tissue applications. *Biotechnol Bioeng* **2018**;115:989–99.
36. Salmi M. Additive manufacturing processes in medical applications. *Materials* **2021**;14:191–16.
37. Gungor-Ozkerim PS, Inci I, Zhang YS, Khademhosseini A, Dokmeci MR. Bioinks for 3D bioprinting: an overview. *Biomater Sci* **2018**;6:915–46.
38. Mierzejewska ZA, Hudák R, Sidun J. Mechanical properties and microstructure of DMLS Ti6Al4V alloy dedicated to biomedical applications. *Materials* **2019**;12:176.
39. Sing SL, An J, Yeong WY, Wiria FE. Laser and electron-beam powder-bed additive manufacturing of metallic implants: a review on processes, materials and designs. *J Orthop Res* **2016**; 34:369–85.
40. Lv X, Zhan Z, Cao H. Microstructure evolution and mechanical properties of Needle-Like ZrB2 reinforced Cu composites manufactured by laser direct energy deposition. *Micromachines* **2022**;13:212.
41. Chen Y, Zhang X, Parvez MM, Liou F. A review on metallic alloys fabrication using elemental powder blends by laser powder directed energy deposition process. *Materials* **2020**;13:3562.
42. Tan XP, Tan YJ, Chow CSL, Tor SB, Yeong WY. Metallic powder-bed based 3D printing of cellular scaffolds for orthopaedic implants: a state-of-the-art review on manufacturing, topological design, mechanical properties and biocompatibility. *Mater Sci Eng C Mater Biol Appl* **2017**;76:1328–43.
43. Awad A, Fina F, Goyanes A, Gaisford S, Basit AW. Advances in powder bed fusion 3D printing in drug delivery and healthcare. *Adv Drug Deliv Rev* **2021**;174:406–24.
44. Fina F, Goyanes A, Gaisford S, Basit AW. Selective laser sintering (SLS) 3D printing of medicines. *Int J Pharm* **2017**;529:285–93.
45. Zeng Z, Deng X, Cui J, Jiang H, Yan S, Peng B. Improvement on selective laser sintering and post-processing of polystyrene. *Polymers* **2019**;11:956.
46. Vande Ryse R, Edeleva M, Van Stichel O, D'hooge DR, Pille F, Fiorio R, De Baets P, Cardon L. Setting the optimal laser power for sustainable powder bed fusion processing of elastomeric polyesters: a combined experimental and theoretical study. *Materials (Basel)* **2022**;15:385.
47. Awad A, Fina F, Goyanes A, Gaisford S, Basit AW. 3D printing: principles and pharmaceutical applications of selective laser sintering. *Int J Pharm* **2020**;586:119594.
48. Roskies M, Jordan JO, Fang D, Abdallah M-N, Hier MP, Mlynarek A, Tamimi F, Tran SD. Improving PEEK bioactivity for

craniofacial reconstruction using a 3D printed scaffold embedded with mesenchymal stem cells. *J Biomater Appl* **2016**;31:132–9.
49. Williams JM, Adewunmi A, Schek RM, Flanagan CL, Krebsbach PH, Feinberg SE, Hollister SJ, Das S. Bone tissue engineering using polycaprolactone scaffolds fabricated via selective laser sintering. *Biomaterials* **2005**;26:4817–27.
50. Čapek J, Machová M, Fousová M, Kubásek J, Vojtěch D, Fojt J. Highly porous, low elastic modulus 316L stainless steel scaffold prepared by selective laser melting. *Mater Sci Eng C Mater Biol Appl* **2016**;69:631–9.
51. Yang Y, Wang G, Liang H, Gao C, Peng S, Shen L. Additive manufacturing of bone scaffolds. *Int J Bioprint* **2019**;5:1–25.
52. Galati M, Minetola P, Rizza G. Surface roughness characterisation and analysis of the electron beam melting (EBM) process. *Materials (Basel)* **2019**;12:2211.
53. Tamayo JA, Riascos M, Vargas CA, Baena LM. Additive manufacturing of Ti6Al4V alloy via electron beam melting for the development of implants for the biomedical industry. *Heliyon* **2021**;7:e06892.
54. Murr LE, Amato KN, Li SJ, Tian YX, Cheng XY, Gaytan SM, Martinez E, Shindo PW, Medina F, Wicker RB. Microstructure and mechanical properties of open-cellular biomaterials prototypes for total knee replacement implants fabricated by electron beam melting. *J Mech Behav Biomed Mater* **2011**;4:1396–411.
55. Fousová M, Vojtěch D, Doubrava K, Daniel M, Lin CF. Influence of inherent surface and internal defects on mechanical properties of additively manufactured Ti6Al4V alloy: comparison between selective laser melting and electron beam melting. *Materials* **2018**;11:537.
56. Jang TS, Kim DE, Han G, Yoon CB, Jung HD. Powder based additive manufacturing for biomedical application of titanium and its alloys: a review. *Biomed Eng Lett* **2020**;10:505–16.
57. Zhang H, Chen Z, He Y, Guo X, Li Q, Ji S, Zhao Y, Li D. High performance NbMoTa-Al(2)O(3) multilayer composite structure manufacturing by laser directed energy deposition. *Materials (Basel)* **2021**;14:1685.
58. Balla VK, Bodhak S, Bose S, Bandyopadhyay A. Porous tantalum structures for bone implants: fabrication, mechanical and in vitro biological properties. *Acta Biomater* **2010**;6:3349–59.
59. Marattukalam JJ, Singh AK, Datta S, Das M, Balla VK, Bontha S, Kalpathy SK. Microstructure and corrosion behavior of laser processed NiTi alloy. *Mater Sci Eng C Mater Biol Appl* **2015**;57:309–13.
60. Xue W, Krishna BV, Bandyopadhyay A, Bose S. Processing and biocompatibility evaluation of laser processed porous titanium. *Acta Biomater* **2007**;3:1007–18.
61. Zhang L, Yang G, Johnson BN, Jia X. Three-dimensional (3D) printed scaffold and material selection for bone repair. *Acta Biomater* **2019**;84:16–33.
62. Jungst T, Smolan W, Schacht K, Scheibel T, Groll J. Strategies and molecular design criteria for 3D printable hydrogels. *Chem Rev* **2016**;116:1496–539.
63. Holzapfel BM, Rudert M, Hutmacher DW. [Scaffold-based bone tissue engineering.]. *Orthopäde* **2017**;46:701–10.
64. Tharakan S, Khondkar S, Ilyas A. Bioprinting of stem cells in multimaterial scaffolds and their applications in bone tissue engineering. *Sensors (Basel, Switzerland)* **2021**;21:7477.
65. Lim KS, Levato R, Costa PF, Castilho MD, Alcala-Orozco CR, van Dorenmalen KMA, Melchels FPW, Gawlitta D, Hooper GJ, Malda J, Woodfield TBF. Bio-resin for high resolution lithography-based biofabrication of complex cell-laden constructs. *Biofabrication* **2018**;10:034101.
66. Kang HJ, Hossain M, Park SS, Bin IS, Lee BT. Microstructures and biological properties of 3D-printed titanium intervertebral spacer with the tri-calcium phosphate loaded demineralized bone matrix hydrogel. *Mater Lett* **2021**;303:130519.
67. Amin Yavari S, Ahmadi SM, van der Stok J, Wauthle R, Riemslag AC, Janssen M, Schrooten J, Weinans H, Zadpoor AA. Effects of bio-functionalizing surface treatments on the mechanical behavior of open porous titanium biomaterials. *J Mech Behav Biomed Mater* **2014**;36:109–19.
68. Attar H, Ehtemam-Haghighi S, Soro N, Kent D, Dargusch MS. Additive manufacturing of low-cost porous titanium-based composites for biomedical applications: advantages, challenges and opinion for future development. *J Alloys Compounds* **2020**;827:154263.
69. Velásquez-García LF, Kornbluth Y. Biomedical applications of metal 3D printing. *Annu Rev Biomed Eng* **2021**;23:307–38.
70. Tang Y, Zhou X, Zhang Q, Chen L, Zhao K, Wu Z. Enhanced mechanical properties of porous titanium implants via in-situ synthesized titanium carbide in lamellar pore walls. *Ceram Int* **2022**;48:5083–90.
71. Pramanik S, Agarwal AK, Rai KN. Chronology of total hip joint replacement and materials development. *Trends Biomater Artif Organs* **2005**;19:15–26.
72. Geis-Gerstorfer J, Sauer KH, Pässler K. Ion release from Ni-Cr-Mo and Co-Cr-Mo casting alloys. *Int J Prosthodont* **1991**;4:152–8.
73. Geis-Gerstorfer J, Weber H. In vitro corrosion behavior of four Ni-Cr dental alloys in lactic acid and sodium chloride solutions. *Dental Mater* **1987**;3:289–95.
74. Al Jabbari YS. Physico-mechanical properties and prosthodontic applications of Co-Cr dental alloys: a review of the literature. *J Adv Prosthodont* **2014**;6:138–45.
75. Chen H, Li H, Zhao Y, Zhang X, Wang Y, Lyu P. Adaptation of removable partial denture frameworks fabricated by selective laser melting. *J Prosthet Dent* **2019**;122:316–24.
76. Dolfini Alexandrino L, Martinez Antunes LH, Jardini Munhoz AL, Ricomini Filho AP, da Silva WJ. Mechanical and surface properties of Co-Cr alloy produced by additive manufacturing for removable partial denture frameworks. *J Prosthet Dent* **2022**;S0022-3913(22)00009-9. doi: 10.1016/j.prosdent.2021.12.019.
77. Kim H, Jang S-H, Kim Y, Son J, Min B, Kim K-H, Kwon T-Y. Microstructures and mechanical properties of Co-Cr dental alloys fabricated by three CAD/CAM-based processing techniques. *Materials* **2016**;9:596.
78. Popov VV, Muller-Kamskii G, Kovalevsky A, Dzhenzhera G, Strokin E, Kolomiets A, Ramon J. Design and 3D-printing of titanium bone implants: brief review of approach and clinical cases. *Biomed Eng Lett* **2018**;8:337–44.
79. Toop N, Gifford C, Motiei-Langroudi R, Farzadi A, Boulter D, Forghani R, Farhadi HF. Can activated titanium interbody cages accelerate or enhance spinal fusion? A review of the literature and a design for clinical trials. *J Mater Sci: Mater Med* **2022**;33:33.
80. Alghamdi HS, Jansen JA. The development and future of dental implants. *Dent Mater J* **2020**;39:167–72.
81. Eisenbarth E, Velten D, Müller M, Thull R, Breme J. Biocompatibility of beta-stabilizing elements of titanium alloys. *Biomaterials* **2004**;25:5705–13.
82. Narra SP, Mittwede PN, DeVincent Wolf S, Urish KL. Additive manufacturing in total joint arthroplasty. *Orthop Clin North Am* **2019**;50:13–20.
83. Jing Z, Zhang T, Xiu P, Cai H, Wei Q, Fan D, Lin X, Song C, Liu Z. Functionalization of 3D-printed titanium alloy orthopedic implants: a literature review. *Biomed Mater* **2020**;15:052003.

84. Buser D, Janner SFM, Wittneben J-G, Brägger U, Ramseier CA, Salvi GE. 10-year survival and success rates of 511 titanium implants with a sandblasted and acid-etched surface: a retrospective study in 303 partially edentulous patients. *Clin Implant Dent Relat Res* **2012**;14:839–51.
85. Fischer K, Stenberg T. Prospective 10-year cohort study based on a randomized controlled trial (RCT) on implant-supported full-arch maxillary prostheses. Part 1: sandblasted and acid-etched implants and mucosal tissue. *Clin Implant Dent Relat Res* **2012**;14:808–15.
86. Schwarz F, Derks J, Monje A, Wang H-L. Peri-implantitis. *J Periodontol* **2018**;89(Suppl 1):S267–90.
87. Zhao DW, Ma ZJ, Wang TN, Liu BY. Biocompatible porous tantalum metal plates in the treatment of tibial fracture. *Orthop Surg* **2019**;11:325–9.
88. Fan H, Deng S, Tang W, Muheremu A, Wu X, He P, Tan C, Wang G, Tang J, Guo K, Yang L, Wang F. Highly porous 3D printed tantalum scaffolds have better biomechanical and microstructural properties than titanium scaffolds. *BioMed Res Int* **2021**;2021:1–8.
89. Hua L, Lei T, Qian H, Zhang Y, Hu Y, Lei P. 3D-printed porous tantalum: recent application in various drug delivery systems to repair hard tissue defects. *Expert Opin Drug Deliv* **2021**; 18:625–34.
90. Luo C, Wang C, Wu X, Xie X, Wang C, Zhao C, Zou C, Lv F, Huang W, Liao J. Influence of porous tantalum scaffold pore size on osteogenesis and osteointegration: a comprehensive study based on 3D-printing technology. *Mater Sci Eng C Mater Biol Appl* **2021**;129:112382.
91. Wang H, Su K, Su L, Liang P, Ji P, Wang C. Comparison of 3D-printed porous tantalum and titanium scaffolds on osteointegration and osteogenesis. *Mater Sci Eng C Mater Biol Appl* **2019**;104:109908.
92. Tang HP, Yang K, Jia L, He WW, Yang L, Zhang XZ. Tantalum bone implants printed by selective electron beam manufacturing (SEBM) and their clinical applications. *JOM* **2020**; 72:1016–21.
93. Lu T, Wen J, Qian S, Cao H, Ning C, Pan X, Jiang X, Liu X, Chu PK. Enhanced osteointegration on tantalum-implanted polyetheretherketone surface with bone-like elastic modulus. *Biomaterials* **2015**;51:173–83.
94. Rodzeń K, Sharma PK, McIlhagger A, Mokhtari M, Dave F, Tormey D, Sherlock R, Meenan BJ, Boyd A. The direct 3D printing of functional PEEK/hydroxyapatite composites via a fused filament fabrication approach. *Polymers* **2021**;13:545–18.
95. Tang Z, Xie Y, Yang F, Huang Y, Wang C, Dai K, Zheng X, Zhang X. Porous tantalum coatings prepared by vacuum plasma spraying enhance BMSCs osteogenic differentiation and bone regeneration in vitro and in vivo. *PLoS ONE* **2013**;8:e66263.
96. Wang L, Hu X, Ma X, Ma Z, Zhang Y, Lu Y, Li X, Lei W, Feng Y. Promotion of osteointegration under diabetic conditions by tantalum coating-based surface modification on 3-dimensional printed porous titanium implants. *Colloids Surf B Biointerfaces* **2016**;148:440–52.
97. Henderson SE, Verdelis K, Maiti S, Pal S, Chung WL, Chou D-T, Kumta PN, Almarza AJ. Magnesium alloys as a biomaterial for degradable craniofacial screws. *Acta Biomater* **2014**;10:2323–32.
98. Oliver AA, Sikora-Jasinska M, Demir AG, Guillory RJ. Recent advances and directions in the development of bioresorbable metallic cardiovascular stents: insights from recent human and in vivo studies. *Acta Biomater* **2021**;127:1–23.
99. Lee J-W, Han H-S, Han K-J, Park J, Jeon H, Ok M-R, Seok H-K, Ahn J-P, Lee KE, Lee D-H, Yang S-J, Cho S-Y, Cha P-R, Kwon H, Nam T-H, Han JHL, Rho H-J, Lee K-S, Kim Y-C, Mantovani D. Long-term clinical study and multiscale analysis of in vivo biodegradation mechanism of Mg alloy. *Proc Natl Acad Sci USA* **2016**;113:716–21.
100. Bär F, Berger L, Jauer L, Kurtuldu G, Schäublin R, Schleifenbaum JH, Löffler JF. Laser additive manufacturing of biodegradable magnesium alloy WE43: a detailed microstructure analysis. *Acta Biomater* **2019**;98:36–49.
101. Guo J, Zhou Y, Liu C, Wu Q, Chen X, Lu J. Wire arc additive manufacturing of AZ31 magnesium alloy: grain refinement by adjusting pulse frequency. *Materials (Basel)* **2016**;9:823.
102. Rössig C, Angrisani N, Helmecke P, Besdo S, Seitz J-M, Welke B, Fedchenko N, Kock H, Reifenrath J. In vivo evaluation of a magnesium-based degradable intramedullary nailing system in a sheep model. *Acta Biomater* **2015**;25:369–83.
103. Bobe K, Willbold E, Morgenthal I, Andersen O, Studnitzky T, Nellesen J, Tillmann W, Vogt C, Vano K, Witte F. In vitro and in vivo evaluation of biodegradable, open-porous scaffolds made of sintered magnesium W4 short fibres. *Acta Biomater* **2013**;9:8611–23.
104. Farraro KF, Sasaki N, Woo SL-Y, Kim KE, Tei MM, Speziali A, McMahon PJ. Magnesium ring device to restore function of a transected anterior cruciate ligament in the goat stifle joint. *J Orthop Res* **2016**;34:2001–8.
105. Grün NG, Holweg P, Tangl S, Eichler J, Berger L, van den Beucken J, Löffler JF, Klestil T, Weinberg AM. Comparison of a resorbable magnesium implant in small and large growing-animal models. *Acta Biomater* **2018**;78:378–86.
106. Windhagen H, Radtke K, Weizbauer A, Diekmann J, Noll Y, Kreimeyer U, Schavan R, Stukenborg-Colsman C, Waizy H. Biodegradable magnesium-based screw clinically equivalent to titanium screw in hallux valgus surgery: short term results of the first prospective, randomized, controlled clinical pilot study. *BioMed Eng OnLine* **2013**;12:1.
107. Wang JL, Xu JK, Hopkins C, Chow DHK, Qin L. Biodegradable magnesium-based implants in orthopedics—a general review and perspectives. *Adv Sci* **2020**;7:1902443.
108. Yu X, Zhao D, Huang S, Wang B, Zhang X, Wang W, Wei X. Biodegradable magnesium screws and vascularized iliac grafting for displaced femoral neck fracture in young adults. *BMC Musculoskelet Disord* **2015**;16:329.
109. Zhao D, Huang S, Lu F, Wang B, Yang L, Qin L, Yang K, Li Y, Li W, Wang W, Tian S, Zhang X, Gao W, Wang Z, Zhang Y, Xie X, Wang J, Li J. Vascularized bone grafting fixed by biodegradable magnesium screw for treating osteonecrosis of the femoral head. *Biomaterials* **2016**;81:84–92.
110. Alipal J, Mohd Pu'ad NAS, Nayan NHM, Sahari N, Abdullah HZ, Idris MI, Lee TC. An updated review on surface functionalisation of titanium and its alloys for implants applications. *Mater Today: Proc* **2021**;42:270–82.
111. Wang X, Xu S, Zhou S, Xu W, Leary M, Choong P, Qian M, Brandt M, Xie YM. Topological design and additive manufacturing of porous metals for bone scaffolds and orthopaedic implants: a review. *Biomaterials* **2016**;83:127–41.
112. Zhang Y, Gulati K, Li Z, Di P, Liu Y. Dental implant nano-engineering: advances, limitations and future directions. *Nanomaterials (Basel)* **2021**;11:2489.
113. Soylu HM, Chevallier P, Copes F, Ponti F, Candiani G, Yurt F, Mantovani D. A novel strategy to coat dopamine-functionalized titanium surfaces with agarose-based hydrogels for the controlled release of gentamicin. *Front Cell Infect Microbiol* **2021**;11:678081.

114. Park KH, Kim SJ, Jeong YH, Moon HJ, Song HJ, Park YJ. Fabrication and biological properties of calcium phosphate/chitosan composite coating on titanium in modified SBF. *Mater Sci Eng C Mater Biol Appl* **2018**;90:113–8.
115. Nguyen TDT, Jang YS, Kim YK, Kim SY, Lee MH, Bae TS. Osteogenesis-related gene expression and guided bone regeneration of a strontium-doped calcium-phosphate-coated titanium mesh. *ACS Biomater Sci Eng* **2019**;5:6715–24.
116. Jung H-D, Yook S-W, Han C-M, Jang T-S, Kim H-E, Koh Y-H, Estrin Y. Highly aligned porous Ti scaffold coated with bone morphogenetic protein-loaded silica/chitosan hybrid for enhanced bone regeneration. *J Biomed Mater Res B Appl Biomater* **2014**;102:913–21.
117. Guo X, Chen M, Feng W, Liang J, Zhao H, Tian L, Chao H, Zou X. Electrostatic self-assembly of multilayer copolymeric membranes on the surface of porous tantalum implants for sustained release of doxorubicin. *Int J Nanomed* **2011**;6:3057–64.
118. He Y, Li Y, Zuo E, Chai S, Ren X, Fei T, Ma G, Wang X, Liu H. A novel antibacterial titanium modification with a sustained release of pac-525. *Nanomaterials* **2021**;11:3306.
119. Wu K, Liu M, Li N, Zhang L, Meng F, Zhao L, Liu M, Zhang Y. Chitosan-miRNA functionalized microporous titanium oxide surfaces via a layer-by-layer approach with a sustained release profile for enhanced osteogenic activity. *J Nanobiotechnol* **2020**;18:127.
120. Nancy D, Rajendran N. Vancomycin incorporated chitosan/gelatin coatings coupled with TiO(2)-SrHAP surface modified cp-titanium for osteomyelitis treatment. *Int J Biol Macromol* **2018**;110:197–205.
121. Carpenter K, Tabei A. On residual stress development, prevention, and compensation in metal additive manufacturing. *Materials* **2020**;13:255.
122. Ye C, Zhang C, Zhao J, Dong Y. Effects of post-processing on the surface finish, porosity, residual stresses, and fatigue performance of additive manufactured metals: a review. *J Mater Eng Perform* **2021**;30:6407–25.
123. Raheem AA, Hameed P, Whenish R, Elsen RS, G A, Jaiswal AK, Prashanth KG, Manivasagam G. A review on development of bio-inspired implants using 3D printing. *Biomimetics* **2021**;6:65.
124. Jaber H, Kónya J, Kulcsár K, Kovács T. Effects of annealing and solution treatments on the microstructure and mechanical properties of Ti6Al4V manufactured by selective laser melting. *Materials (Basel)* **2022**;15:1978.
125. Vrancken B, Thijs L, Kruth JP, Van Humbeeck J. Heat treatment of Ti6Al4V produced by selective laser melting: microstructure and mechanical properties. *J Alloys Compounds* **2012**;541:177–85.
126. Rupp F, Liang L, Geis-Gerstorfer J, Scheideler L, Hüttig F. Surface characteristics of dental implants: a review. *Dent Mater* **2018**;34:40–57.
127. John M, Kalvala PR, Misra M, Menezes PL. Peening techniques for surface modification: processes, properties and applications. *Materials* **2021**;14:3841–30.
128. Li N, Li YD, Li YX, Wu YH, Zheng YF, Han Y. Effect of surface mechanical attrition treatment on biodegradable Mg-1Ca alloy. *Mater Sci Eng C Mater Biol Appl* **2014**;35:314–21.
129. Huang R, Zhang L, Huang L, Zhu J. Enhanced in-vitro osteoblastic functions on β-type titanium alloy using surface mechanical attrition treatment. *Mater Sci Eng C Mater Biol Appl* **2019**;97:688–97.
130. Nkonta DT, Drevet R, Fauré J, Benhayoune H. Effect of surface mechanical attrition treatment on the microstructure of cobalt–chromium–molybdenum biomedical alloy. *Microsc Res Tech* **2021**;84:238–45.
131. Lai M, Cai K, Hu Y, Yang X, Liu Q. Regulation of the behaviors of mesenchymal stem cells by surface nanostructured titanium. *Colloids Surf B Biointerfaces* **2012**;97:211–20.
132. Wen M, Wen C, Hodgson P, Li Y. Improvement of the biomedical properties of titanium using SMAT and thermal oxidation. *Colloids Surf B Biointerfaces* **2014**;116:658–65.
133. Lumetti S, Manfredi E, Ferraris S, Spriano S, Passeri G, Ghiacci G, Macaluso G, Galli C. The response of osteoblastic MC3T3-E1 cells to micro- and nano-textured, hydrophilic and bioactive titanium surfaces. *J Mater Sci Mater Med* **2016**;27:68.
134. Vishnu J, K Manivasagam V, Gopal V, Bartomeu Garcia C, Hameed P, Manivasagam G, Webster TJ. Hydrothermal treatment of etched titanium: a potential surface nanomodification technique for enhanced biocompatibility. *Nanomedicine* **2019**;20:102016.
135. Yuan Z, Liu P, Liang Y, Tao B, He Y, Hao Y, Yang W, Hu Y, Cai K. Investigation of osteogenic responses of Fe-incorporated micro/nano-hierarchical structures on titanium surfaces. *J Mater Chem B* **2018**;6:1359–72.
136. Müller F, Al-Nawas B, Storelli S, Quirynen M, Hicklin S, Castro-Laza J, Bassetti R, Schimmel M; On behalf of the Roxolid Study Group. Small-diameter titanium grade IV and titanium-zirconium implants in edentulous mandibles: five-year results from a double-blind, randomized controlled trial. *BMC Oral Health* **2015**;15:1–10.
137. Hotchkiss KM, Reddy GB, Hyzy SL, Schwartz Z, Boyan BD, Olivares-Navarrete R. Titanium surface characteristics, including topography and wettability, alter macrophage activation. *Acta Biomater* **2016**;31:425–34.
138. Wang Q, Wang W, Li Y, Li W, Tan L, Yang K. Biofunctional magnesium coating of implant materials by physical vapour deposition. *Biomater Transl* **2021**;2:248–56.
139. Ballo AM, Bjöörn D, Astrand M, Palmquist A, Lausmaa J, Thomsen P. Bone response to physical-vapour-deposited titanium dioxide coatings on titanium implants. *Clin Oral Implants Res* **2013**;24:1009–17.
140. Kim B-S, Kim JS, Park YM, Choi B-Y, Lee J. Mg ion implantation on SLA-treated titanium surface and its effects on the behavior of mesenchymal stem cell. *Mater Sci Eng C Mater Biol Appl* **2013**;33:1554–60.
141. Hannig M, Kriener L, Hoth-Hannig W, Becker-Willinger C, Schmidt H. Influence of nanocomposite surface coating on biofilm formation in situ. *j Nanosci Nanotechnol* **2007**;7:4642–8.
142. Kligman S, Ren Z, Chung C-H, Perillo MA, Chang Y-C, Koo H, Zheng Z, Li C. The impact of dental implant surface modifications on osseointegration and biofilm formation. *JCM* **2021**;10:1641.
143. Zhong J, Li X, Yao Y, Zhou J, Cao S, Zhang X, Jian Y, Zhao K. Effect of acid-alkali treatment on serum protein adsorption and bacterial adhesion to porous titanium. *J Mater Sci Mater Med* **2022**;33:20.
144. Zhao G, Schwartz Z, Wieland M, Rupp F, Geis-Gerstorfer J, Cochran DL, Boyan BD. High surface energy enhances cell response to titanium substrate microstructure. *J Biomed Mater Res A* **2005**;74:49–58.
145. Polo-Corrales L, Latorre-Esteves M, Ramirez-Vick JE. Scaffold design for bone regeneration. *J Nanosci Nanotechnol* **2014**;14:15–56.
146. Jiang H, Zhang T, Zhou W, Lin Z, Liu Z. Effect of plasma oxidation-treated TiOx film on early osseointegration. *Int J Oral Maxillofac Implants* **2018**;33:1011–8.

147. Feller L, Jadwat Y, Khammissa RAG, Meyerov R, Schechter I, Lemmer J. Cellular responses evoked by different surface characteristics of intraosseous titanium implants. *Biomed Res Int* **2015**;2015:171945.
148. Al-Radha ASD, Dymock D, Younes C, O'Sullivan D. Surface properties of titanium and zirconia dental implant materials and their effect on bacterial adhesion. *J Dent* **2012**;40:146–53.
149. Ribeiro AR, Oliveira F, Boldrini LC, Leite PE, Falagan-Lotsch P, Linhares ABR, Zambuzzi WF, Fragneaud B, Campos APC, Gouvêa CP, Archanjo BS, Achete CA, Marcantonio E, Rocha LA, Granjeiro JM. Micro-arc oxidation as a tool to develop multifunctional calcium-rich surfaces for dental implant applications. *Mater Sci Eng C Mater Biol Appl* **2015**;54:196–206.
150. Shah FA, Thomsen P, Palmquist A. Osseointegration and current interpretations of the bone-implant interface. *Acta Biomater* **2019**;84:1–15.
151. Huang Q, Liu X, Elkhooly TA, Zhang R, Yang X, Shen Z, Feng Q. Preparation and characterization of TiO2/silicate hierarchical coating on titanium surface for biomedical applications. *Mater Sci Eng C Mater Biol Appl* **2016**;60:308–16.
152. Dohan Ehrenfest DM, Coelho PG, Kang B-S, Sul Y-T, Albrektsson T. Classification of osseointegrated implant surfaces: materials, chemistry and topography. *Trends Biotechnol* **2010**;28:198–206.
153. Civantos A, Martínez-Campos E, Ramos V, Elvira C, Gallardo A, Abarrategi A. Titanium coatings and surface modifications: toward clinically useful bioactive implants. *ACS Biomater Sci Eng* **2017**;3:1245–61.
154. Sedelnikova MB, Komarova EG, Sharkeev YP, Ugodchikova AV, Tolkacheva TV, Rau JV, Buyko EE, Ivanov VV, Sheikin VV. Modification of titanium surface via Ag-, Sr- and Si-containing micro-arc calcium phosphate coating. *Bioact Mater* **2019**;4:224–35.
155. Zhou L, Pan M, Zhang Z, Diao Z, Peng X. Enhancing osseointegration of TC4 alloy by surficial activation through biomineralization method. *Front Bioeng Biotechnol* **2021**;9:639835.
156. Yang J, Zhang K, Que K, Hou S, Chen Z, Li Y, Wang Y, Song Y, Guan B, Zhang W, Zhu D, Li C, Wang D, Geng P, Zhang X. Surface modification of titanium with hydroxyapatite layer induced by phase-transited lysozyme coating. *Mater Sci Eng C Mater Biol Appl* **2018**;92:206–15.
157. Chen Y-L, Lin T, Liu A, Shi M-M, Hu B, Shi Z-l, Yan S-G. Does hydroxyapatite coating have no advantage over porous coating in primary total hip arthroplasty? A meta-analysis. *J Orthop Surg Res* **2015**;10:21. doi: 10.1186/s13018-015-0161-4.
158. Jung JH, Kim SY, Yi YJ, Lee BK, Kim YK. Hydroxyapatite-coated implant: clinical prognosis assessment via a retrospective followup study for the average of 3 years. *J Adv Prosthodont* **2018**;10:85–92.
159. Simmons DE, Palaiologou A, Teitelbaum AG, Billiot S, Popat LJ, Maney P. Immediate and early loading of hydrothermally treated, hydroxyapatite-coated dental implants: 2-year results from a prospective clinical study. *J Oral Implantol* **2016**;42:17–25.
160. Sun Y, Zhang X, Luo M, Hu W, Zheng L, Huang R, Greven J, Hildebrand F, Yuan F. Plasma spray vs. electrochemical deposition: toward a better osteogenic effect of hydroxyapatite coatings on 3D-Printed titanium scaffolds. *Front Bioeng Biotechnol* **2021**;9:1–16.
161. Wei M, Ruys AJ, Milthorpe BK, Sorrell CC. Precipitation of hydroxyapatite nanoparticles: effects of precipitation method on electrophoretic deposition. *J Mater Sci: Mater Med* **2005**;16:319–24.
162. Jaafar A, Hecker C, Árki P, Joseph Y. Sol-gel derived hydroxyapatite coatings for titanium implants: a review. *Bioengineering* **2020**;7:127–3.
163. Dinda GP, Shin J, Mazumder J. Pulsed laser deposition of hydroxyapatite thin films on Ti-6Al-4V: effect of heat treatment on structure and properties. *Acta Biomater* **2009**;5:1821–30.
164. Chen C, Li H, Kong X, Zhang S-M, Lee I-S. Immobilizing osteogenic growth peptide with and without fibronectin on a titanium surface: effects of loading methods on mesenchymal stem cell differentiation. *Int J Nanomed* **2015**;10:283–95.
165. Lu M, Chen H, Yuan B, Zhou Y, Min L, Xiao Z, Zhu X, Tu C, Zhang X. Electrochemical deposition of nanostructured hydroxyapatite coating on titanium with enhanced early stage osteogenic activity and osseointegration. *IJN* **2020**;15:6605–18.
166. Ke D, Vu AA, Bandyopadhyay A, Bose S. Compositionally graded doped hydroxyapatite coating on titanium using laser and plasma spray deposition for bone implants. *Acta Biomater* **2019**;84:414–23.
167. Cui FZ, Luo ZS, Feng QL. Highly adhesive hydroxyapatite coatings on titanium alloy formed by ion beam assisted deposition. *J Mater Sci Mater Med* **1997**;8:403–5.
168. Chen C, Qiu ZY, Zhang SM, Lee IS. Biomimetic fibronectin/mineral and osteogenic growth peptide/mineral composites synthesized on calcium phosphate thin films. *Chem Commun (Camb)* **2011**;47:11056–8.
169. Choi JM, Kim HE, Lee IS. Ion-beam-assisted deposition (IBAD) of hydroxyapatite coating layer on Ti-based metal substrate. *Biomaterials* **2000**;21:469–73.
170. Bigi A, Boanini E, Bracci B, Facchini A, Panzavolta S, Segatti F, Sturba L. Nanocrystalline hydroxyapatite coatings on titanium: a new fast biomimetic method. *Biomaterials* **2005**;26:4085–9.
171. Wang X, Mei L, Jiang X, Jin M, Xu Y, Li J, Li X, Meng Z, Zhu J, Wu F. Hydroxyapatite-coated titanium by micro-arc oxidation and steam–hydrothermal treatment promotes osseointegration. *Front Bioeng Biotechnol* **2021**;9:1–12.
172. Eliaz N, Metoki N. Calcium phosphate bioceramics: a review of their history, structure, properties, coating technologies and biomedical applications. *Materials (Basel)* **2017**;10:334.
173. Le Guéhennec L, Soueidan A, Layrolle P, Amouriq Y. Surface treatments of titanium dental implants for rapid osseointegration. *Dent Mater* **2007**;23:844–54.
174. Sun L, Berndt CC, Gross KA, Kucuk A. Material fundamentals and clinical performance of plasma-sprayed hydroxyapatite coatings: a review. *J Biomed Mater Res* **2001**;58:570–92.
175. Wang G, Brewer JR, Namavar F, Sabirianov RF, Haider H, Garvin KL, Cheung CL. Structural study of titanium oxide films synthesized by ion beam-assisted deposition. *Scanning* **2008**;30:59–64.
176. Utke I, Michler J, Winkler R, Plank H. Mechanical properties of 3D nanostructures obtained by focused electron/ion beam-induced deposition: a review. *Micromachines* **2020**;11:397.
177. Liu Y, Layrolle P, de Bruijn J, van Blitterswijk C, de Groot K. Biomimetic coprecipitation of calcium phosphate and bovine serum albumin on titanium alloy. *J Biomed Mater Res* **2001**;57:327–35.
178. Chen C, Lee I-S, Zhang S-M, Yang HC. Biomimetic apatite formation on calcium phosphate-coated titanium in Dulbecco's phosphate-buffered saline solution containing CaCl(2) with and without fibronectin. *Acta Biomater* **2010**;6:2274–81.
179. Puleo DA, Nanci A. Understanding and controlling the bone-implant interface. *Biomaterials* **1999**;20:2311–21.

180. Xiu P, Jia Z, Lv J, Yin C, Cheng Y, Zhang K, Song C, Leng H, Zheng Y, Cai H, Liu Z. Tailored surface treatment of 3D printed porous Ti6Al4V by microarc oxidation for enhanced osseointegration via optimized bone in-growth patterns and interlocked bone/implant interface. *ACS Appl Mater Interfaces* **2016**;8:17964–75.
181. Li Y, Yang W, Li X, Zhang X, Wang C, Meng X, Pei Y, Fan X, Lan P, Wang C, Li X, Guo Z. Improving osteointegration and osteogenesis of three-dimensional porous Ti6Al4V scaffolds by polydopamine-assisted biomimetic hydroxyapatite coating. *ACS Appl Mater Interfaces* **2015**;7:5715–24.
182. Zhao Z, Gao W, Bai H. A mineral layer as an effective binder to achieve strong bonding between a hydrogel and a solid titanium substrate. *J Mater Chem B* **2018**;6:3859–64.
183. Yang J, Liu F, Zhou C, Li H, Yang G, Fang S, Lee I-S, Liu Y, Bai H, Chen C. Journal of materials science & technology 3D printed porous titanium filled with mineralized UV-responsive chitosan hydrogel promotes cell proliferation and osteogenesis in vitro. *J Mater Sci Technol* **2023**;142:34–44.
184. Sánchez-Bodón J, Del Olmo JA, Alonso JM, Moreno-Benítez I, Vilas-Vilela JL, Pérez-Álvarez L. Bioactive coatings on titanium: a review on hydroxylation, self-assembled monolayers (SAMs) and surface modification strategies. *Polymers* **2021**;14:165.
185. Kumari S, Tiyyagura HR, Pottathara YB, Sadasivuni KK, Ponnamma D, Douglas TE, Skirtach AG, Mohan MK. Surface functionalization of chitosan as a coating material for orthopaedic applications: a comprehensive review. *Carbohydr Polym* **2021**;255:117487.
186. Qi H, Chen Q, Ren H, Wu X, Liu X, Lu T. Electrophoretic deposition of dexamethasone-loaded gelatin nanospheres/chitosan coating and its dual function in anti-inflammation and osteogenesis. *Colloids Surf B Biointerfaces* **2018**;169:249–56.
187. Abinaya B, Prasith TP, Ashwin B, Viji Chandran S, Selvamurugan N. Chitosan in surface modification for bone tissue engineering applications. *Biotechnol J* **2019**;14:e1900171.
188. Ding I, Shendi DM, Rolle MW, Peterson AM. Growth-factor-releasing polyelectrolyte multilayer films to control the cell culture environment. *Langmuir* **2018**;34:1178–89.
189. del Mercato LL, Ferraro MM, Baldassarre F, Mancarella S, Greco V, Rinaldi R, Leporatti S. Biological applications of LbL multilayer capsules: from drug delivery to sensing. *Adv Colloid Interface Sci* **2014**;207:139–54.
190. Koenig O, Neumann B, Schlensak C, Wendel HP, Nolte A. Hyaluronic acid/poly(ethylenimine) polyelectrolyte multilayer coatings for siRNA-mediated local gene silencing. *PLoS One* **2019**;14:e0212584.
191. Han L, Wang M, Sun H, Li P, Wang K, Ren F, Lu X. Porous titanium scaffolds with self-assembled micro/nano-hierarchical structure for dual functions of bone regeneration and anti-infection. *J Biomed Mater Res* **2017**;105:3482–92.
192. Li W, Yang Y, Zhang H, Xu Z, Zhao L, Wang J. Improvements on biological and antimicrobial properties of titanium modified by AgNPs-loaded chitosan-heparin polyelectrolyte multilayers. *J Mater Sci Mater Med* **2019**;30:52.
193. Song W, Seta J, Chen L, Bergum C, Zhou Z, Kanneganti P, Kast RE, Auner GW, Shen M, Markel DC, Ren W, Yu X. Doxycycline-loaded coaxial nanofiber coating of titanium implants enhances osseointegration and inhibits *Staphylococcus aureus* infection. *Biomed Mater* **2017**;12:045008.
194. Zhang L, Yan J, Yin Z, Tang C, Guo Y, Li D, Wei B, Xu Y, Gu Q, Wang L. Electrospun vancomycin-loaded coating on titanium implants for the prevention of implant-associated infections. *Int J Nanomed* **2014**;9:3027–36.
195. Kim YK, Lee KB, Kim SY, Jang YS, Kim JH, Lee MH. Improvement of osteogenesis by a uniform PCL coating on a magnesium screw for biodegradable applications. *Sci Rep* **2018**;8:1–11.
196. Tian P, Xu D, Liu X. Mussel-inspired functionalization of PEO/PCL composite coating on a biodegradable AZ31 magnesium alloy. *Colloids Surf B Biointerfaces* **2016**;141:327–37.
197. Karageorgiou V, Kaplan D. Porosity of 3D biomaterial scaffolds and osteogenesis. *Biomaterials* **2005**;26:5474–91.
198. Wu C, Chang J. A review of bioactive silicate ceramics. *Biomed Mater* **2013**;8:032001.
199. Samavedi S, Whittington AR, Goldstein AS. Calcium phosphate ceramics in bone tissue engineering: a review of properties and their influence on cell behavior. *Acta Biomater* **2013**;9:8037–45.
200. Kowal TJ, Golovchak R, Chokshi T, Harms J, Thamma U, Jain H, Falk MM. Role of phase separation on the biological performance of 45S5 bioglass(®). *J Mater Sci Mater Med* **2017**;28:161.
201. Hajiali H, Hosseinalipour M, Karbasi S, Shokrgozar MA. The influence of bioglass nanoparticles on the biodegradation and biocompatibility of poly (3-hydroxybutyrate) scaffolds. *Int J Artif Organs* **2012**;35:1015–24.
202. Zhang H, Liu S, Xiao H, Zhang X. Synthesis and tribological properties of bio-inspired Nacre-like composites. *Materials* **2018**;11:1563.
203. Spirandeli BR, Ribas RG, Amaral SS, Martins EF, Esposito E, Vasconcellos LMR, Campos TMB, Thim GP, Trichês ES. Incorporation of 45S5 bioglass via sol-gel in β-TCP scaffolds: bioactivity and antimicrobial activity evaluation. *Mater Sci Eng C Mater Biol Appl* **2021**;131:112453.
204. Lin K, Sheikh R, Romanazzo S, Roohani I. 3D printing of bioceramic scaffolds—barriers to the clinical translation: from promise to reality. *Materials* **2019**;12:2660.
205. Trombetta R, Inzana JA, Schwarz EM, Kates SL, Awad HA. 3D printing of calcium phosphate ceramics for bone tissue engineering and drug delivery. *Ann Biomed Eng* **2017**;45:23–44.
206. Zhou H, Lee J. Nanoscale hydroxyapatite particles for bone tissue engineering. *Acta Biomater* **2011**;7:2769–81.
207. Qayoom I, Teotia AK, Meena M, Singh P, Mishra A, Singh S, Kumar A. Enhanced bone mineralization using hydroxyapatite-based ceramic bone substitute incorporating *Withania somnifera* extracts. *Biomed Mater* **2020**;15:055015.
208. Khotib J, Gani MA, Budiatin AS, Lestari MLAD, Rahadiansyah E, Ardianto C. Signaling pathway and transcriptional regulation in osteoblasts during bone healing: direct involvement of hydroxyapatite as a biomaterial. *Pharmaceuticals (Basel)*. **2021**;14:615.
209. Song Y, Wu H, Gao Y, Li J, Lin K, Liu B, Lei X, Cheng P, Zhang S, Wang Y, Sun J, Bi L, Pei G. Zinc silicate/nano-hydroxyapatite/collagen scaffolds promote angiogenesis and bone regeneration via the p38 MAPK pathway in activated monocytes. *ACS Appl Mater Interfaces* **2020**;12:16058–75.
210. Fernandes MH, Alves MM, Cebotarenco M, Ribeiro IA, Grenho L, Gomes PS, Carmezim MJ, Santos CF. Citrate zinc hydroxyapatite nanorods with enhanced cytocompatibility and osteogenesis for bone regeneration. *Mater Sci Eng C Mater Biol Appl* **2020**;115:111147.
211. Tronco MC, Cassel JB, Dos Santos LA. α-TCP-based calcium phosphate cements: a critical review. *Acta Biomater* **2022**;151:70–87.
212. Gallinetti S, Canal C, Ginebra M-P, Ferreira J. Development and characterization of biphasic hydroxyapatite/β-TCP cements. *J Am Ceram Soc* **2014**;97:1065–73.

213. Bohner M, Santoni BLG, Döbelin N. β-Tricalcium phosphate for bone substitution: synthesis and properties. *Acta Biomater* **2020**;113:23–41.
214. Zhao N, Wang Y, Qin L, Guo Z, Li D. Effect of composition and macropore percentage on mechanical and in vitro cell proliferation and differentiation properties of 3D printed HA/β-TCP scaffolds. *RSC Adv* **2017**;7:43186–96.
215. Liu F, Liu Y, Li X, Wang X, Li D, Chung S, Chen C, Lee I-S. Osteogenesis of 3D printed macro-pore size biphasic calcium phosphate scaffold in rabbit calvaria. *J Biomater Appl* **2019**;33:1168–77.
216. Bertol LS, Schabbach R, Dos Santos LAL. Dimensional evaluation of patient-specific 3D printing using calcium phosphate cement for craniofacial bone reconstruction. *J Biomater Appl* **2017**;31:799–806.
217. Wu Q, Wang X, Jiang F, Zhu Z, Wen J, Jiang X. Study of Sr-Ca-Si-based scaffolds for bone regeneration in osteoporotic models. *Int J Oral Sci* **2020**;12:25.
218. Wang CY, Chiu YC, Lee AKX, Lin YA, Lin PY, Shie MY. Article biofabrication of gingival fibroblast cell-laden collagen/strontium-doped calcium silicate 3d-printed bi-layered scaffold for osteoporotic periodontal regeneration. *Biomedicines* **2021**;9:431.
219. Shie M-Y, Ding S-J. Integrin binding and MAPK signal pathways in primary cell responses to surface chemistry of calcium silicate cements. *Biomaterials* **2013**;34:6589–606.
220. Chen YW, Hsu TT, Wang K, Shie MY. Preparation of the fast setting and degrading Ca-Si-Mg cement with both odontogenesis and angiogenesis differentiation of human periodontal ligament cells. *Mater Sci Eng C Mater Biol Appl* **2016**;60:374–83.
221. He F, Lu T, Fang X, Li Y, Zuo F, Deng X, Ye J. Effects of strontium amount on the mechanical strength and cell-biological performance of magnesium-strontium phosphate bioceramics for bone regeneration. *Mater Sci Eng C Mater Biol Appl* **2020**;112:110892.
222. Rizwan M, Hamdi M, Basirun WJ. Bioglass® 45S5-based composites for bone tissue engineering and functional applications. *J Biomed Mater Res* **2017**;105:3197–223.
223. Fiume E, Barberi J, Verné E, Baino F. Bioactive glasses: from parent 45S5 composition to scaffold-assisted tissue-healing therapies. *JFB* **2018**;9:24.
224. Rahaman MN, Liu X, Bal BS, Day DE, Bi L, Bonewald LF. Bioactive glass in bone tissue engineering. *Ceram Trans* **2012**;237:73–82.
225. Wetzel R, Blochberger M, Scheffler F, Hupa L, Brauer DS. Mg or Zn for Ca substitution improves the sintering of bioglass 45S5. *Sci Rep* **2020**;10:1–10.
226. Huang W, Day DE, Kittiratanapiboon K, Rahaman MN. Kinetics and mechanisms of the conversion of silicate (45S5), borate, and borosilicate glasses to hydroxyapatite in dilute phosphate solutions. *J Mater Sci: Mater Med* **2006**;17:583–96.
227. Huan Z, Leeflang S, Zhou J, Zhai W, Chang J, Duszczyk J. In vitro degradation behavior and bioactivity of magnesium-Bioglass(®) composites for orthopedic applications. *J Biomed Mater Res B Appl Biomater* **2012**;100:437–46.
228. Aitasalo KMJ, Piitulainen JM, Rekola J, Vallittu PK. Craniofacial bone reconstruction with bioactive fiber-reinforced composite implant. *Head Neck* **2014**;36:722–8.
229. Wu C, Zhang Y, Zhou Y, Fan W, Xiao Y. A comparative study of mesoporous glass/silk and non-mesoporous glass/silk scaffolds: physiochemistry and in vivo osteogenesis. *Acta Biomater* **2011**;7:2229–36.
230. Sepulveda P, Jones JR, Hench LL. Characterization of melt-derived 45S5 and sol-gel-derived 58S bioactive glasses. *J Biomed Mater Res* **2001**;58:734–40.
231. Zhang J, Zhao S, Zhu Y, Huang Y, Zhu M, Tao C, Zhang C. Three-dimensional printing of strontium-containing mesoporous bioactive glass scaffolds for bone regeneration. *Acta Biomater* **2014**;10:2269–81.
232. Qi X, Pei P, Zhu M, Du X, Xin C, Zhao S, Li X, Zhu Y. Three dimensional printing of calcium sulfate and mesoporous bioactive glass scaffolds for improving bone regeneration in vitro and in vivo. *Sci Rep* **2017**;7:42556–13.
233. Song W, Li S, Tang Q, Chen L, Yuan Z. In vitro biocompatibility and bioactivity of calcium silicate-based bioceramics in endodontics (review). *Int J Mol Med* **2021**;48:48.
234. Zhao C, Liu W, Zhu M, Wu C, Zhu Y. Bioceramic-based scaffolds with antibacterial function for bone tissue engineering: a review. *Bioact Mater* **2022**;18:383–98.
235. Charbonnier B, Manassero M, Bourguignon M, Decambron A, El-Hafci H, Morin C, Leon D, Bensidoum M, Corsia S, Petite H, Marchat D, Potier E. Custom-made macroporous bioceramic implants based on triply-periodic minimal surfaces for bone defects in load-bearing sites. *Acta Biomater* **2020**;109:254–66.
236. Bidan CM, Kommareddy KP, Rumpler M, Kollmannsberger P, Fratzl P, Dunlop JWC. Geometry as a factor for tissue growth: towards shape optimization of tissue engineering scaffolds. *Adv Healthc Mater* **2013**;2:186–94.
237. Zadpoor AA. Bone tissue regeneration: the role of scaffold geometry. *Biomater Sci* **2015**;3:231–45.
238. Gariboldi MI, Best SM. Effect of ceramic scaffold architectural parameters on biological response. *Front Bioeng Biotechnol* **2015**;3:1–11.
239. Zhu Y, Liu K, Deng J, Ye J, Ai F, Ouyang H, Wu T, Jia J, Cheng X, Wang X. 3D printed zirconia ceramic hip joint with precise structure and broad-spectrum antibacterial properties. *IJN* **2019**;14:5977–87.
240. Wen Y, Xun S, Haoye M, Baichuan S, Peng C, Xuejian L, Kaihong Z, Xuan Y, Jiang P, Shibi L. 3D printed porous ceramic scaffolds for bone tissue engineering: a review. *Biomater Sci* **2017**;5:1690–8.
241. Ansari MAA, Golebiowska AA, Dash M, Kumar P, Jain PK, Nukavarapu SP, Ramakrishna S, Nanda HS. Engineering biomaterials to 3D-print scaffolds for bone regeneration: practical and theoretical consideration. *Biomater Sci* **2022**;10:2789–816.
242. Shao H, Yang X, He Y, Fu J, Liu L, Ma L, Zhang L, Yang G, Gao C, Gou Z. Bioactive glass-reinforced bioceramic ink writing scaffolds: sintering, microstructure and mechanical behavior. *Biofabrication* **2015**;7:035010.
243. Rumpler M, Woesz A, Dunlop JWC, Van Dongen JT, Fratzl P. The effect of geometry on three-dimensional tissue growth. *J R Soc Interface* **2008**;5:1173–80.
244. Vu AA, Burke DA, Bandyopadhyay A, Bose S. Effects of surface area and topography on 3D printed tricalcium phosphate scaffolds for bone grafting applications. *Additive Manufac* **2021**;39:101870.
245. Luo Y, Zhai D, Huan Z, Zhu H, Xia L, Chang J, Wu C. Three-dimensional printing of Hollow-Struts-Packed bioceramic scaffolds for bone regeneration. *ACS Appl Mater Interfaces* **2015**;7:24377–83.
246. Zhang M, Lin R, Wang X, Xue J, Deng C, Feng C, Zhuang H, Ma J, Qin C, Wan L, Chang J, Wu C. 3D printing of haversian bone-mimicking scaffolds for multicellular delivery in bone regeneration. *Sci Adv* **2020**;6:eaaz6725.
247. Luo S, Wu J, Jia Z, Tang P, Sheng J, Xie C, Liu C, Gan D, Hu D, Zheng W, Lu X. An injectable, bifunctional hydrogel with photothermal effects for tumor therapy and bone regeneration. *Macromol Biosci* **2019**;19:e1900047.

248. Liu X, Miao Y, Liang H, Diao J, Hao L, Shi Z, Zhao N, Wang Y. 3D-printed bioactive ceramic scaffolds with biomimetic micro/nano-HAp surfaces mediated cell fate and promoted bone augmentation of the bone–implant interface in vivo. *Bioact Mater* **2022**;12:120–32.
249. Raymond Y, Bonany M, Lehmann C, Thorel E, Benítez R. Acta biomaterialia hydrothermal processing of 3D-printed calcium phosphate scaffolds enhances bone formation in vivo: a comparison with biomimetic treatment. *Acta Biomater* **2021**;135:671–88.
250. Lee H, Dellatore SM, Miller WM, Messersmith PB. Mussel-inspired surface chemistry for multifunctional coatings. *Science* **2007**;318:426–30.
251. Liu Y, Ai K, Liu J, Deng M, He Y, Lu L. Dopamine-melanin colloidal nanospheres: an efficient near-infrared photothermal therapeutic agent for in vivo cancer therapy. *Adv Mater* **2013**;25:1353–9.
252. Fang Z, Chen J, Pan J, Liu G, Zhao C. The development tendency of 3D-printed bioceramic scaffolds for applications ranging from bone tissue regeneration to bone tumor therapy. *Front Bioeng Biotechnol* **2021**;9:1–13.
253. Dang W, Li T, Li B, Ma H, Zhai D, Wang X, Chang J, Xiao Y, Wang J, Wu C. A bifunctional scaffold with CuFeSe 2 nanocrystals for tumor therapy and bone reconstruction. *Biomaterials* **2018**;160:92–106.
254. Yang B, Yin J, Chen Y, Pan S, Yao H, Gao Y, Shi J. 2D-black-phosphorus-reinforced 3D-printed scaffolds:a stepwise countermeasure for osteosarcoma. *Adv Mater* **2018**;30:1705611–2.
255. Liao J, Han R, Wu Y, Qian Z. Review of a new bone tumor therapy strategy based on bifunctional biomaterials. *Bone Res* **2021**;9:18.
256. Zhang X, Li H, Liu J, Wang H, Sun W, Lin K, Wang X, Shen SG. Amorphous carbon modification on implant surface: a general strategy to enhance osteogenic differentiation for diverse biomaterials via FAK/ERK1/2 signaling pathways. *J Mater Chem B* **2019**;7:2518–33.
257. Zhang Y, Zhai D, Xu M, Yao Q, Chang J, Wu C. 3D-printed bioceramic scaffolds with a Fe3O4/graphene oxide nanocomposite interface for hyperthermia therapy of bone tumor cells. *J Mater Chem B* **2016**;4:2874–86.
258. Fu Y, Cui S, Luo D, Liu Y. Novel inorganic nanomaterial-based therapy for bone tissue regeneration. *Nanomaterials* **2021**;11:789–18.
259. Wang S, Liu L, Zhou X, Yang D, Shi Z, Hao Y. Effect of strontium-containing on the properties of Mg-doped wollastonite bioceramic scaffolds. *BioMed Eng OnLine* **2019**;18:1–14.
260. Truong LB, Medina Cruz D, Mostafavi E, O'Connell CP, Webster TJ. Advances in 3D-printed surface-modified Ca-Si bioceramic structures and their potential for bone tumor therapy. *Materials (Basel)* **2021**;14:3844.
261. Hurle K, Oliveira JM, Reis RL, Pina S, Goetz-Neunhoeffer F. Ion-doped brushite cements for bone regeneration. *Acta Biomater* **2021**;123:51–71.
262. Luo Y, Chen S, Shi Y, Ma J. 3D printing of strontium-doped hydroxyapatite based composite scaffolds for repairing critical-sized rabbit calvarial defects. *Biomed Mater* **2018**;13:065004.
263. Li J, Deng C, Liang W, Kang F, Bai Y, Ma B, Wu C, Dong S. Mn-containing bioceramics inhibit osteoclastogenesis and promote osteoporotic bone regeneration via scavenging ROS. *Bioact Mater* **2021**;6:3839–50.
264. Dang W, Wang X, Li J, Deng C, Liu Y, Yao Q, Wang L, Chang J, Wu C. 3D printing of Mo-containing scaffolds with activated anabolic responses and bi-lineage bioactivities. *Theranostics* **2018**;8:4372–92.
265. Lin R, Deng C, Li X, Liu Y, Zhang M, Qin C, Yao Q, Wang L, Wu C. Copper-incorporated bioactive glass-ceramics inducing anti-inflammatory phenotype and regeneration of cartilage/bone interface. *Theranostics* **2019**;9:6300–13.
266. Bose S, Tarafder S, Bandyopadhyay A. Effect of chemistry on osteogenesis and angiogenesis towards bone tissue engineering using 3D printed scaffolds. *Ann Biomed Eng* **2017**;45:261–72.
267. Bose S, Banerjee D, Robertson S, Vahabzadeh S. Enhanced in vivo bone and blood vessel formation by iron oxide and silica doped 3D printed tricalcium phosphate scaffolds. *Ann Biomed Eng* **2018**;46:1241–53.
268. Guduric V, Belton N, Richter RF, Bernhardt A, Spangenberg J, Wu C, Lode A, Gelinsky M. Tailorable zinc-substituted mesoporous bioactive glass/alginate-methylcellulose composite bioinks. *Materials* **2021**;14:1225–1.
269. Lin YH, Lee AKX, Ho CC, Fang MJ, Kuo TY, Shie MY. The effects of a 3D-printed magnesium-/strontium-doped calcium silicate scaffold on regulation of bone regeneration via dual-stimulation of the AKT and WNT signaling pathways. *Mater Sci Eng C* **2022**;133:112660.
270. Zhang Y, Zhai D, Xu M, Yao Q, Zhu H, Chang J, Wu C. 3D-printed bioceramic scaffolds with antibacterial and osteogenic activity. *Biofabrication* **2017**;9:025037.
271. Liu Y, Li T, Ma H, Zhai D, Deng C, Wang J, Zhuo S, Chang J, Wu C. 3D-printed scaffolds with bioactive elements-induced photothermal effect for bone tumor therapy. *Acta Biomater* **2018**;73:531–46.
272. Rastogi P, Kandasubramanian B. Review of alginate-based hydrogel bioprinting for application in tissue engineering. *Biofabrication* **2019**;11:042001.
273. Axpe E, Oyen ML. Applications of alginate-based bioinks in 3D bioprinting. *IJMS* **2016**;17:1976.
274. Ooi HW, Mota C, Tessa Ten Cate A, Calore A, Moroni L, Baker MB. Thiol-Ene alginate hydrogels as versatile bioinks for bioprinting. *Biomacromolecules* **2018**;19:3390–400.
275. Zhang J, Ke J, Zhu Y, Song J, Yang J, Wen C, Zhang L. Influence of divalent cations on the biofouling behaviors of alginate hydrogels. *Biomed Mater* **2019**;15:015003.
276. Hu C, Lu W, Mata A, Nishinari K, Fang Y. Ions-induced gelation of alginate: mechanisms and applications. *Int J Biol Macromol* **2021**;177:578–88.
277. Sarker M, Izadifar M, Schreyer D, Chen X. Influence of ionic crosslinkers (Ca(2+)/Ba(2+)/Zn(2+)) on the mechanical and biological properties of 3D bioplotted hydrogel scaffolds. *J Biomater Sci Polym Edn* **2018**;29:1126–54.
278. Tijore A, Behr J-M, Irvine SA, Baisane V, Venkatraman S. Bioprinted gelatin hydrogel platform promotes smooth muscle cell contractile phenotype maintenance. *Biomed Microdevices* **2018**;20:32.
279. Zhao N, Wang X, Qin L, Zhai M, Yuan J, Chen J, Li D. Effect of hyaluronic acid in bone formation and its applications in dentistry. *J Biomed Mater Res* **2016**;104:1560–9.
280. Yazan M, Kocyigit ID, Atil F, Tekin U, Gonen ZB, Onder ME. Effect of hyaluronic acid on the osseointegration of dental implants. *Br J Oral Maxillofac Surg* **2019**;57:53–7.
281. Hamlet SM, Vaquette C, Shah A, Hutmacher DW, Ivanovski S. 3-Dimensional functionalized polycaprolactone-hyaluronic acid hydrogel constructs for bone tissue engineering. *J Clin Periodontol* **2017**;44:428–37.
282. Li M, Zhang X, Jia W, Wang Q, Liu Y, Wang X, Wang C, Jiang J, Gu G, Guo Z, Chen Z. Improving in vitro biocompatibility on

biomimetic mineralized collagen bone materials modified with hyaluronic acid oligosaccharide. *Mater Sci Eng C Mater Biol Appl* **2019**;104:110008.
283. Highley CB, Rodell CB, Burdick JA. Direct 3D printing of shear-thinning hydrogels into self-healing hydrogels. *Adv Mater* **2015**;27:5075–9.
284. Ouyang L, Highley CB, Rodell CB, Sun W, Burdick JA. 3D printing of shear-thinning hyaluronic acid hydrogels with secondary cross-linking. *ACS Biomater Sci Eng* **2016**;2:1743–51.
285. Muxika A, Etxabide A, Uranga J, Guerrero P, de la Caba K. Chitosan as a bioactive polymer: processing, properties and applications. *Int J Biol Macromol* **2017**;105:1358–68.
286. Pahlevanzadeh F, Emadi R, Valiani A, Kharaziha M, Poursamar SA, Bakhsheshi-Rad HR, Ismail AF, RamaKrishna S, Berto F. Three-dimensional printing constructs based on the chitosan for tissue regeneration: state of the art, developing directions and prospect trends. *Materials* **2020**;13:2663.
287. Siddiqui N, Asawa S, Birru B, Baadhe R, Rao S. PCL-based composite scaffold matrices for tissue engineering applications. *Mol Biotechnol* **2018**;60:506–32.
288. Górecka Ż, Idaszek J, Kołbuk D, Choińska E, Chlanda A, Święszkowski W. The effect of diameter of fibre on formation of hydrogen bonds and mechanical properties of 3D-printed PCL. *Mater Sci Eng C Mater Biol Appl* **2020**;114:111072.
289. Miszuk JM, Xu T, Yao Q, Fang F, Childs JD, Hong Z, Tao J, Fong H, Sun H. Functionalization of PCL-3D electrospun nanofibrous scaffolds for improved BMP2-Induced bone formation. *Appl Mater Today* **2018**;10:194–202.
290. D'souza AA, Shegokar R. Polyethylene glycol (PEG): a versatile polymer for pharmaceutical applications. *Expert Opin Drug Deliv* **2016**;13:1257–75.
291. Cui Y, Jin R, Zhou Y, Yu M, Ling Y, Wang L-Q. Crystallization enhanced thermal-sensitive hydrogels of PCL-PEG-PCL triblock copolymer for 3D printing. *Biomed Mater* **2021**;16:035006.
292. Yesildag C, Ouyang Z, Zhang Z, Lensen MC. Micro-patterning of PEG-based hydrogels with gold nanoparticles using a reactive micro-contact-printing approach. *Front Chem* **2019**;6:667.
293. Rutz AL, Hyland KE, Jakus AE, Burghardt WR, Shah RN. A multimaterial bioink method for 3D printing tunable, cell-compatible hydrogels. *Adv Mater* **2015**;27:1607–14.
294. Gu X, Sun X, Sun Y, Wang J, Liu Y, Yu K, Wang Y, Zhou Y. Bioinspired modifications of PEEK implants for bone tissue engineering. *Front Bioeng Biotechnol* **2021**;8:1–15.
295. Han X, Sharma N, Xu Z, Scheideler L, Geis-Gerstorfer J, Rupp F, Thieringer FM, Spintzyk S. An in vitro study of osteoblast response on fused-filament fabrication 3D printed PEEK for dental and Cranio-Maxillofacial implants. *JCM* **2019**;8:771.
296. Honigmann P, Sharma N, Okolo B, Popp U, Msallem B, Thieringer FM. Patient-specific surgical implants made of 3D printed PEEK: material, technology, and scope of surgical application. *Biomed Res Int* **2018**;2018:4520636.
297. Torstrick FB, Klosterhoff BS, Westerlund LE, Foley KT, Gochuico J, Lee CS, Gall K, Safranski DL. Impaction durability of porous polyether-ether-ketone (PEEK) and titanium-coated PEEK interbody fusion devices. *Spine J* **2018**;18:857–65.
298. Seaman S, Kerezoudis P, Bydon M, Torner JC, Hitchon PW. Titanium vs. polyetheretherketone (PEEK) interbody fusion: meta-analysis and review of the literature. *J Clin Neurosci* **2017**;44:23–9.
299. Najeeb S, Zafar MS, Khurshid Z, Siddiqui F. Applications of polyetheretherketone (PEEK) in oral implantology and prosthodontics. *J Prosthodont Res* **2016**;60:12–9.
300. Basgul C, Yu T, MacDonald DW, Siskey R, Marcolongo M, Kurtz SM. Does annealing improve the interlayer adhesion and structural integrity of FFF 3D printed PEEK lumbar spinal cages? *J Mech Behav Biomed Mater* **2020**;102:103455.
301. Yang C, Tian X, Li D, Cao Y, Zhao F, Shi C. Influence of thermal processing conditions in 3D printing on the crystallinity and mechanical properties of PEEK material. *J Mater Process Technol* **2017**;248:1–7.
302. Liaw C-Y, Tolbert JW, Chow LW, Guvendiren M. Interlayer bonding strength of 3D printed PEEK specimens. *Soft Matter* **2021**;17:4775–89.
303. Basgul C, Yu T, MacDonald DW, Siskey R, Marcolongo M, Kurtz SM. Structure-property relationships for 3D printed PEEK intervertebral lumbar cages produced using fused filament fabrication. *J Mater Res* **2018**;33:2040–51.
304. Yang M, Wu Z, Yu H, Cheng J. Reconstruction for diverse fronto-orbital defects with computer-assisted designed and computer-assisted manufactured PEEK implants in one-stage operation: case reports. *Medicine (Baltimore)* **2021**;100:e27452.
305. Chen C, Yin Y, Xu H, Li Z, Wang F, Chen G. Personalized three-dimensional printed polyether-ether-ketone prosthesis for reconstruction after subtotal removal of chronic clavicle osteomyelitis: a case report. *Medicine (Baltimore)* **2021**;100:e25703.
306. Liu D, Fu J, Fan H, Li D, Dong E, Xiao X, Wang L, Guo Z. Application of 3D-printed PEEK scapula prosthesis in the treatment of scapular benign fibrous histiocytoma: a case report. *J Bone Oncol* **2018**;12:78–82.
307. Hak DJ, Mauffrey C, Seligson D, Lindeque B. Use of carbon-fiber-reinforced composite implants in orthopedic surgery. *Orthopedics* **2014**;37:825–30.
308. Laux CJ, Hodel SM, Farshad M, Müller DA. Carbon fibre/polyether ether ketone (CF/PEEK) implants in orthopaedic oncology. *World J Surg Oncol* **2018**;16:241.
309. Loeb AE, Mitchell SL, Osgood GM, Shafiq B. Catastrophic failure of a carbon-fiber-reinforced polyetheretherketone tibial intramedullary nail: a case report. *JBJS Case Connect* **2018**;8:e83.
310. Goudriaan WA, Tordoir RL, Broekhuis D, van der Wal RJP. Early failure of a carbon-fiber-reinforced polyetheretherketone distal femur plate: a case report. *JBJS Case Connect* **2020**;10:e20.00041.
311. Reddy R, Reddy N. Biomimetic approaches for tissue engineering. *J Biomater Sci Polym Edn* **2018**;29:1667–85.
312. Hoffman AS. Stimuli-responsive polymers: biomedical applications and challenges for clinical translation. *Adv Drug Deliv Rev* **2013**;65:10–6.
313. Sponchioni M, Capasso Palmiero U, Moscatelli D. Thermo-responsive polymers: applications of smart materials in drug delivery and tissue engineering. *Mater Sci Eng C Mater Biol Appl* **2019**;102:589–605.
314. Rennert K, Nitschke M, Wallert M, Keune N, Raasch M, Lorkowski S, Mosig AS. Thermo-responsive cell culture carrier: effects on macrophage functionality and detachment efficiency. *J Tissue Eng* **2017**;8:2041731417726428.
315. Cao M, Wang Y, Hu X, Gong H, Li R, Cox H, Zhang J, Waigh TA, Xu H, Lu JR. Reversible thermoresponsive Peptide-PNIPAM hydrogels for controlled drug delivery. *Biomacromolecules* **2019**;20:3601–10.
316. Sun X, Tyagi P, Agate S, McCord MG, Lucia LA, Pal L. Highly tunable bioadhesion and optics of 3D printable PNIPAm/cellulose nanofibrils hydrogels. *Carbohydr Polym* **2020**;234:115898.
317. Ohya S, Nakayama Y, Matsuda T. Thermoresponsive artificial extracellular matrix for tissue engineering: hyaluronic acid

bioconjugated with poly(N-isopropylacrylamide) grafts. *Biomacromolecules* **2001**;2:856–63.
318. Peroglio M, Eglin D, Benneker LM, Alini M, Grad S. Thermoreversible hyaluronan-based hydrogel supports in vitro and ex vivo disc-like differentiation of human mesenchymal stem cells. *Spine J* **2013**;13:1627–39.
319. Peroglio M, Grad S, Mortisen D, Sprecher CM, Illien-Jünger S, Alini M, Eglin D. Injectable thermoreversible hyaluronan-based hydrogels for nucleus pulposus cell encapsulation. *Eur Spine J* **2012**;21(Suppl 6):S839–49.
320. Kesti M, Müller M, Becher J, Schnabelrauch M, D'Este M, Eglin D, Zenobi-Wong M. A versatile bioink for three-dimensional printing of cellular scaffolds based on thermally and photo-triggered tandem gelation. *Acta Biomater* **2015**;11:162–72.
321. Koetting MC, Peters JT, Steichen SD, Peppas NA. Stimulus-responsive hydrogels: theory, modern advances, and applications. *Mater Sci Eng R: Rep* **2015**;93:1–49.
322. Kelly PV, Cheng P, Gardner DJ, Gramlich WM. Aqueous polymer modification of cellulose nanofibrils by Grafting-through a reactive methacrylate group. *Macromol Rapid Commun* **2021**;42:e2000531.
323. Yue K, Trujillo-de Santiago G, Alvarez MM, Tamayol A, Annabi N, Khademhosseini A. Synthesis, properties, and biomedical applications of gelatin methacryloyl (GelMA) hydrogels. *Biomaterials* **2015**;73:254–71.
324. Hoch E, Hirth T, Tovar GEM, Borchers K. Chemical tailoring of gelatin to adjust its chemical and physical properties for functional bioprinting. *J Mater Chem B* **2013**;1:5675–85.
325. Hu J, Hou Y, Park H, Choi B, Hou S, Chung A, Lee M. Visible light crosslinkable chitosan hydrogels for tissue engineering. *Acta Biomater* **2012**;8:1730–8.
326. Lim KS, Schon BS, Mekhileri NV, Brown GCJ, Chia CM, Prabakar S, Hooper GJ, Woodfield TBF. New visible-light photoinitiating system for improved print fidelity in gelatin-based bioinks. *ACS Biomater Sci Eng* **2016**;2:1752–62.
327. Abbadessa A, Mouser VHM, Blokzijl MM, Gawlitta D, Dhert WJA, Hennink WE, Malda J, Vermonden T. A synthetic thermosensitive hydrogel for cartilage bioprinting and its biofunctionalization with polysaccharides. *Biomacromolecules* **2016**;17:2137–47.
328. Lam T, Dehne T, Krüger JP, Hondke S, Endres M, Thomas A, Lauster R, Sittinger M, Kloke L. Photopolymerizable gelatin and hyaluronic acid for stereolithographic 3D bioprinting of tissue-engineered cartilage. *J Biomed Mater Res B Appl Biomater* **2019**;107:2649–57.
329. Fan Y, Yue Z, Lucarelli E, Wallace GG. Hybrid printing using cellulose nanocrystals reinforced GelMA/Hama hydrogels for improved structural integration. *Adv Healthcare Mater* **2020**;9:2001410–1.
330. Kufelt O, El-Tamer A, Sehring C, Meißner M, Schlie-Wolter S, Chichkov BN. Water-soluble photopolymerizable chitosan hydrogels for biofabrication via two-photon polymerization. *Acta Biomater* **2015**;18:186–95.
331. Li B, Wang L, Xu F, Gang X, Demirci U, Wei D, Li Y, Feng Y, Jia D, Zhou Y. Hydrosoluble, UV-crosslinkable and injectable chitosan for patterned cell-laden microgel and rapid transdermal curing hydrogel in vivo. *Acta Biomater* **2015**;22:59–69.
332. Torstrick FB, Lin ASP, Safranski DL, Potter D, Sulchek T, Lee CSD, Gall K, Guldberg RE. Effects of surface topography and chemistry on polyether-ether-ketone (PEEK) and titanium osseointegration. *Spine (Phila Pa 1976)* **2020**;45:E417–24.
333. Declercq HA, Desmet T, Berneel EEM, Dubruel P, Cornelissen MJ. Synergistic effect of surface modification and scaffold design of bioplotted 3-D poly-ε-caprolactone scaffolds in osteogenic tissue engineering. *Acta Biomater* **2013**;9:7699–708.
334. Park S, Kim JE, Han J, Jeong S, Lim JW, Lee MC, Son H, Kim HB, Choung Y-H, Seonwoo H, Chung JH, Jang K-J. 3D-Printed poly(E-caprolactone)/hydroxyapatite scaffolds modified with alkaline hydrolysis enhance osteogenesis in vitro. *Polymers* **2021**;13:257–11.
335. Han X, Yang D, Yang C, Spintzyk S, Scheideler L, Li P, Li D, Geis-Gerstorfer J, Rupp F. Carbon fiber reinforced PEEK composites based on 3D-printing technology for orthopedic and dental applications. *JCM* **2019**;8:240.
336. Park J, Lee SJ, Jung TG, Lee JH, Kim WD, Lee JY, Park SA. Surface modification of a three-dimensional polycaprolactone scaffold by polydopamine, biomineralization, and BMP-2 immobilization for potential bone tissue applications. *Colloids Surf B Biointerfaces* **2021**;199:111528.
337. Dong L, Wang SJ, Zhao XR, Zhu YF, Yu JK. 3D-printed poly (ϵ-caprolactone) scaffold integrated with cell-laden chitosan hydrogels for bone tissue engineering. *Sci Rep* **2017**;7:4–12.
338. Wu DT, Munguia-Lopez JG, Cho YW, Ma X, Song V, Zhu Z, Tran SD. Polymeric scaffolds for dental, oral, and craniofacial regenerative medicine. *Molecules (Basel)* **2021**;26:7043.
339. Kamaraj M, Sreevani G, Prabusankar G, Rath SN. Mechanically tunable photo-cross-linkable bioinks for osteogenic differentiation of MSCs in 3D bioprinted constructs. *Mater Sci Eng C Mater Biol Appl* **2021**;131:112478.
340. Oladapo BI, Ismail SO, Bowoto OK, Omigbodun FT, Olawumi MA, Muhammad MA. Lattice design and 3D-printing of PEEK with Ca10(OH)(PO4)3 and in-vitro bio-composite for bone implant. *Int J Biol Macromol* **2020**;165:50–62.
341. Zhu W, Cui H, Boualam B, Masood F, Flynn E, Rao RD, Zhang Z-Y, Zhang LG. 3D bioprinting mesenchymal stem cell-laden construct with core-shell nanospheres for cartilage tissue engineering. *Nanotechnology* **2018**;29:185101.
342. Soltan N, Ning L, Mohabatpour F, Papagerakis P, Chen X. Printability and cell viability in bioprinting alginate dialdehyde-gelatin scaffolds. *ACS Biomater Sci Eng* **2019**;5:2976–87.
343. Schuurman W, Levett PA, Pot MW, van Weeren PR, Dhert WJA, Hutmacher DW, Melchels FPW, Klein TJ, Malda J. Gelatin-methacrylamide hydrogels as potential biomaterials for fabrication of tissue-engineered cartilage constructs. *Macromol Biosci* **2013**;13:551–61.
344. Dranseikiene D, Schrüfer S, Schubert DW, Reakasame S, Boccaccini AR. Cell-laden alginate dialdehyde–gelatin hydrogels formed in 3D printed sacrificial gel. *J Mater Sci Mater Med* **2020**;31:31–7.
345. Poldervaart MT, Goversen B, de Ruijter M, Abbadessa A, Melchels FPW, Öner FC, Dhert WJA, Vermonden T, Alblas J. 3D bioprinting of methacrylated hyaluronic acid (MeHA) hydrogel with intrinsic osteogenicity. *PLoS One* **2017**;12:e0177628.
346. Wang Z, Abdulla R, Parker B, Samanipour R, Ghosh S, Kim K. A simple and high-resolution stereolithography-based 3D bioprinting system using visible light crosslinkable bioinks. *Biofabrication* **2015**;7:045009.
347. Piluso S, Skvortsov GA, Altunbek M, Afghah F, Khani N, Koç B, Patterson J. 3D bioprinting of molecularly engineered PEG-based hydrogels utilizing gelatin fragments. *Biofabrication* **2021**;13:045008.
348. Weber LM, Lopez CG, Anseth KS. Effects of PEG hydrogel crosslinking density on protein diffusion and encapsulated islet survival and function. *J Biomed Mater Res* **2009**;90A:720–9.
349. Wen J, Lu T, Wang X, Xu L, Wu Q, Pan H, Wang D, Liu X, Jiang X. In vitro and in vivo evaluation of silicate-coated

polyetheretherketone fabricated by electron beam evaporation. *ACS Appl Mater Interfaces* **2016**;8:13197–206.

350. Ouyang L, Zhao Y, Jin G, Lu T, Li J, Qiao Y, Ning C, Zhang X, Chu PK, Liu X. Influence of sulfur content on bone formation and antibacterial ability of sulfonated PEEK. *Biomaterials* **2016**;83:115–26.
351. Gao A, Liao Q, Xie L, Wang G, Zhang W, Wu Y, Li P, Guan M, Pan H, Tong L, Chu PK, Wang H. Tuning the surface immunomodulatory functions of polyetheretherketone for enhanced osseointegration. *Biomaterials* **2020**;230:119642.
352. Jang CH, Koo Y, Kim G. ASC/chondrocyte-laden alginate hydrogel/PCL hybrid scaffold fabricated using 3D printing for auricle regeneration. *Carbohydr Polym* **2020**;248:116776.
353. Nguyen D, Hägg DA, Forsman A, Ekholm J, Nimkingratana P, Brantsing C, Kalogeropoulos T, Zaunz S, Concaro S, Brittberg M, Lindahl A, Gatenholm P, Enejder A, Simonsson S. Cartilage tissue engineering by the 3D bioprinting of iPS cells in a nanocellulose/alginate bioink. *Sci Rep* **2017**;7:658.
354. Purohit SD, Singh H, Bhaskar R, Yadav I, Chou C-F, Gupta MK, Mishra NC. Gelatin-alginate-cerium oxide nanocomposite scaffold for bone regeneration. *Mater Sci Eng C Mater Biol Appl* **2020**;116:111111.
355. Ashammakhi N, Hasan A, Kaarela O, Byambaa B, Sheikhi A, Gaharwar AK, Khademhosseini A. Advancing frontiers in bone bioprinting. *Adv Healthcare Mater* **2019**;8:1801048–24.
356. Cui H, Zhu W, Nowicki M, Zhou X, Khademhosseini A, Zhang LG. Hierarchical fabrication of engineered vascularized bone biphasic constructs via dual 3D bioprinting: integrating regional bioactive factors into architectural design. *Adv Healthc Mater* **2016**;5:2174–81.
357. Walladbegi J, Schaefer C, Pernevik E, Sämfors S, Kjeller G, Gatenholm P, Sándor G, Rasmusson L. Three-dimensional bioprinting using a coaxial needle with viscous inks in bone tissue engineering—an in vitro study. *Ann Maxillofac Surg* **2020**;10:370–6.
358. Feng F, He J, Li J, Mao M, Li D. Multicomponent bioprinting of heterogeneous hydrogel constructs based on microfluidic printheads. *Int J Bioprint* **2019**;5:202.
359. Colosi C, Shin SR, Manoharan V, Massa S, Costantini M, Barbetta A, Dokmeci MR, Dentini M, Khademhosseini A. Microfluidic bioprinting of heterogeneous 3D tissue constructs using low-viscosity bioink. *Adv Mater* **2016**;28:677–84.
360. Raja N, Yun HS. A simultaneous 3D printing process for the fabrication of bioceramic and cell-laden hydrogel core/shell scaffolds with potential application in bone tissue regeneration. *J Mater Chem B* **2016**;4:4707–16.
361. Shanjani Y, Pan CC, Elomaa L, Yang Y. A novel bioprinting method and system for forming hybrid tissue engineering constructs. *Biofabrication* **2015**;7:045008.